CHEMICALLY AND PHOTOCHEMICALLY CROSSLINKED NETWORKS AND ACID-FUNCTIONALIZED MWCNT COMPOSITES

Ali Nebipasagil

Thesis submitted to the faculty of the
Virginia Polytechnic Institute and State University
in partial fulfillment of the requirements for the degree of

Masters of Science in
Macromolecular Science and Engineering

Timothy E. Long (Chair)
Robert B. Moore
S. Richard Turner

May 17, 2011
Blacksburg, Virginia

Keywords: Telechelic, urethane H-bonding, Michael carbon addition, multiwalled carbon nanotubes, urethane composites, UV curing, thermo-mechanical property

CHEMICALLY AND PHOTOCHEMICALLY CROSSLINKED NETWORKS and FUNCTIONALIZED MWCNT COMPOSITES

Ali Nebipasagil

ABSTRACT

PTMO-urethane and urea diacrylates (UtDA, UrDA) were synthesized from a two-step reactions of bis (4-isocyanatocyclohexyl) methane (HMDI) with either α,ω-hydroxy-terminated poly (tetramethylene oxide) (PTMO M_n 250, 1000, 2000 and 2900 g/mol**)** or α,ω-aminopropyl-terminated PTMO and 2-hydroxyethyl acrylate (HEA). PTMO-based ester precursors (EtDA) were also synthesized from α,ω-hydroxy-terminated PTMO (M_n 1000 and 2000 g/mol**)**. Two bis acetoacetates were synthesized from acetoacetylation of 1,4-butanediol and 250 g/mol hydroxy-terminated PTMO with tert-butyl acetoacetate. ^{1}H NMR spectroscopy confirmed the structure and average molecular weights (M_n)of diacrylates. M_n of these precursors were in the range of 950 to 3670 g/mol by ^{1}H NMR. The rheological properties of diacrylates were studied and activation energies for flow were calculated. Activation energies increased with increasing M_n and hydrogen-bond segment content. Michael carbon addition was employed to covalently crosslink the precursors resulting in networks with gel fractions better than 90%. DSC and DMA experiments revealed that networks had a broad distribution of glass transition temperatures depending on M_n and degree of hydrogen bonding present in the diacrylates. Their T_g's varied from -61 ºC to 63 ºC depending on the crosslinking density and hydrogen-bonding segment content. TGA revealed that UtDA and UrDA networks had an improved thermal stability compared to their EtDA counterparts. Tensile properties showed a variation depending on the structure and M_n of diacrylate and BisAcAc precursors. The storage moduli of networks precursor change from 25.3 MPa to 2.0 MPa with increasing M_n of the urethane diacrylate Elongation at break increased from 255% to 755 % for the same networks. The Young's moduli

increased from 3.27 MPa for EtDA 2000 to 311.1 MPa for UrDA 2000 which was attributed to increasing degree of hydrogen-bonding.

Acid functionalization of C70 P Baytubes multiwalled carbon nanotubes (MWCNT) generated acid-functionalized nanotubes (MWCNT-COOH). Suspension of MWCNT-COOH in organic solvents (chloroform, toluene, THF, DMF and 2-propanol) were prepared. DLS indicated average particle diameters of MWCNT-COOH in DMF and in 2-propanol were 139 nm and 162 nm respectively. FESEM of suspensions revealed aggregate free dispersion of MWCNT-COOH in DMF and 2-propanol. MWCNT-COOH containing composite networks were prepared. FESEM images of fracture surfaces of UtDA showed MWCNT-COOH were well-dispersed in the composites. DMA showed an increase in the rubbery plateau modulus which correlated with the MWCNT-COOH content in the networks. Tensile testing also revealed a relationship between MWCNT-COOH content and young's moduli and strain at break of networks. Storage moduli of networks increased from 25 MPa to 211 MPa with increasing MWCNT-COOH content whereas elongation at break decreased from 255 % to 146 %.

UtDAs and pentaerythritol tetraacrylate (PETA) were crosslinked under UV radiation (6 passes, 1.42 ± 0.05 $W.cm^2$ for each pass) in the presence of 2,2-dimethoxy-2-phenylacetophenone (DMPA) (1 wt. % of the mixture) UV initiator. DMA demonstrated the presence of broad glass transition regions with a range of T_g's which varied from -60 °C to -30°C. Tensile testing also revealed the relationship between Young's moduli, strain at break and the molecular weight of the diacrylates. The increasing molecular weight of urethane diacrylate precursors caused a drop in the storage moduli of networks from 15.8 MPa to 1.4 MPa and an increase in elongation at break from 76 % to 132 %.

ACKNOWLEDGEMENTS

I would like to express my sincere gratitude to my advisor, Dr. Timothy E. Long, for giving me the opportunity to work in a distinguished research group and most of all for his encouragement and tremendous support from the first day of my graduate career. I would like to thank my committee members, Dr. S. Richard Turner, and Robert B. Moore for their very valuable time and guidance during my studies at Virginia Tech.

I would like to recognize all my group members, previous and present, including Dr. Erin Murphy, Dr. Matthew Hunley, Dr. Philippe Bissel, Dr. Gozde Karabiyik, Matthew Green, Tianyu Wu, Renlong Gao, Michael Allen, Nancy Zhang, Mana Tamami, Shijing Cheng, Steve June, Sean Hemp, David Inglefield, Ashley Nelson, Alison Schultz, Chainika Jangu, Alex Fersner and Dr. Daisuke Yamamoto for their advice, discussions, and time. I also would like to thank staff members including Vicki Long, Valerie Owens, Laurie Good, Mary Jane Smith for their assistance.

I would like to send my gratitude to İskender and Emel Yılgör, my advisors at Koç University, who always encouraged and supported me throughout my undergraduate studies.

I am forever grateful to my family. I would not have been where I am today without them. I especially thank my mother for supporting and encouraging me in every step of my life, nothing can mean more to me than making her proud. I can never pay sacrifices she made to allow me to pursue my life goals.

Table of Contents

List of Figures

List of Tables

List of Schemes

Chapter 1. Introduction to Polyurethanes and Polyurethane Nanocomposites: Applications to Structure-Property Characterizations

1.1 Abstract

Polyurethanes (PUs) exhibit properties ranging from soft elastomers to rigid thermoplastics depending on the chemical composition, backbone structure, and morphology. Most have high elongations, moduli, strength, and good processability. PUs can incorporate covalent and/or physical crosslinks due to presence of hydrogen bonding and/or covalent crosslinking through monomers with functionality greater than two. Michael carbon addition utilizing acrylate functional telechelics with bis- or tris-acetoacetates yield covalent networks. The chemical structure, functionality, molecular weight of oligomers, molecular weight between crosslinks points, and hydrogen bonding influences the thermal stability and mechanical properties of networks. Incorporation of nanoparticles improves the overall network properties. Treatment of nanoparticles to yield homogeneous dispersion within the polymer matrix is of crucial importance to achieve ultimate composite properties. Carbon nanotubes improve a range of polymer properties which can be exploited for many applications. This chapter discusses the synthesis and structure-property relationship of polyurethanes, synthetic strategies to prepare polyurethane networks, nanocomposites in particular carbon nanotube composites and their potential applications.

Key words: polyurethanes, Michael addition, crosslinking, carbon nanotubes, polyurethane nanocomposites

1.2 Polyurethanes: Synthesis and Structure-Property Relationships

Segmented linear polyurethanes (SPU) have a wide range of emerging applications, such as membranes,[1] biomedical and bioengineering applications, [2-4] and actuators.[5] Polyurethanes contain urethane linkages, along their backbone structure. The reaction of a diisocyanate with an α,ω-hydroxyl terminated polyol alone or coupled with low molecular weight glycol (chain extender) produces linear segmented polyurethanes. **Figure 1.1** depicts the structure of a segmented polyurethane in which the flexible (soft) segment consists of a polyol and rigid (hard) segment consist of a diisocyanate and a chain extender.[6,7]

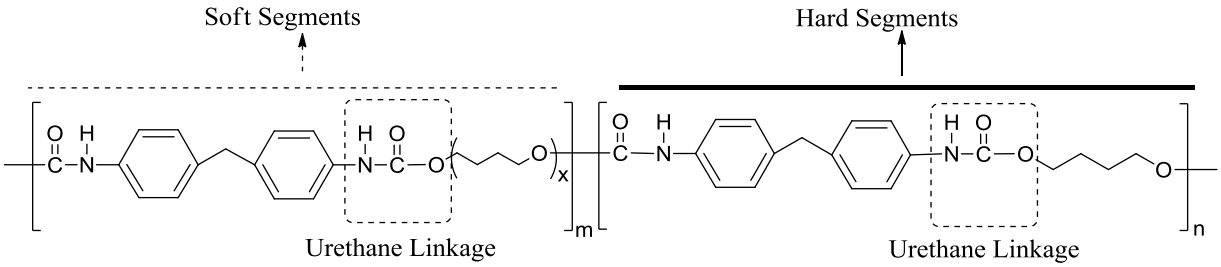

Figure 1.1. Schematic representation of a linear segmented polyurethane

Polyols consist primarily of polyether-, polyester-, polycarbonate-, or polysiloxane-based oligomers with glass transition temperatures below room temperature and number average molecular weights (M_n) between 1000 and 5000 g/mol. The conventional methods to synthesize segmented polyurethanes include single-step "one-shot" and two-step "prepolymer" methods. In single step "one-shot" synthesis, all constituents react simultaneously. In the "prepolymer" method, the reaction of excess isocyanate with α,ω-hydroxyl terminated polyol yields isocyanate-terminated prepolymer which later is allowed to react chain extender to form high molecular weight segmented polyurethane with alternating soft (SS) and hard segments(HS). **Figure 1.2** depicts the synthesis of segmented polyurethanes through prepolymer method.

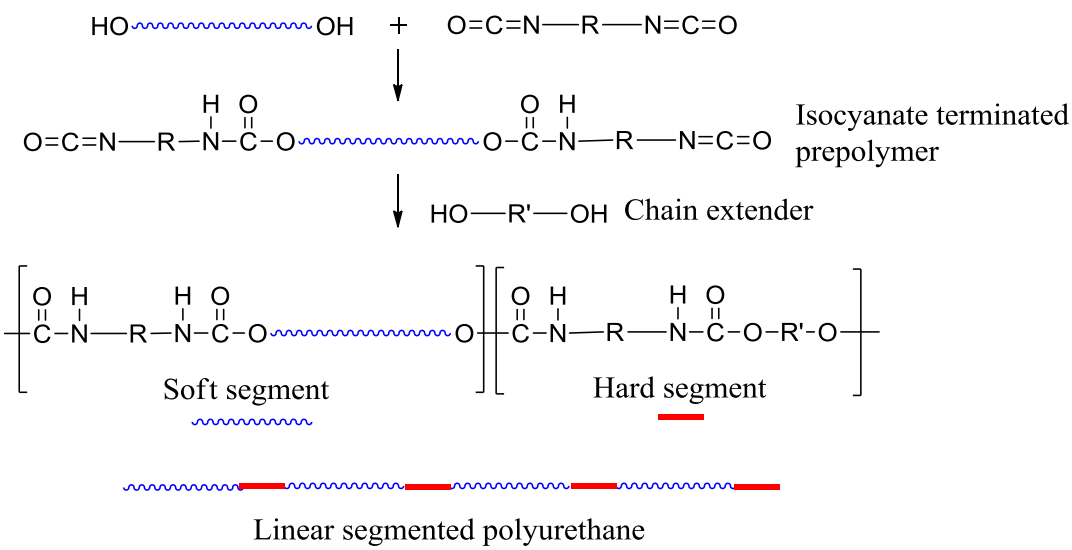

Figure 1.2. Representation of the preparation of segmented polyurethane using the prepolymer method.[7]

Several studies report the synthesis, and structure-property relationships of polyether segmented polyurethanes.[8-14] SS structure and molecular weights vary depending on the targeted applications. Poly(tetramethylene oxide), poly(ethylene glycol), poly(propylene glycol), and poly(ethylene oxide-*co*-propylene oxide) copolyol (PTMO, PEG, PPG, and PEG-co-PPG, respectively) represent some of the most-often studied polyether polyols. Hernandez *et al.* [15] reported SPU with the same HS and a different polyether SS (PTMO, poly(hexamethylene oxide), PHMO) have significantly different phase morphologies and different degrees of hydrogen-bonding. Similar studies also showed the SS molecular weight, structure, and composition affect water solubility, biodegradability, biocompatibility, morphology and microphase separation, and physical phenomena such as hydrogen-bonding and crystallization.[1,7,9-12,15,16]

Polyester based soft-segmented polyurethanes have also received significant interest. Synthesis of SPU with different ester-based SS yields several different SPU with unique properties. Small difunctional molecules such as short chain diols (1,6-hexanediol, 1,5-

pentanediol) with diacids (adipic acid, pimelic acid) react to synthesize hydroxyl-terminated ester polyols.[17] In addition to diol reactions with diacids, reactions of diisocyanates with poly (ε-caprolactone)[18,19] or their derivatives at different mol ratios with or without presence of chain extenders yields polyester-based polyurethanes.[18,20,21] Compatibility of polyester SS with HS, SS chain length, mobility of HS in SS domains affect the properties of polyurethanes. Utilization of polyester SS in polyurethanes has several advantages over polyether-based SS. Different from ether-based SS, ester SS bear carbonyl units along their backbone. Carbonyl units allow ester SS to form hydrogen-bonds with amide groups of the HS. Recent research efforts reported crystallization and melting of ester SS domains.[17-19,22] Moreover, since carbonyl units along the ester SS adds polarity and hydrogen-bonding to the molecule; they change morphology, [21] increase mechanical properties and introduce shape-memory properties [23] to polyurethanes, compared to their polyether counterparts.

Incorporation of polycarbonate based SS into SPU have attracted significant attention over the years. The presence of carbonate units along their backbone structure increases polarity of SS and add hydrogen-bonding sites along the SS backbone. Polar carbonyl units cause differences in intersegment hydrogen-bonding between the polar hard and soft segments, which ultimately lead to partial phase mixing between HS and SS domains.[15] Polycarbonate diol based polyurethanes exhibit high tensile strength, modulus, and low elasticity, and improved resistance and to organic solvents and hydrolysis than polyether based polyurethanes.[24-30] Transesterification reaction of short chain diols (1,5-pentanediol or 1,6-hexanediol) with alkyl carbonate diols yields poly(alkyl carbonate) diols. The degree of phase separation and the degree of crystallinity of SS determine tensile properties of polycarbonate based SPU. Higher SS M_n increase the degree of crystallinity of SS and thereby increase the stiffness of SPU. [31] Therefore

structure and M_n of SS plays an integral role in mechanical properties. Lee *et al.*[32] reported polyurethanes with polycarbonate SS have significantly higher modulus than those polyester and polyether-based SS polyurethanes. Tanaka *et al.*[33] concluded that long alkyl chain polycarbonate SS repeating units had higher degree of crystallinity than their short-chain counterparts and thus they had improved modulus and improved thermal resistance.

Presence of silicone-based PDMS polyols in PU introduces unique properties of PDMS into PU.[34] PDMS exhibits low glass transition temperature (−120 °C), low degrees of intermolecular interaction and providing great molecular flexibility, excellent thermal stability and oxidation resistance, hydrophobicity, resistance to temperature extremes, low surface energy, and high impact resistance.[34-36] PDMS exhibit high degree of incompatibility with polar HS, which result high degree of phase separation in polyurethanes.[35] Moreover, excellent biostability and unique mechanical properties make PDMS an alternative for biological applications.[37] Lin *et al.*[35] summarized the effect of soft segment on polyurethane properties. The authors compared the effect of PDMS-based SS to PTMO-based SS. DSC and DMA results confirmed the immiscibility of PDMS segment with other segments of PU.

HS type, symmetry, and structure have a profound impact on properties of SPU. Several different diisocyanates, aliphatic, cycloaliphatic, aromatic, exist for SPU synthesis as shown in **Figure 1.3**.

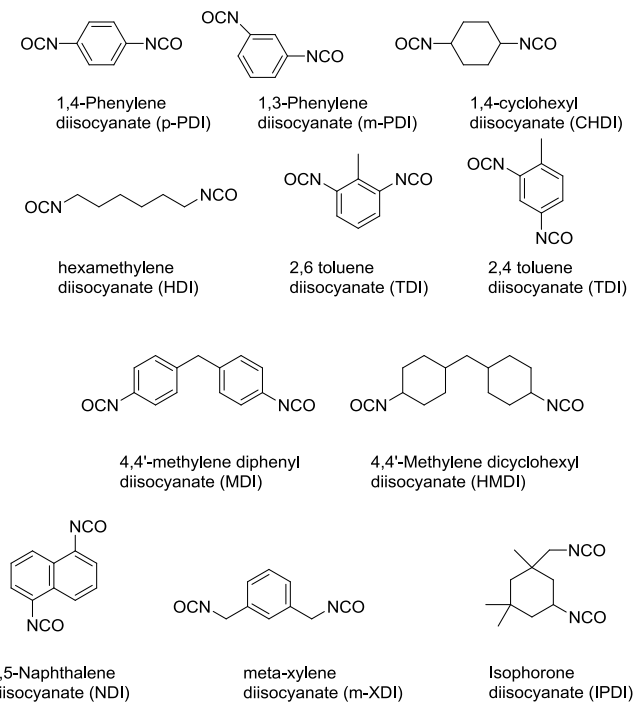

Figure 1.3. Common diisocyanates used for the synthesis of segmented polyurethanes

Yilgor *et al*.,[14] and Das *et al*., [6] suggested that the symmetry of diisocyanates influenced the degree of crystallinity of polyurethanes. These studies suggested that symmetric diisocyanates organized to form crystalline domains; however, the presence of non-symmetric diisocyanates in the PU backbone disrupted the degree of organization and inhibited the self-organization of HS domains. DMA analyses of different SPU with different diisocyanates indicated that the PU bearing symmetric diisocyanate units have higher transition temperatures and showed better mechanical properties over a wider range of temperatures than asymmetric diisocyanate SPU. AFM images of PU with different HS composition in **Figure 1.4** reveal that the difference in surface morphology of symmetrical and asymmetrical diisocyanate containing HS PUs. SAXS and tensile testing methods also confirm the symmetry of the diisocyanate affected the crystallinity of PU.

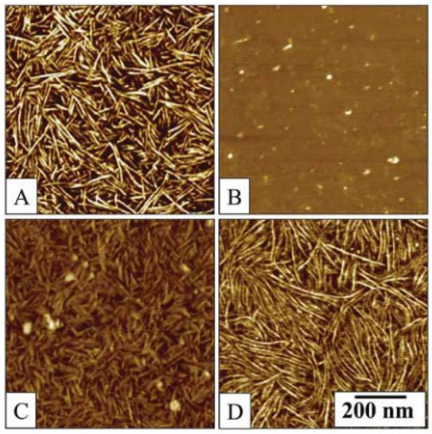

Figure 1.4. Tapping-mode phase images of polyurethanes with hard segments based on (A)p-PDI (B) MDI (C) HDI (D) CHDI diisocyanates.[6]

Figure 1.5 presents SAXS profiles of each film. Yilgor and co-workers indicated that MDI, TDI, and m-PDI containing polyurethanes did not have interference peaks in SAXS profile. All the symmetric polyurethanes that show phase-separated surface morphologies in AFM also show a first order interference peak in their SAXS profiles. SAXS data validated that SPU with symmetrical diisocyanates have higher degree of crystallinity than those with non-symmetrical diisocyanates.[6]

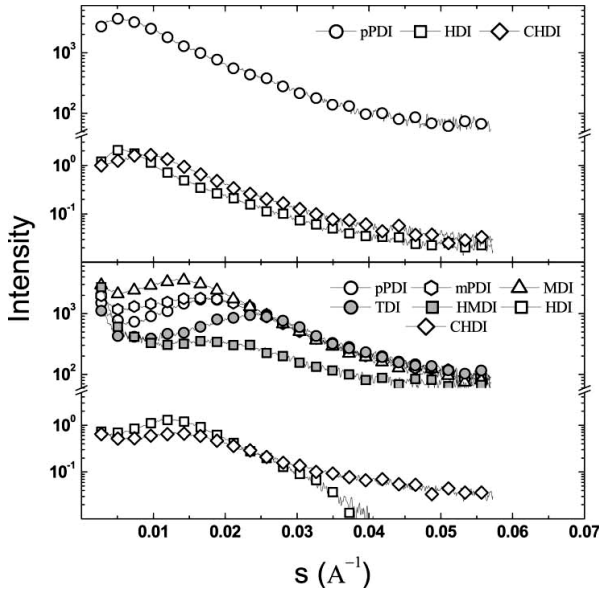

Figure 1.5. SAXS profiles of polyurethanes.[6]

The second constituent of the HS consists of chain extenders. Chattopadhyay *et al.*[8] studied the effect of chain extender on the properties of SPU. They investigated the effect of various chain extenders such as 1,4-butanediol, 1,2-propanediol, 2,2-diethyl-1,3-propanediol, and 2-butyl-2-ethyl-1,3-propanediol. They reported mechanical, tensile, impact properties of polyurethanes with different chain extenders. Chattopadhyay proposed a direct correlation between the structure of chain extenders, and degree of phase separation. They suggested that the molecular weight and nature of the chain extenders (bulky diol chain extenders promote phase separation compared to small diol chain extenders) controlled the phase separation and thus mechanical and thermal properties of polyurethanes.

Several factors directly affect the properties of segmented polyurethanes. In a polyurethane system, either covalent and/or physical crosslinks exist. The physical crosslinking originates from inter-molecular and intra-molecular H-bonding or from the interaction of charged segments present in the polymer unit.[6,8,11,22,31,38] **Figure 1.6** shows the physical crosslinking due to inter-molecular hydrogen bonds in a polyurethane synthesized from a diester diphenol and hexamethylene diisocyanate.

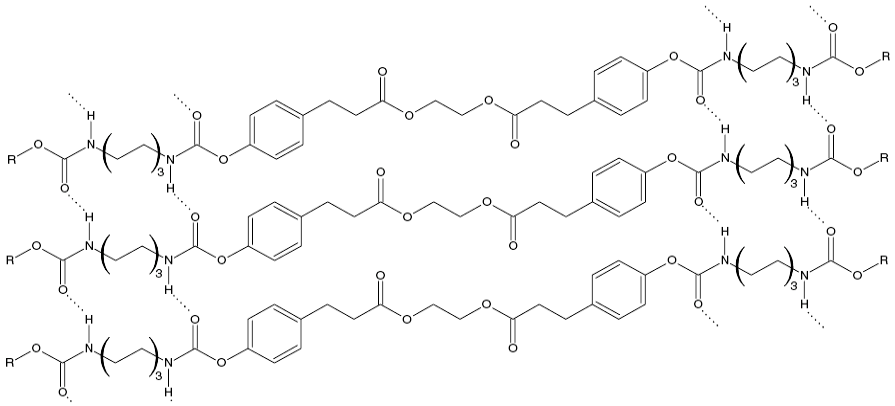

Figure 1.6. Physical crosslinking in hard segment of a segmented polyurethane.[22]

1.3. Synthetic Strategies to Achieve Polyurethane Networks

Crosslinked polyurethanes have a wide range of applications in membranes, coatings[39], adhesives[40,41], medicine[42], biomedical and bioengineering applications[43-45], and in electronic devices[46]. The major advantages of crosslinking introduce to polyurethanes are additional mechanical resistance and high temperatures of deformation and/or degradation. The presence of crosslinks provides enhanced tensile strength, abrasion resistance as well as acid and solvent resistance. Crosslinking in the urethane elastomer initiates by reaction of isocyanate end groups with triols or higher functional hydroxyls instead of a difunctional glycol. Increasing the functionality of the monomers also increase the crosslinking density. Crosslinked PUs have high T_g's, ability to form high quality films, good solvent resistance and ease of synthesis and processing. Hydroxy-terminated polyester and hydroxy-functional acrylic resins are the most common polyols. Alternative methods also exist to prepare polyurethane networks.

1.3.1 Utilization of Multi-Functional Monomers to Achieve Networks

Utilization of non-linear variation of a conventional monomer yields a polyurethane network. The type of covalent crosslinking depends on the crosslinking agent's properties.[47] Non-linear derivatives of linear SPU consist of dendrimeric and hyperbranched (or highly branched) polyurethanes. Unal *et al.*[48] studied the synthesis of highly branched segmented poly(ester urethanes). Unal synthesized branched polyurethanes from reaction of HMDI-terminated 1,4-butanediol-based difunctional hard segment and poly(caprolactone)-based trifunctional soft segment. Results indicated that reaction conditions determine the degree of branching, gel formation, polydispersity, and M_n of the product. Unal and colleagues reported crosslinking of highly branched polyurethanes produced polyurethane networks with high (above

90%) gel fraction. Tensile properties of polyurethane networks showed dramatic increase compared to highly branched analogs. Fornof *et al*.[49] reported the synthesis of branched segmented poly(ester urethane) based on difunctional PEG, PPG, and PTMO soft segments and hard segments comprised of trifunctional trimethylol propane and HMDI. Characterizations suggested that the degree of branching depends on M_n and type of soft segments, molar ratio of trifunctional and difunctional monomers. Furthermore, others showed that hyperbranched crosslinkers such as hyperbranched polyesters or multifunctional polyols crosslink linear polyurethanes.[50-52]

1.3.2 Michael Carbon Addition of Acrylate Functional Telechelics

Michael addition reaction[53-55] of telechelic precursors provides an alternative to crosslinking with hyperbranched crosslinking agents. Michael addition is a versatile method suitable for various applications.[53-57] Michael addition reaction offers many advantages such as mild conditions, functional group tolerance, and variety of precursors.[53] Mather and others [56] studied the PEG diacrylates Michael addition to synthesized of PPG-based bis acetoacetates. They investigated and the effect of PPG precursor M_n on the mechanical properties of Michael addition networks in relation to the critical molecular weight for entanglement. Moreover, they focused on the gelation process, by which they discovered ideal bisAcAc to diacrylate ration to be 1:1.4 and base catalyst to be 0.0027 mol equivalence relative to bisAcAc. Authors showed the onset of gelation was faster and gel fraction percent of the networks were higher for the lower M_n precursors. They attribute this result to higher concentration thus higher accessibility of the acrylate end groups in the lower M_n samples. Tensile and DMA results revealed that a strong correlation between the M_n of PPG diacrylate and mechanical strength exists. The authors

showed that the T_g of the networks increased with decreasing PPG M_n. Tensile strength and Young's moduli of the networks were also higher for networks with lower PPG M_n precursors. These result both attribute to crosslinking density of the networks. Mather *et al.* reported the synthesis of acid-cleavable diacrylate crosslinker containing Michael addition networks. The researchers synthesized PEG bisAcAc and dicumyl alcohol diacrylate. Authors showed that these precursors cure and room temperature and the networks can degrade in the presence of strong acids. Ozturk and Long[58] showed the synthesis of covalently crosslinked PCL-based biodegradable networks using Michael carbon addition. Authors also reported the biodegradation rates are controlled with morphology changes, which they achieved by using bis- or tris- functionalized poly (caprolactone) with M_n varying from 1000 to 4800 g/mol.

Long *et al.*[53] investigated the preparation of hydrogen-bond containing networks that utilizes Michael addition reaction. This approach consisted of synthesis of Michael donors from PEG of various M_n and tert-butyl acetoacetate and later crosslinking of the Michael donors with hydroxy ethyl acrylate functionalized HMDI or neopentyl glycol diacrylate (NPGDA) with a base catalyst. Gel fraction analysis confirmed polyurethane networks from both methods yield high gel fractions. Tensile and DMA results revealed the existence of a strong correlation between the M_n of PPG diacrylate and mechanical strength. Williams and others also showed that the T_g of the networks increased with decreasing PPG M_n. Tensile strength and Young's moduli of the hydrogen-bonding networks were higher compared to networks with non-hydrogen-bonded couterparts. These result both attribute to covalent crosslinking density of the networks and physical crosslinking due to presence of hydrogen-bonds.

1.3.3 UV Curing of Acrylate-Methacrylate Functional Telechelics

UV radiation curing [35,59-66] of acrylate or methacrylate functional telechelics offer an alternative to crosslinking with hyperbranched crosslinking agents. Kim *et al.*[59] investigated the properties of UV-curable acrylates based on PPG SS and IPDI-HEA HS along with, tripropyleneglycol diacrylate, and trimethylolpropane triacrylate. Kim employed benzophenone as UV initiator and N-methyldiethanolamine as the accelerator. Kim and colleagues showed the effect of molecular weight of SS and acrylate group type on tensile strength of crosslinked films. Results revealed that both content and functionality of acrylic monomer affected to tensile strength of the crosslinked polyurethane films. Tensile testing and DMA traces showed that mechanical properties improved with the amount of acrylic molecule content and increasing functionality of acrylic molecules. Kim *et al.*[64] studied the synthesis and properties of PEG based UV curable hydrogels. They functionalized PEG-based prepolymers (molecular weight of PEG ranging from 400 to 4000 g/mol and various isocyanates HDI, IPDI, TDI, and HMDI) with HEMA. Kim preferred benzophenone as UV initiator to cure hydrogels. The SS type and molecular weight affects the distance between crosslinking points and mechanical properties of this type of crosslinked polyurethanes. Moreover, Kim showed that the nature of isocyanate plays an important part to control mechanical behavior, phase separation, and hydrogen-bonding of polyurethane networks. Tensile testing and dynamic mechanical analysis indicated significant improvement in mechanical and thermal properties of crosslinked polyurethanes.

1.4 Introduction to Polyurethane Nanocomposites

Polymer nanocomposites are polymers containing nanofillers. The size of nano particles are in the range of nanometers. Fillers are used for a long time to enhance properties of

thermoplastic polymers. Previous literature report the enhancement of properties of polymer nanocomposites compared to the pristine polymers. Common inorganic fillers are frequently used to reduce cost and to increase stiffness, but the improvements in modulus usually mean a compromise in elastomer properties.

Researchers are currently focused on two types of nanofillers: nanoparticles and nanoclays. The main hypothesis is that a valuable nanocomposite is achieved through the largest possible surface of nanofiller. Avoiding aggregation of nanoparticles and exfoliation of nanoclays provide large particle surface area. Layered silicates and especially montrillomonite are widely employed in nanocomposites. Silicates have inorganic cations such as Na^+ between layers that hold negatively charged particles together. The replacement of the inorganic cations with larger alkyl cations leads to intercalation of polymer molecules into the increased space between layers and thus to a better compatibility between polymer and nanoparticles. There is a number of ways to increase the degree of exfoliation in a nanocomposite, such as in situ polymerization, melt blending, solution blending, sonication, high shear mixing, and melt intercalation[67-69].

PU nanocomposites with silica and alumina were prepared and their physical properties were studied.[70] Some beneficial properties of silica nanocomposites of PU were observed. Storage moduli of elastomers with nanosilica demonstrated an increase in the rubbery plateau with increasing silica content.[70] Nanosilica has a profound effect on tensile strength and elongation-at-break of PU composites below 10 wt. % nanosilica content.[70]

Previous literature also demonstrated an important application of organoclay.[71] Researchers were able to polymerize ε-caprolactam with organoclay, which yielded a Nylon 6-clay hybrid. They showed that presence of 4.2 wt. % of organoclay doubled the tensile modulus,

and increased the tensile strength more than 50% compared to the pristine polymer. They attributed this outcome to complete exfoliation of the clay nanolayers in the polymer matrix [71]. Others also studied the effects of organoclay on the properties of PU using many different procedures. Researchers employed (i) distribution of clay in polyol and reaction with diisocyanate; (ii) dispersing clay in reaction solvent with a subsequent evaporation of solvent; (iii) reaction of diisocyanate with hydroxyalkyls in the clay with a subsequent reaction with polyol. The research showed dispersion of clay in reaction solvent yielded an improvement in both elasticity and tensile modulus.[72] Clay nanolayers, even in aggregated state, strengthen and toughen the matrix of the composites. The enhancement in strength and modulus is directly attributed to the reinforcement provided by the disperse clay nanolayers. Chang *et al*. studied several PU nanocomposites containing 0–8 wt. % organoclay. [73] They reported 3–4 wt. % organoclay content yielded the most desired tensile properties. The authors also showed ultimate strength and initial modulus of the nanocomposites increased. Moreover, they demonstrated gas barrier properties, and the thermal stability of one nanocomposite increased with increasing clay content [73]. Finnigan *et al.*[74] showed the interaction of unmodified, hydrophilic, exfoliated clay with polar soft segments (polyol) in PU like poly(ethylene oxide) where as in PU with hydrophobic soft segments like poly(tetramethylene oxide) clay interacts with the hard segment.[74] They reported, a decrease toughness and elongation-to-break for polar soft segments, whereas an increase of the same properties for non-polar soft segments..[74]

Discovery of multi-walled carbon nanotubes (MWCNTs) in 1991 and single-walled carbon nanotubes (SWCNTs) in 1993 attracted significant interest. [75,76] Carbon nanotubes (CNTs) have tubular structures that are typically of nanometer diameter and many micrometers in length. Due to their size and unique shape, these nanotubes exhibit fascinating properties.

Their lightweight, high tensile strength (50-100 GPa) and high modulus (1-2 TPa) make them good reinforcing fillers for lightweight composite applications.[77]

Efforts focused on various methods to disperse CNTs in composite matrix such as ultrasonication, [78-80] high shear mixing of CNTs composites, [81-85] melt mixing, [86-90] using polymeric compatiblizers, [91] and chemical functionalization.[77,92-109] The van der Waals interactions hold nanotubes together as bundles and ropes, resulting in CNTs having very low dispersion, which causes aggregation in organic solvents.[77] The desired application determines the choice of functional group. Several methods exist to functionalize CNTs such as fluorination[109], alkyl lithium reactions, [73] Grignard reagents, diazonium salts, [68] amines, and organic radicals.[16] All these methods have different procedures to attach various molecules on the CNT surface; most methods require extremely reactive reaction media and harsh reaction conditions.

Acid functionalization of CNT provides an alternative as a recently investigated method. Acid functionalization of CNT surface provides many advantages over other methods. Carboxylic acid groups on CNT (CNT-COOH) (i) increase solubility and dispersion in polar solvents such as water and ethanol; (ii) improve dispersion of CNT in polymers matrices; and (iii) introduces the ability to functionalize CNT further with thionyl chloride and long-chain amines.[93,101,106,107,110,111] Several procedures exist to attach carboxylic acid on CNT surface. Some of these methods include reacting CNT with organic acyl peroxides of dicarboxylic acids,[106] acid treatment of CNT followed by sonication and agitation,[101] growing –COOH bearing amino acid groups on fluorinated CNT,[107] and HCl treatment during the purification of CNT.[111] Several studies investigated solubility and dispersion of CNT-COOH in water and in organic solvents such as toluene, chloroform, dichloromethane, and benzene. The studies

revealed that acid functionalization greatly improves the solubility and dispersion of CNT in different organic solvents. Lin *et al*.[101] investigated the change in the dispersion of CNT in water and in toluene. **Figure 1.7** illustrates their findings on the effect of surface functionalization on dispersion in water and toluene. CNT exhibited a phase selective behavior between toluene and water depending on the nature of surface groups.

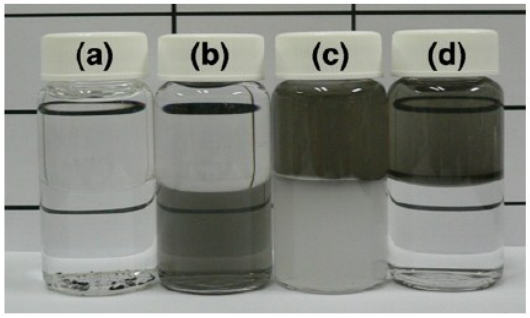

Figure 1.7. Comparative solubility of the modified MWCNT-amides in toluene (top)/water(bottom) phases: (a)MWNT, (b) MWNT-COOH, (c) MWNT-amine I, (d) MWNT-amine II.[101]

Several efforts concentrated on investigating CNT-polymer composites. Zhu *et al.*[77] investigated the dispersion of acid-functionalized SWCNT in epoxy matrices. Zhu and co-workers prepared fluorinated SWCNT from acid-functionalized SWCNT. They dispersed functionalized SWCNT in DMF and in epoxy matrix (prior to curing) via sonication. This study suggested that due to the presence of acid groups and the dispersion of SWCNT in DMF significantly improved. ATR-IR and RAMAN spectroscopy confirmed the presence of COOH on SWCNT surface. As shown in **Figure 1.8**, optical micrographs of non-functionalized SWCNT in DMF showed large aggregates (average aggregate size 3 μm size by light scattering) but fluorinated SWCNT-COOH in DMF showed no signs of aggregation (average aggregate size 300 nm by light scattering).

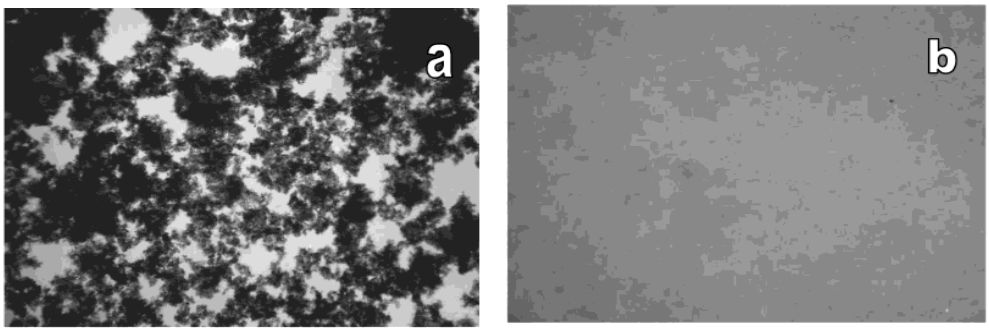

Figure 1.8. Optical microscopy of the nanotube dispersions (2 mg/mL) in DMF:
(a) Neat SWNT (b) F-SWNT-COOH.[77]

Zhu[77] indicated that they homogenously dispersed SWCNT-COOH in epoxy composites. SEM images of fracture surfaces below (**Figure 1.9**) have two-micron scale bars. The authors claimed that they measured the average size of F-SWNT-COOH aggregates as 300 nm. SEM images in **Figure 1.9** F-SWCNT-COOH show homogeneous dispersion compared to SWCNT in polymer matrix.

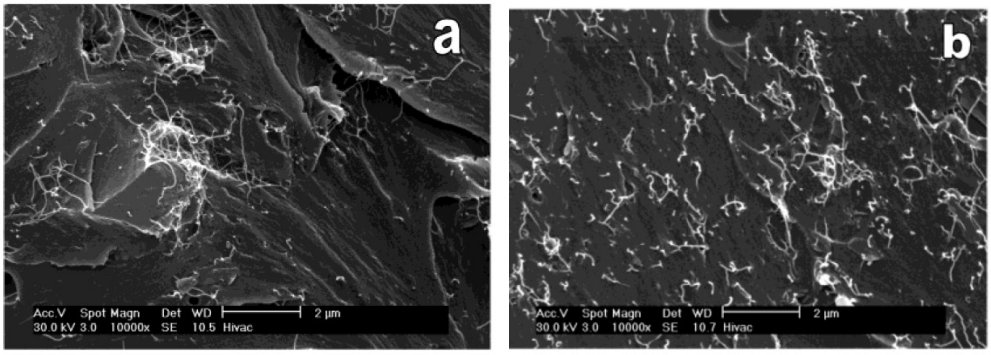

Figure 1.9. SEM images of fracture surfaces of 1 wt % nanotube/epoxy composites
(a) SWNT in epoxy matrix (b) F-SWNT-COOH nanotube in epoxy matrix.[77]

^{13}C NMR, ATR-FTIR, and RAMAN spectroscopy confirmed these results. Peng and co-workers[106] claimed that surface functionalization improved solubility and thus improved dispersion of SWCNT in polymer matrix.These results show modification of CNT significantly improve the dispersion of nanoparticles within the polymer matrix.

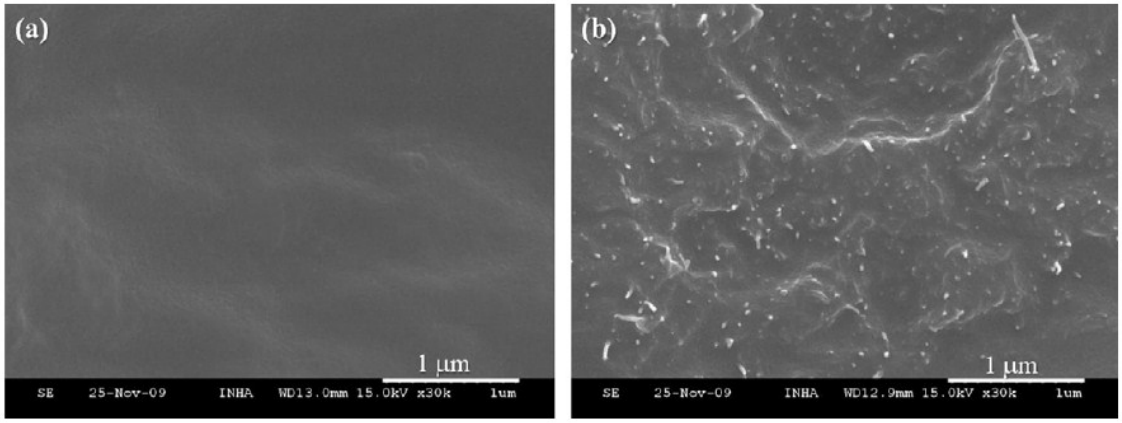

Figure 1.10. SEM images of fracture surfaces of 1 wt % nanotube/epoxy composites (a) SWNT in epoxy matrix. (b) F-SWNT-COOH nanotube in epoxy matrix.[77]

SEM images in **Figure 1.10** show that PEG-modified MWCNT dispersed well in PU matrix. Lee *et al.*[112] covalently modified MWCNT with PEG. They reacted the –OH groups on the surface of PEG modified MWCNT with the –NCO groups of methylene diphenyl diisocyanate (MDI). Therefore, they obtained the polyurethane/MWCNT composite film by means of condensation polymerization and solution casting

1.5 Potential Applications of Polyurethane CNT Nanocomposites

Fabrication of conducting polymer composites requires polymer matrix and fillers with good mechanical properties, processability, and high conductivity. In recent years, studies concentrated around the new potential applications of conductive carbon nanotube-polyurethanes. Potential applications discussed in the literature vary from biomedical applications, [113] actuators, [114] microelectronics, and microsensors,[115] electrical dissipative and conductive composites.[116]

Williams *et al.*[113] targeted to produce neural interfacing electrode implants. Williams and co-workers aimed to prepare a conductive elastomeric polymer electrode. To achieve the properties the application required, the authors manufactured polymer electrode from commercial biocompatible polyurethane (PU)-based elastomer and SWCNT. The cytotoxicity studies indicated that those PU-SWCNT composites have low cell inhibition percentages and they did not exhibit cytotoxic behavior. **Figure 1.11** present the conductivity measurements of composites over containing 5 wt. % of SWCNT reached desired conductivity values. Williams and co-workers stated that although nanotubes significantly improved the electrical conductivity properties of composites compared to polyurethanes composite matrix, high-loading percentages presents a challenge.

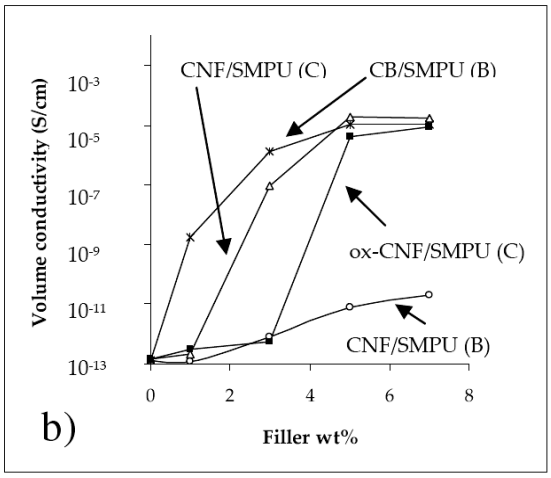

Figure 1.11. Electrical percolation in PU composites.[117]

CNT-containing polyurethane composites have potential application as actuators. Paik and collegues[114] studied the fabrication of conducting shape memory polyurethane actuators. They synthesized PU based on polycaprolactone diol (PCL), MDI, and 1,4-butanediol. Researchers incorporated MWCNT into polyurethane matrix during the prepolymer step. Paik reported PU composites with varying CNT filler and hard segment contents. Actuation

performance tests showed that the presence of CNT in PU matrix reduced the resistivity of the PU matrix. They also reported that resistivity has increased under strain (**Figure 1.12**). They attributed this result to increasing distance between MWCNT fragments present in the surface.

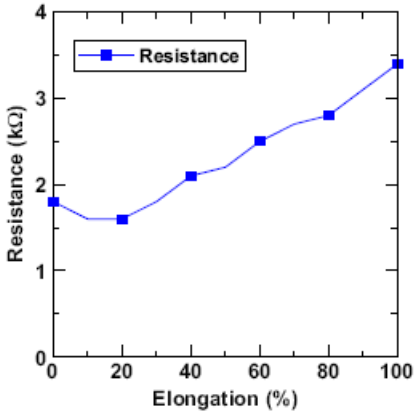

Figure 1.12. Resistance vs. elongation of composites.[114]

Zhao *et al.*[118] synthesized PU-MWCNT nanocomposites for specific aerospace coating applications. In this study, the carboxylic acid groups on the surface of acid-treated multiwalled carbon nanotubes (MWNTs) were converted to acid chloride groups, followed by reaction with para-phenylenediamine (PPD). PPD-modified MWNTs were used as initiator to start the polymerization reaction in the prepolymer of PU that resulted in a homogeneous dispersion of MWNTs in the PU matrix with strong interfacial adhesion. The authors suggested that electrostatic dissipation (ESD) is important due to exposure of the aerospace coatings to the charged environments. They showed that the DC electrical resistivity of MWNT/PU composite films (**Figure 1.13**) compared with pure PU film decreased from 10^{13} Ω cm for the pristine PU to the order of 10^{8} Ω cm for the 0.5 wt.-% MWNTs and to the order of 10^{7} Ω cm for the 3.0 wt.-% MWNTs composites. They also reported that these results were within the required ESD limits.

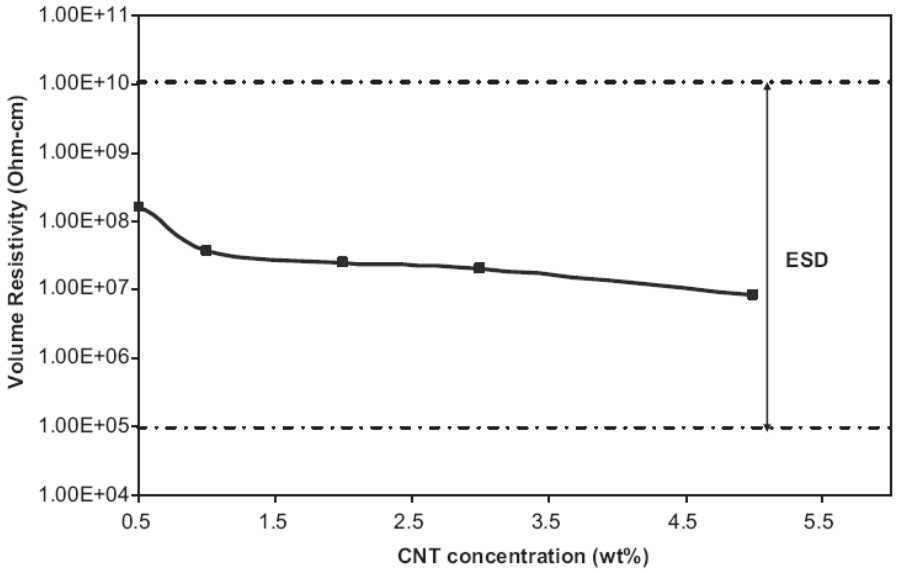

Figure 1.13. Volume resistivity as a function of MWNT concentration in MWNT/PU composites.

Zhao *et al.*[118] showed rapidity of the heat propagation improved with incorporation of MWCNT in the polymer matrix. **Figure 1.14** show at 1.0 wt.-% of carbon nanotube loading, the thermal diffusivity of composite film was improved by 24% compared to pure PU film.

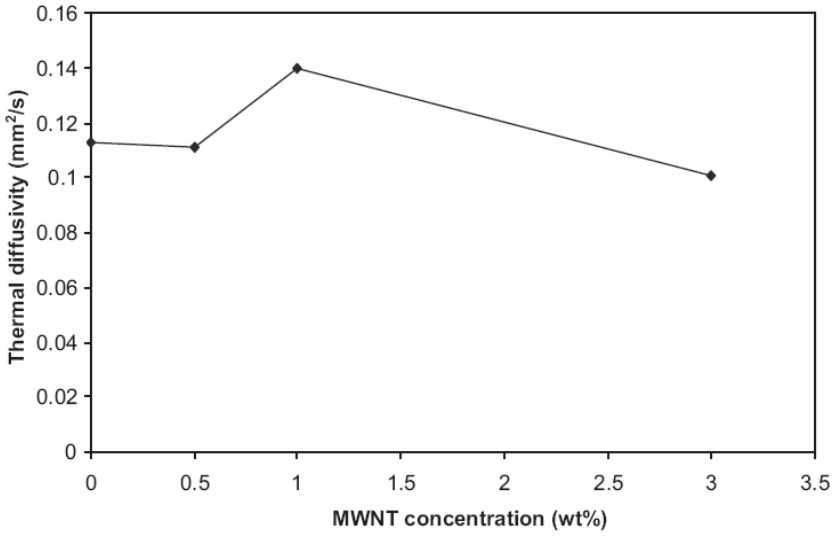

Figure 1.14. Thermal diffusivity of MWNT/PU films with different MWNT content at ambient temperature.

Blizniyuk *et al.*[115] studied the electrical dissipative and conductive properties of CNT-PU composites. Results indicated that CNT-PU composites had either electrically dissipative or conductive properties. The results indicated electrical conductivity of composites depended upon an excellent dispersability. Resistivity studies showed resistivity decreased significantly (from 10^{12} Ohm/cm to 10^{3} Ohm/cm) over two weight percent MWCNT content. Blizniyuk suggested the conductivity of material changes with the depth from the composite surface. Although Blizniyuk and co-workers confronted the conductivity changes depending on the depth, control of conductive nanotube distribution within the thickness of phase-segregated polymer film may present a solution to the preparation conductive nanocomposites. Ultimately, conductive polymer composites have promising applications such as molecular electronic devices and micro sensors.

1.6 Conclusions

This chapter briefly described the synthesis and structure property relationships of polyurethanes. Moreover, it consists of the synthetic strategies to prepare polyurethane networks, and their structure-property relationships. The chemical structure, functionality, molecular weight of oligomers, molecular weight between crosslinks points, and hydrogen bonding determines the thermal and mechanical properties of networks. This section also discusses the preparation of nanocomposites in particular carbon nanotube composites and their potential applications. Treatment of nanoparticles to yield homogeneous dispersion within the polymer matrix is of crucial importance to achieve ultimate composite properties. Carbon nanotubes improve a range of polymer properties which can be exploited for many applications ranging from biomedical applications, to actuators, microsensors, and aerospace coatings.

1.7 References

(1) Silver, J. H.; Karayianni, E.; Cooper, S. L. *Journal of Colloid and Interface Science* **1996**, *178*, 219.
(2) Tsui, Y. K.; Gogolewski, S. *Journal of Materials Science: Materials in Medicine* **2009**, *20*, 1729.
(3) Ciardelli, G.; Rechichi, A.; Cerrai, P.; Tricoli, M.; Barbani, N.; Giusti, P. *Macromolecular Symposia* **2004**, *218*, 261.
(4) Grenier, S.; Sandig, M.; Mequanint, K. *Journal of Biomedical Materials Research, Part A* **2007**, *82A*, 802.
(5) Lim, H.-O.; Bark, G.-M.; Jo, N.-J. *Proceedings of SPIE* **2007**, *6423*, 64234F/1.
(6) Das, S.; Cox, D. F.; Wilkes, G. L.; Klinedinst, D. B.; Yilgor, I.; Yilgor, E.; Beyer, F. L. *Journal of Macromolecular Science, Part B: Physics* **2007**, *46*, 853.
(7) Yilgor, I.; Yilgor, E. *Polymer Reviews (Philadelphia, PA, United States)* **2007**, *47*, 487.
(8) Chattopadhyay, D. K.; Sreedhar, B.; Raju, K. V. S. N. *Industrial & Engineering Chemistry Research* **2005**, *44*, 1772.
(9) Gong, C. Y.; Fu, S. Z.; Gu, Y. C.; Liu, C. B.; Kan, B.; Deng, H. X.; Luo, F.; Qian, Z. Y. *Journal of Applied Polymer Science* **2009**, *113*, 1111.
(10) Ioan, S.; Lupu, M.; Epure, V.; Ioanid, A.; Macocinschi, D. *Journal of Applied Polymer Science* **2008**, *107*, 1414.
(11) Kojio, K.; Mitsui, Y.; Furukawa, M. *Polymer* **2009**, *50*, 3693.
(12) Simonovsky, F. I.; Porter, S. C.; Ratner, B. D. *Journal of Biomaterials Science, Polymer Edition* **2005**, *16*, 267.
(13) Tsai, H.-C.; Hong, P.-D.; Yen, M.-S. *Journal of Applied Polymer Science* **2008**, *108*, 2266.
(14) Yilgor, I.; Yilgor, E.; Guclu Guler, I.; Ward, T. C.; Wilkes, G. L. *Polymer* **2006**, *47*, 4105.
(15) Hernandez, R.; Weksler, J.; Padsalgikar, A.; Choi, T.; Angelo, E.; Lin, J. S.; Xu, L.-C.; Siedlecki, C. A.; Runt, J. *Macromolecules (Washington, DC, United States)* **2008**, *41*, 9767.
(16) Lomax, G. R. *Journal of Materials Chemistry* **2007**, *17*, 2775.
(17) Chen, K.-S.; Yu, T. L.; Chen, Y.-S.; Lin, T.-L.; Liu, W.-J. *Journal of Polymer Research* **2001**, *8*, 99.
(18) Peng, P.; Wang, W.; Chen, X.; Jing, X. *Biomacromolecules* **2005**, *6*, 587.
(19) Zhu, Y.; Hu, J.; Choi, K.-F.; Yeung, K.-W.; Meng, Q.; Chen, S. *Journal of Applied Polymer Science* **2008**, *107*, 599.
(20) Yen, M.-S.; Kuo, S.-C. *Journal of Applied Polymer Science* **1996**, *61*, 1639.
(21) Yen, M.-S.; Kuo, S.-C. *Journal of Polymer Research* **1998**, *5*, 125.
(22) Caracciolo, P. C.; Buffa, F.; Abraham, G. A. *Journal of Materials Science: Materials in Medicine* **2009**, *20*, 145.
(23) Pierce, B. F.; Brown, A. H.; Sheares, V. V. *Macromolecules (Washington, DC, United States)* **2008**, *41*, 3866.
(24) Harris, R. F.; Joseph, M. D.; Davidson, C.; Deporter, C. D.; Dais, V. A. *Journal of Applied Polymer Science* **1990**, *41*, 509.
(25) Harris, R. F.; Joseph, M. D.; Davidson, C.; Deporter, C. D.; Dais, V. A. *Journal of Applied Polymer Science* **1990**, *41*, 487.

(26) Furukawa, M. *Journal of Applied Polymer Science: Applied Polymer Symposium* **1994**, *53*, 61.
(27) Gunatillake, P. A.; Meijs, G. F.; McCarthy, S. J.; Adhikari, R.; Sherriff, N. *Journal of Applied Polymer Science* **1998**, *69*, 1621.
(28) Christenson, E. M.; Anderson, J. M.; Hiltner, A. *Journal of Biomedical Materials Research, Part A* **2004**, *70A*, 245.
(29) Kojio, K.; Nonaka, Y.; Masubuchi, T.; Furukawa, M. *Journal of Polymer Science, Part B: Polymer Physics* **2004**, *42*, 4448.
(30) Wiggins, M. J.; MacEwan, M.; Anderson, J. M.; Hiltner, A. *Journal of Biomedical Materials Research, Part A* **2004**, *68A*, 668.
(31) Eceiza, A.; Martin, M. D.; de la Caba, K.; Kortaberria, G.; Gabilondo, N.; Corcuera, M. A.; Mondragon, I. *Polymer Engineering and Science* **2008**, *48*, 297.
(32) Lee, D.-K.; Tsai, H.-B.; Tsai, R.-S.; Chen, P. H. *Polymer Engineering and Science* **2007**, *47*, 695.
(33) Tanaka, H.; Kunimura, M. *Polymer Engineering and Science* **2002**, *42*, 1333.
(34) Choi, T.; Weksler, J.; Padsalgikar, A.; Runt, J. *Polymer* **2009**, *50*, 2320.
(35) Lin, Y.-H.; Chou, N.-K.; Chen, K.-F.; Ho, G.-H.; Chang, C.-H.; Wang, S.-S.; Chu, S.-H.; Hsieh, K.-H. *Polymer International* **2007**, *56*, 1415.
(36) Yen, M.-S.; Tsai, P.-Y.; Hong, P.-D. *Colloids and Surfaces, A: Physicochemical and Engineering Aspects* **2006**, *279*, 1.
(37) Choi, T.; Weksler, J.; Padsalgikar, A.; Hernandez, R.; Runt, J. *Australian Journal of Chemistry* **2009**, *62*, 794.
(38) Williams, S. R.; Wang, W.; Winey, K. I.; Long, T. E. *Macromolecules (Washington, DC, United States)* **2008**, *41*, 9072.
(39) Crawford, D. M.; Escarsega, J. A. *Thermochimica Acta* **2000**, *357-358*, 161.
(40) Lawson, G.; Bartram, S.; Fitchner, S.; Woodland, E. D. *Analyst (Cambridge, United Kingdom)* **2000**, *125*, 115.
(41) Cho, Y. B.; Jeong, H. M.; Kim, B. K. *Macromolecular Research* **2009**, *17*, 879.
(42) Abraham, G. A.; de Queiroz, A. A. A.; Roman, J. S. *Biomaterials* **2001**, *22*, 1971.
(43) Karabanova, L. V.; Lloyd, A. W.; Mikhalovsky, S. V.; Helias, M.; Phillips, G. J.; Rose, S. F.; Mikhalovska, L.; Boiteux, G.; Sergeeva, L. M.; Lutsyk, E. D.; Svyatyna, A. *Journal of materials science. Materials in medicine* **2006**, *17*, 1283.
(44) Jaffrennou, B.; Droger, N.; Mechin, F.; Halary, J.-L.; Pascault, J.-P. *e-Polymers* **2005**, No pp given.
(45) Bruin, P.; Meeuwsen, E. A.; van Andel, M. V.; Worst, J. G.; Pennings, A. J. *Biomaterials* **1993**, *14*, 1089.
(46) Figovsky, O. L.; Sklyarsky, L. S.; Sklyarsky, O. N. *Journal of Adhesion Science and Technology* **2000**, *14*, 915.
(47) Okrasa, L.; Czech, P.; Boiteux, G.; Mechin, F.; Ulanski, J. *Polymer* **2008**, *49*, 2662.
(48) Unal, S.; Ozturk, G.; Sisson, K.; Long, T. E. *Journal of Polymer Science, Part A: Polymer Chemistry* **2008**, *46*, 6285.
(49) Fornof, A. R.; Glass, T. E.; Long, T. E. *Macromolecular Chemistry and Physics* **2006**, *207*, 1197.
(50) Czech, P.; Okrasa, L.; Boiteux, G.; Mechin, F.; Ulanski, J. *Journal of Non-Crystalline Solids* **2005**, *351*, 2735.

(51) Monteavaro, L. L.; da Silva, E. O.; Costa, A. P. O.; Samios, D.; Gerbase, A. E.; Petzhold, C. L. *Journal of the American Oil Chemists' Society* **2005**, *82*, 365.
(52) Czech, P.; Okrasa, L.; Ulanski, J.; Boiteux, G.; Mechin, F.; Cassagnau, P. *Journal of Applied Polymer Science* **2007**, *105*, 89.
(53) Williams, S. R.; Mather, B. D.; Miller, K. M.; Long, T. E. *Journal of Polymer Science, Part A: Polymer Chemistry* **2007**, *45*, 4118.
(54) Williams, S. R.; Mather, B. D.; Miller, K. M.; Long, T. E. *Polymer Preprints (American Chemical Society, Division of Polymer Chemistry)* **2007**, *48*, 833.
(55) Williams, S. R.; Miller, K. M.; Long, T. E. *Progress in Reaction Kinetics and Mechanism* **2007**, *32*, 165.
(56) Mather, B. D.; Miller, K. M.; Long, T. E. *Macromolecular Chemistry and Physics* **2006**, *207*, 1324.
(57) Mather, B. D.; Williams, S. R.; Long, T. E. *Macromolecular Chemistry and Physics* **2007**, *208*, 1949.
(58) Ozturk, G.; Long, T. E. *Journal of Polymer Science, Part A: Polymer Chemistry* **2009**, *47*, 5437.
(59) Kim, B. K.; Lee, K. H.; Kim, H. D. *Journal of Applied Polymer Science* **1996**, *60*, 799.
(60) Ghosh, S.; Krishnamurti, N. *Polymer-Plastics Technology and Engineering* **2001**, *40*, 539.
(61) Srivastava, A.; Agarwal, D.; Mistry, S.; Singh, J. *Pigment & Resin Technology* **2008**, *37*, 217.
(62) Kumari, S.; Mishra, A. K.; Chattopadhyay, D. K.; Raju, K. V. S. N. *Journal of Polymer Science, Part A: Polymer Chemistry* **2007**, *45*, 2673.
(63) Wang, F.; Hu, J. Q.; Tu, W. P. *Progress in Organic Coatings* **2008**, *62*, 245.
(64) Kim, B. K.; Paik, S. H. *Journal of Polymer Science, Part A: Polymer Chemistry* **1999**, *37*, 2703.
(65) Ahn, B. U.; Lee, S. K.; Lee, S. K.; Park, J. H.; Kim, B. K. *Progress in Organic Coatings* **2008**, *62*, 258.
(66) Lin, Y. H.; Liao, K. H.; Chou, N. K.; Wang, S. S.; Chu, S. H.; Hsieh, K. H. *European Polymer Journal* **2008**, *44*, 2927.
(67) LeBaron, P. C.; Wang, Z.; Pinnavaia, T. J. *Applied Clay Science* **1999**, *15*, 11.
(68) Viovy, J.-L.; Weber, J.; Paul, D.; (Institut Curie, Fr.; Centre National de la Recherche Scientifique; Fluigent Paris-Biotech-Faculte de Medecine Cochin Port Royal). Application: US, 2008, p 17pp.
(69) Paul, D. R.; Robeson, L. M. *Polymer* **2008**, *49*, 3187.
(70) Petrovic, Z. S.; Javni, I.; Waddon, A.; Banhegyi, G. *Journal of Applied Polymer Science* **2000**, *76*, 133.
(71) Usuki, A.; Kojima, Y.; Kawasumi, M.; Okada, A.; Fukushima, Y.; Kurauchi, T.; Kamigaito, O. *Journal of Materials Research* **1993**, *8*, 1179.
(72) Wang, Z.; Pinnavaia, T. J. *Chemistry of Materials* **1998**, *10*, 3769.
(73) Chang, J.-H.; An, Y. U. *Journal of Polymer Science, Part B: Polymer Physics* **2002**, *40*, 670.
(74) Finnigan, B.; Halley, P.; Jack, K.; McDowell, A.; Truss, R.; Casey, P.; Knott, R.; Martin, D. *Journal of Applied Polymer Science* **2006**, *102*, 128.
(75) Iijima, S. *Nature (London, United Kingdom)* **1991**, *354*, 56.
(76) Iijima, S.; Ichihashi, T. *Nature (London, United Kingdom)* **1993**, *363*, 603.

(77) Zhu, J.; Kim, J.; Peng, H.; Margrave, J. L.; Khabashesku, V. N.; Barrera, E. V. *Nano Letters* **2003**, *3*, 1107.
(78) Biercuk, M. J.; Llaguno, M. C.; Radosavljevic, M.; Hyun, J. K.; Johnson, A. T.; Fischer, J. E. *Applied Physics Letters* **2002**, *80*, 2767.
(79) Coleman, J. N.; Dalton, A. B.; Curran, S.; Rubio, A.; Davey, A. P.; Drury, A.; McCarthy, B.; Lahr, B.; Ajayan, P. M.; Roth, S.; Barklie, R. C.; Blau, W. J. *Advanced Materials (Weinheim, Germany)* **2000**, *12*, 213.
(80) Ajayan, P. M.; Schadler, L. S.; Giannaris, C.; Rubio, A. *Advanced Materials (Weinheim, Germany)* **2000**, *12*, 750.
(81) Cao, S.-z.; Sun, X.-g.; Zeng, X.-s. *Jixie Gongcheng Cailiao* **2008**, *32*, 50.
(82) Andrews, R.; Jacques, D.; Minot, M.; Rantell, T. *Macromolecular Materials and Engineering* **2002**, *287*, 395.
(83) Chen, G.-X.; Shimizu, H. *PMSE Preprints* **2007**, *96*, 685.
(84) Obrzut, J.; Douglas, J. F.; Kharchenko, S. B.; Migler, K. B. *Physical Review B: Condensed Matter and Materials Physics* **2007**, *76*, 195420/1.
(85) Chen, G.-X.; Li, Y.; Shimizu, H. *Carbon* **2007**, *45*, 2334.
(86) Masuda, J. i.; Torkelson, J. M. *Macromolecules (Washington, DC, United States)* **2008**, *41*, 5974.
(87) Broza, G.; Schulte, K. *Polymer Engineering and Science* **2008**, *48*, 2033.
(88) Poetschke, P.; Bhattacharyya, A. R.; Abdel-Goad, M.; Janke, A.; Goering, H. *ACS Symposium Series* **2005**, *898*, 164.
(89) Pujari, S.; Ramanathan, T.; Kasimatis, K.; Masuda, J. i.; Andrews, R.; Torkelson, J. M.; Brinson, L. C.; Burghardt, W. R. *Journal of Polymer Science, Part B: Polymer Physics* **2009**, *47*, 1426.
(90) Manchado, M. A. L.; Valentini, L.; Biagiotti, J.; Kenny, J. M. *Carbon* **2005**, *43*, 1499.
(91) Zhang, J. X.; Zheng, Y. P.; Yu, P. Y.; Mo, S.; Wang, R. M. *Carbon* **2009**, *47*, 2776.
(92) Gotovac, S.; Yang, C.-M.; Hattori, Y.; Takahashi, K.; Kanoh, H.; Kaneko, K. *Journal of Colloid and Interface Science* **2007**, *314*, 18.
(93) Balasubramanian, K.; Burghard, M. *Small* **2005**, *1*, 180.
(94) Titus, E.; Ali, N.; Cabral, G.; Gracio, J.; Babu, P. R.; Jackson, M. J. *Journal of Materials Engineering and Performance* **2006**, *15*, 182.
(95) Liang, F.; Sadana, A. K.; Peera, A.; Chattopadhyay, J.; Gu, Z.; Hauge, R. H.; Billups, W. E. *Nano Letters* **2004**, *4*, 1257.
(96) Dyke, C. A.; Tour, J. M. *Journal of Physical Chemistry A* **2004**, *108*, 11151.
(97) Agrawal, S.; Raghuveer, M. S.; Kroger, R.; Ramanath, G. *Journal of Applied Physics* **2006**, *100*, 094314/1.
(98) Bekyarova, E.; Itkis, M. E.; Cabrera, N.; Zhao, B.; Yu, A.; Gao, J.; Haddon, R. C. *Journal of the American Chemical Society* **2005**, *127*, 5990.
(99) Wang, C.; Cao, Q.; Ozel, T.; Gaur, A.; Rogers, J. A.; Shim, M. *Journal of the American Chemical Society* **2005**, *127*, 11460.
(100) Tobias, G.; Shao, L. D.; Ballesteros, B.; Green, M. L. H. In *2nd ChemOnTubes International Conference* Zaragoza, SPAIN, 2008; Vol. 9, p 6072.
(101) Lin, S.-T.; Wei, K.-L.; Lee, T.-M.; Chiou, K.-C.; Lin, J.-J. *Nanotechnology* **2006**, *17*, 3197.
(102) Xia, W.; Jin, C.; Kundu, S.; Muhler, M. *Carbon* **2009**, *47*, 919.

(103) Yu, H.; Jin, Y.; Peng, F.; Wang, H.; Yang, J. *Journal of Physical Chemistry C* **2008**, *112*, 6758.
(104) de Heer, W. A. *MRS Bulletin* **2004**, *29*, 281.
(105) Escobar, M.; Goyanes, S.; Corcuera, M. A.; Eceiza, A.; Mondragon, I.; Rubiolo, G. H.; Candal, R. J. In *2nd ChemOnTubes International Conference* Zaragoza, SPAIN, 2008; Vol. 9, p 6228.
(106) Peng, H.; Alemany, L. B.; Margrave, J. L.; Khabashesku, V. N. *Journal of the American Chemical Society* **2003**, *125*, 15174.
(107) Zeng, L.; Zhang, L.; Barron, A. R. *Nano Letters* **2005**, *5*, 2001.
(108) Long, B.; Wu, T. M.; Stellacci, F. *Chemical Communications (Cambridge, United Kingdom)* **2008**, 2788.
(109) Geng, H.; Rosen, R.; Zheng, B.; Shimoda, H.; Fleming, L.; Liu, J.; Zhou, O. *Advanced Materials (Weinheim, Germany)* **2002**, *14*, 1387.
(110) Zhang, L.; Kiny, V. U.; Peng, H.; Zhu, J.; Lobo, R. F. M.; Margrave, J. L.; Khabashesku, V. N. *Chemistry of Materials* **2004**, *16*, 2055.
(111) Jian Chen, M. A. H., Hui Hu, Yongsheng Chen,; Apparao M. Rao, P. C. E., Robert C. Haddon **1998**, *282*, 95.
(112) Lee, J.; Park, E. J.; Choi, J.; Hong, J.; Shim, S. E. *Synthetic Metals* **2010**, *160*, 566.
(113) Williams, C. M.; Nash, M. A.; Poole-Warren, L. A. *Proceedings of SPIE-The International Society for Optical Engineering* **2005**, *5651*, 329.
(114) Paik, I. H.; Goo, N. S.; Jung, Y. C.; Cho, J. W. *Smart Materials and Structures* **2006**, *15*, 1476.
(115) Bliznyuk, V.; Singamaneni, S.; Kattumenu, R.; Atashbar, M. *Applied Physics Letters* **2006**, *88*, 164101/1.
(116) Poetschke, P.; Haeussler, L.; Pegel, S.; Steinberger, R.; Scholz, G. *KGK, Kautschuk Gummi Kunststoffe* **2007**, *60*, 432.
(117) Gunes, I. S.; Jimenez, G. A.; Jana, S. C. *Materials Research Society Symposium Proceedings* **2008**, *1129*, No pp given.
(118) Zhao, W.; Li, M.; Peng, H.-X. *Macromolecular Materials and Engineering* **2010**, *295*, 838.
(119) Klinedinst, D. B.; Yilgor, E.; Yilgor, I.; Beyer, F. L.; Sheth, J. P.; Wilkes, G. L. *Rubber Chemistry and Technology* **2005**, *78*, 737.
(120) Chang, C.-C.; Chen, K.-S.; Yu, T. L.; Chen, Y.-S.; Tsai, C.-L.; Tseng, Y.-H. *Polymer Journal (Tokyo)* **1999**, *31*, 1205.
(121) Sheth, J. P.; Klinedinst, D. B.; Wilkes, G. L.; Yilgor, I.; Yilgor, E. *Polymer* **2005**, *46*, 7317.
(122) Chattopadhyay, D. K.; Raju, K. V. S. N. *Progress in Polymer Science* **2007**, *32*, 352.
(123) Clemens, R. J.; Del Rector, F. *Journal of Coatings Technology* **1989**, *61*, 83.
(124) Kilambi, H.; Stansbury, J. W.; Bowman, C. N. *Journal of Polymer Science, Part A: Polymer Chemistry* **2008**, *46*, 3452.
(125) Yamauchi, K.; Lizotte, J. R.; Long, T. E. *Macromolecules* **2002**, *35*, 8745.
(126) Coca, S.; Jasieczek, C. B.; Beers, K. L.; Matyjaszewski, K. *Journal of Polymer Science, Part A: Polymer Chemistry* **1998**, *36*, 1417.
(127) Lee, H.-J.; Oh, S.-J.; Choi, J.-Y.; Kim, J. W.; Han, J.; Tan, L.-S.; Baek, J.-B. *Chemistry of Materials* **2005**, *17*, 5057.

(128) Chen, G.-X.; Kim, H.-S.; Park, B. H.; Yoon, J.-S. *Journal of Physical Chemistry B* **2005**, *109*, 22237.

Chapter 2. Structure-Property Relationships of Segmented Poly (tetramethylene oxide)-Based Ester, Urethane, and Urea Networks with Michael Addition

2.1 Abstract

Poly (tetramethylene oxide) (PTMO)-based ether precursors (EtDA) were synthesized using the reaction of acryloyl chloride with α,ω-hydroxy-terminated PTMOs (M_n 1000 and 2000 g/mol**)**. PTMO-urethane diacrylates (UtDA) were synthesized from a two-step reaction of bis (4-isocyanatocyclohexyl) methane (HMDI) with α,ω-hydroxy-terminated PTMO (M_n 250, 1000, 2000 and 2900 g/mol**)** and 2-hydroxyethyl acrylate (HEA). PTMO-urea diacrylates were synthesized from the reaction of HMDI with 1100 g/mol α,ω-aminopropyl-terminated polyol (or 4,9-dioxa-1,12dodacanediamine**)** and 2-hydroxyethyl acrylate in two consecutive steps. A 2:1 stoichiometric imbalance between HMDI and PTMO respectively ensured end-capping of PTMO polyols. Two bis acetoacetates (BisAcAc) were synthesized from acetoacetylation of 1,4-butanediol and 250 g/mol hydroxy-terminated PTMO with tert-butyl acetoacetate. Titration studies confirmed the difunctionality of the –NCO capped precursors to urethane- and urea-diacrylates. ^{1}H NMR spectroscopy confirmed structure and molecular weight of all diacrylates. *In situ* FTIR spectroscopy determined the reaction conditions. The rheological properties revealed the viscosity and activation energies for flow of the diacrylates. Michael reaction between diacrylates and BisAcAc yielded covalently crosslinked networks resulting in gel fractions better than 90 %. DSC and DMA experiments exhibited a broad distribution of T_g's depending on the M_n and type of hydrogen-bonding (urethane or urea) present in the diacrylate networks. The network T_g's vary from -61 ºC to 63 ºC depending on the crosslinking density and hydrogen-bonding segment content. TGA revealed that UtDA and UrDA networks have an improved thermal stability compared to EtDA networks. Tensile properties showed a broad variation depending on the presence urethane or urea hydrogen-bonding and M_n of diacrylates

and BisAcAc. The increasing M_n of the urethane diacrylate precursor resulted in a drop in the storage moduli of networks from 25.3 MPa to 2.0 MPa. Elongation at break increased from 255 % to 755 % for the same networks which we attributed to increasing hydrogen-bonding segment content of diacrylates. The Young's moduli increased from 3.27 MPa for EtDA 2000 to 311.1 MPa for UrDA 2000 due to presence of urethane and urea hydrogen-bonding in the networks.

Keywords: crosslinking, hydrogen bond, mechanical properties, Michael addition, thermal properties

2.2 Introduction

Polyurethanes (PURs) and polyureas (PUs) represent a commercially important segment of polymers. They exhibit properties ranging from soft elastomers to rigid thermoplastics depending on the chemical composition, backbone structure, and morphology. Most have high elongations, moduli, strength, and good processability[6,119,120] which makes them useful for a diverse range of emerging applications including membranes,[1] actuators,[5] and biomaterials.[15,16,60,62,121,122] PURs and PUs can incorporate covalent and/or physical crosslinks. Physical networks originate from inter- and intra-molecular hydrogen bonding or the electrostatic interaction of charged species in the polymer; [11,22,31,38] whereas, monomers with a functionality greater than two yield covalent networks.

Michael addition represents a versatile method for synthesizing networks utilizing mild reaction conditions, high functional group tolerance, and absence of by-products[53-57]. Covalently crosslinked networks of telechelic acrylates with bis/tris-acetoacetates through Michael addition resulted in polymers with good mechanical strength.[53,54] Furthermore, chemical structure, functionality, molecular weight of oligomers, molecular weight between crosslinks points, and hydrogen bonding influences the thermal stability and mechanical properties of networks.[53-55] Therefore, Michael addition of telechelic acrylates to bis/tris-acetoacetates offers a reliable alternative to prepare networks with desired properties.

The Michael reaction mechanism consists of three steps. Deprotonation of the β-keto ester with a base catalyst which yields the intermediate known as the Michael donor, is a resonance-stabilized nucleophilic enolate anion. Next, the Michael donor adds to an electrophile such as a β-unsaturated ester known as the Michael acceptor. The Michael acceptor produces a second enolate intermediate, which subsequently reacts with another Michael acceptor. Proton

transfer to the enolate from the reaction media yields the final product.[53] Earlier literature reported[123] the pK values of the hydrogens on the acetoacetate group vary significantly (pK_{a1} ≈12, pK_{a2} ≈ 13); therefore, the reaction rate and the structure of the final product is highly dependent on the strength of the base catalyst. Clemens and Rector[123] demonstrated that amidine and guanidine bases are readily soluble in organic solvents and react in a controlled fashion at ambient temperature; thus they are convenient catalysts for Michael reaction. Kilambi *et.al* [124] synthesized acrylic monomers with carbamate, hydroxyl, or cyano functionalities. The authors established that modifying acrylates with carbamate, hydroxyl, or cyano functionalities improved the reactivity of the adjacent acrylate groups.

Previously our group showed functionalization of hydroxyl-terminated polyols with acetoacetate groups upon esterification of hydroxyl groups with tertiary-butyl acetoacetate.[53-57,125] The readily derivatized polyols with acetoacetate groups are reactive towards acrylates. Crosslinking of the acrylate functionalized polyols facilitate the synthesis of a variety of networks with different chemical compositions and several crosslinking densities, which displayed a wide range of thermo-mechanical properties. Williams *et al*.[53] investigated the influence of hydrogen-bonding on mechanical properties of networks of acrylate-functionalized urethane-based Michael acceptors. This approach consisted of the synthesis of Michael donors from poly(ethylene glycol) (PEG) of various M_n with tertiary-butyl acetoacetate and subsequently crosslinking Michael donors with hydroxy ethyl acrylate-functionalized (urethane) dicyclohexylmethane 4,4'-diisocyanate (HMDI) or (ether) neopentyl glycol diacrylate (NPGDA) with catalytic amounts of 1,8-diazabicycloundec-7-ene (DBU). Williams reported Michael networks with high gel fraction. DMA analysis of networks confirmed polyurethane hydrogen-bond containing networks had higher rubbery plateau storage moduli than ester counterparts,

which confirmed the influence of hydrogen-bonding on the networks' mechanical properties. They also concluded the presence of hydrogen bonding in the networks presented better tensile properties than non-hydrogen bonded counterparts.

In this chapter, we describe a detailed analysis of structure-property relationships of the Michael addition networks as a function of M_n of PTMO oligomers. To compare the influence of nature of hydrogen-bonding segments on thermal and mechanical properties we synthesized PTMO-based telechelic urethane diacrylates, PTMO-based telechelic urea diacrylates, and PTMO-based ester diacrylates with molecular weights ranging from 1000 to 3600 g/mol. 1,4-BD BisAcAc and PTMO 250 BisAcAc were synthesized from 1,4-butanediol and PTMO 250 g/mol to investigate the influence of crosslink density on thermo-mechanical properties of the networks. BisAcAcs reacted with urethane, urea and ester type diacrylates in the presence of DBU at ambient temperature, subsequently forming networks with well-defined networks with uniform molecular weights between crosslink points. The impact of degree of hydrogen bonding on thermal properties of crosslinked systems were investigated using DSC, and rheology. We utilized tensile testing and DMA to analyze the mechanical properties of the crosslinked polymer films, and TGA to explore the thermo-oxidative stability of the networks.

2.3 Experimental

2.3.1 Materials

tert-Butyl acetoacetate (t-BuAcAc, reagent grade, 98%), 1,4-butanediol (1,4-BD, reagent plus, >99%), 1,8-diazobicyclo[5.4.0]undec-7-ene (DBU, 98%), dibutyl tin dilaurate (DBTDL, 95%), 2,6-di-tert-butyl-4-methylphenol (BHT, >99%) acryloyl chloride (99%), triethylamine (98%), magnesium sulfate (reagent plus, anhydrous, 99 %), calcium hydride (reagent grade, >95%) sodium bicarbonate (reagent plus, >99%), and sodium chloride (reagent grade >98%)

were purchased from Sigma-Aldrich and were used as received. 2-hydroxyethyl acrylate (HEA, 96%) was purchased from Aldrich and purified as previously described.[126] Hydroxy-terminated PTMOs (M_n 250, 1000, 2000 and 2900 g/mol) and bis aminopropyl terminated PTMO (M_n 1100 g/mol) were purchased from Sigma-Aldrich, 4,9-dioxa-1,12dodacanediamine (97%) was purchased from Alfa Aesar. They were degassed at 60 °C for ~12 h. Bis (4-isocyanatocyclohexyl) methane (HMDI, >99.5%) was graciously donated by Bayer Material Science. Toluene (Fischer, HPLC grade,) was distilled from magnesium sulfate and stored over activated 4Å molecular sieves immediately prior to use. Chloroform (HPLC grade, Fischer Scientific) was distilled from calcium hydride and stored over 4Å molecular sieves. Anhydrous 2-propanol (>99.5 %) was purchased from Sigma Aldrich and used without further treatment. Dibutyl tin dilaurate (DBTDL, 95%) was dissolved in THF as a 1 wt. % solution. Saturated aqueous solutions of sodium bicarbonate and sodium chloride were prepared. Ultrahigh-purity nitrogen gas was used as inert reaction atmosphere.

2.3.2 Synthesis of PTMO-Ester Michael Acceptors

Freshly distilled $CHCl_3$ (35 mL), PTMO (1100 g/mol by ^1H NMR, 11 g, 10 mmol) and triethylamine (2.23 g, 22 mmol) were introduced into a two-neck, round-bottomed flask equipped with a stir bar, addition funnel and nitrogen inlet. Acryloyl chloride (1.99 g, 22.0 mmol) was dissolved in $CHCl_3$ (10 mL) and charged into an addition funnel. Dropwise addition of acryloyl chloride into the PTMO solution was completed over ~1 h. The reaction was allowed to proceed for 2 h at 0 °C, and then the temperature was raised to ambient temperature and maintained for 1 h. The triethylamine salt was removed by filtration. The reaction mixture was extracted with the saturated aqueous solutions of sodium bicarbonate, sodium chloride and deionized water (3X each). The mixture was dried over $MgSO_4$, filtered, and BHT (50 mg) was

added to prevent polymerization of the product. The resulting viscous liquid was dried at reduced pressure (0.1 mmHg) at room temperature for 24 h to a constant weight. The BisAcAc oligomer structure was confirmed by ^{1}H NMR spectroscopy. ^{1}H NMR (400 MHz, 50 mg/mL, $CDCl_3$) of the EtDA 1000, δ= 1.61 ppm (t, 28H), δ= 3.39 ppm (s, 24H), δ= 4.15 ppm (s, 4H), δ=5.80 ppm (m, 4H), δ=6.09(m, 4H), δ=6.34 ppm (m, 4H).

2.3.3 Synthesis of PTMO-Urethane Michael Acceptors

Freshly distilled toluene (35 mL), HMDI (10.49 g, 40.0 mmol), and DBTDL solution (0.01 mL) were introduced into a two-neck, round-bottomed flask equipped with a stir bar, addition funnel and nitrogen inlet. The PTMO polyol (1100 g/mol by ^{1}H NMR, 22.0 g, 20.0 mmol) was dissolved in toluene (68 mL) and was charged into the addition funnel. Dropwise addition of PTMO into the HMDI solution was completed over ~30 min. The reaction was allowed to proceed at 80 °C for 2 h. The reaction temperature was reduced to 60 °C. HEA (4.70 g, 40.5 mmol) was dissolved in toluene (16 mL), charged into the addition funnel and added dropwise over ~30 min. The reaction proceeded for 3 h at 60 °C after completion of the addition of HEA. BHT (50 mg) was added to prevent polymerization of the product. The solvent was removed in a rotary evaporator. The resulting viscous product was dried at reduced pressure (0.1 mm Hg) at room temperature for 24 h to a constant weight.

^{1}H NMR (400 MHz, 50 mg/mL, *d*-DMSO) of the UtDA 2000, PTMO PROTONS : δ= 1.60 ppm (t, 28H), δ= 3.38 ppm (s, 24H), δ= 3.72 ppm (s, 4H), HMDI PROTONS : δ= 1.08 ppm (m), δ= 1.41 ppm (m), δ= 1.23 ppm (m), HEA PROTONS: δ= 4.32 ppm (m), δ=4.50 ppm (m), δ=5.80 ppm (m, 4H), δ=6.09(m, 4H), δ=6.34 ppm (m, 4H).

2.3.4 Synthesis of PTMO–Urea Michael Acceptors

HMDI (10.49 g, 40.0 mmol) was dissolved in freshly distilled toluene (35 mL), and the solution was introduced into a two-neck, round-bottomed flask equipped with a stir bar, addition funnel and nitrogen inlet. Bis aminopropyl-terminated PTMO (1150 g/mol by ^{1}H NMR, 23.0 g, 20.0 mmol) was dissolved in toluene (68 mL) and was charged into the addition funnel. Dropwise addition of bis amino propyl-PTMO solution into the HMDI solution was completed over ~30 min. The reaction was allowed to proceed for 2 h at ambient temperature. The reaction temperature was raised to 60 °C. HEA (4.70 g, 40.5 mmol) was dissolved in toluene (16 mL), charged into the addition funnel and added dropwise over ~30 min. The reaction proceeded for 3 h at 60 °C after completion of the addition of HEA. BHT (50 mg) was added to prevent polymerization of the product. The solvent was removed in a rotary evaporator. The resulting viscous liquid was dried at reduced pressure (0.1 mm Hg) at room temperature for 24 h to a constant weight.

^{1}H NMR (400 MHz, 50 mg/mL, *d*-DMSO) of the UrDA 2000, PTMO PROTONS : δ= 1.60 ppm (t, 30H), δ= 3.38 ppm (s, 26H), δ= 3.72 ppm (s, 4H), propyl PTMO END-GROUP PROTONS δ= 4.03 ppm, δ= 4.32 ppm, δ= 5.32 ppm ,HMDI PROTONS : δ= 1.08 ppm (m), δ= 1.41 ppm (m), δ= 1.23 ppm (m), HEA PROTONS: δ= 4.32 ppm (m), δ=4.50 ppm (m), δ=5.80 ppm (m, 4H), δ=6.09(m, 4H), δ=6.34 ppm (m, 4H).

2.3.5 Synthesis of 1, 4-Butanediol and PTMO-Based Michael Donors

PTMO BisAcAc and 1,4-BD BisAcAc were prepared from 1,4-butanediol and the PTMO 250 g/mol polyol respectively. These acetoacetates were prepared using the acetoacetylation method described previously in the literature. [53-55,58] Briefly, PTMO polyol and t-BuAcAc (1:4 mol eq.) were dissolved in toluene (30 wt. % solution) and solution was charged to a flask

equipped with a short-path distillation head, receiving flask, and magnetic stirrer. The mixture was maintained at 110 °C for 3 h under mild vacuum (100 mmHg) to remove the tert-butanol by-product and excess t-BuAcAc. An additional 2 mol eq. of t-BuAcAc was added and heating continued for another 3 h at 110 °C. Finally high vacuum (0.1 mmHg) at 110 °C were applied to remove volatile starting reagents, solvent and reaction by products. The BisAcAc oligomer structure was confirmed by ^{1}H NMR spectroscopy. ^{1}H NMR (400 MHz, 50 mg/mL, $CDCl_3$) of the 1,4-BD BisAcAc, δ= 1.49 ppm(t, 4H), δ= 2.26 ppm (s, 6H), δ= 3.4 ppm (s, 4H), δ=4.14 ppm (m,4H), δ=4.90 ppm (s, -enol C=CH-C=O).

2.3.6 Network Formation

1,4-BD BisAcAc (2.26 g, 0.875 mmol), UtDA 1000 (2.260 g, 1.23 mmol, 1.4 mol eq.) and IPA (1 mL) were mixed thoroughly to form a clear, homogeneous liquid. DBU catalyst was quickly added and mixed thoroughly. The mixture was cast on Mylar® substrate with an adjustable film applicator. Mixtures were allowed to crosslink for 24 h at room temperature. The films were dried at reduced pressure (0.1 mmHg) at 60 °C for 24 h. The same procedure was followed to form urea and ester type networks. IPA was employed to facilitate homogeneous mixing.

2.4 Characterization

^{1}H NMR spectroscopy was utilized to determine PTMO diacrylate and bisAcAc oligomer composition, M_n, and percent functionalization. A 400 MHz Varian Inova NMR spectrometer was used to characterize the oligomers in *d*-DMSO or $CDCl_3$ at 23 °C. *In situ* FTIR analysis was performed on a Metler Toledo React IR 45M instrument with a SiComp fiberoptic ATR probe. An average absorbance was plotted per minute from 256 infrared scans with a 4 cm^{-1} resolution

for 6 h. FTIR analysis was performed on thin films cast on polished KBr discs on a Varian 6700 FTIR spectrometer at ambient temperature in transmittance mode. An average absorbance was plotted from 256 infrared scans with a 4 cm^{-1} resolution. FTIR spectrum of a KBr disc was collected as a background before each scan. Thermogravimetric analysis (TGA) was carried on a TA Instruments Q100 under isothermal conditions at 125 ºC and 175 ºC under an air atmosphere for 5 h to determine the thermal oxidative stabilities of networks. The remaining weight percent was measured. Differential scanning calorimetery (DSC) was conducted on a TA Instruments Q100, under nitrogen at 10 ºC/min heating rate. Isothermal DSC was conducted on a TA Instruments Q100, under nitrogen at 90 °C. Rheology analysis was performed on a TA Instruments AR2000 rheometer with a temperature step (45 °C to 65 °C) and a frequency sweep (1 to 100 Hz) using 20 mm parallel plates geometry. A temperature ramp from (45 to 90 °C) at a constant 1 Hz frequency was also performed on a TA Instruments AR2000 rheometer with the same geometry. Dynamic mechanical analysis (DMA) was conducted on a TA Instruments Q800 Dynamic Mechanical Analyzer in tension mode at a frequency of 1 Hz, an oscillatory amplitude of 15 μm, and a static force of 0.01 N. The temperature ramp was 3 °C/min. The glass transition temperatures were determined at the peak of the tan δ curve. Tensile tests were performed on an Instron 4411 universal testing instrument with a cross-head speed of 20 mm/min using manual grips at ambient temperature. Stress–strain experiments were conducted with rectangular film specimens. The reported data represents an average of at least five specimens. The gel fraction of the networks were characterized using Soxhlet extractions in THF for 6 h and extracted films were subsequently dried in an oven at reduced pressure (0.1 mmHg) at 60 °C for 24 h, until constant weight was observed. The gel fraction was determined gravimetrically, dividing the initial mass (m_i) by the final mass (m_f).

2.5 Results and Discussion

2.5.1 Impact of Crosslinking Density on Thermal Properties and Morphology

Michael carbon addition was adopted to prepare networks of ester, urethane or urea-PTMO precursors. These Michael donors were added to Michael acceptors such as 1,4-BD BisAcAc or PTMO 250 BisAcAc. A 2-step "prepolymer" method was selected to prepare urethane (α-ω hydroxyl-terminated PTMO polyol) and urea (α-ω aminopropyl-terminated PTMO polyol) diacrylates from the reaction of HMDI with the corresponding polyol, and HEA. ^{1}H NMR spectroscopy confirmed the intended composition and the absence of by-products in the precursors. **Scheme 2.1** depicts the synthesis of urethane diacrylates (UtDA).

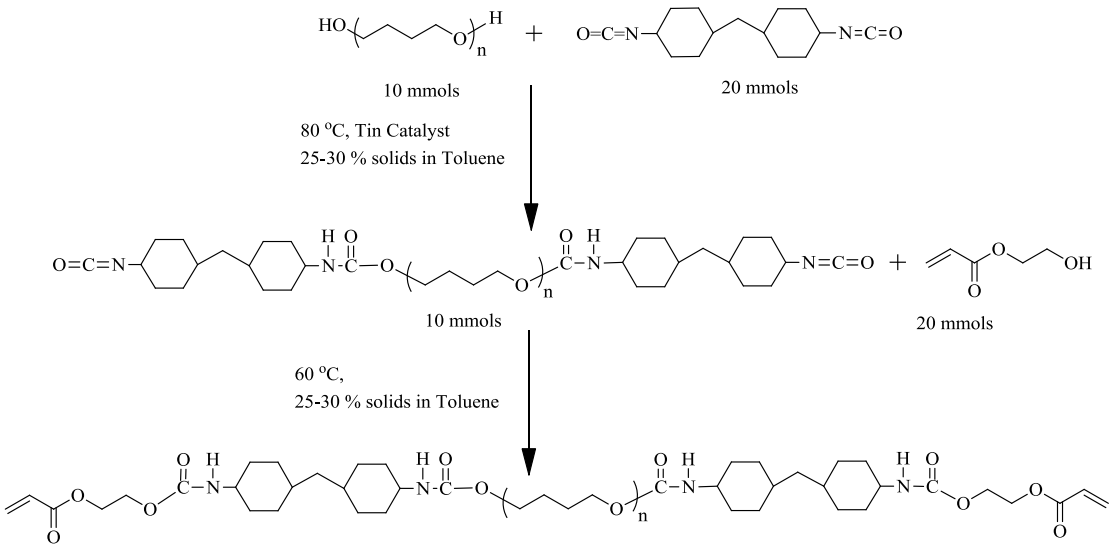

Scheme 2.1. Two-step synthesis of PTMO-based urethane diacrylates (UtDA)

The H-bonding containing PTMO-based Michael acceptors included molecular weights of 1000, 2000, 3000, and 3600 g/mol urethane diacrylates (UtDA 1000, UtDA 2000, UtDA 3000, UtDA 3600) and 1000 and 2000 g/mol urea diacrylates (UrDA 1000, UrDA 2000). **Scheme 2.2** shows the synthesis of the urea diacrylates.

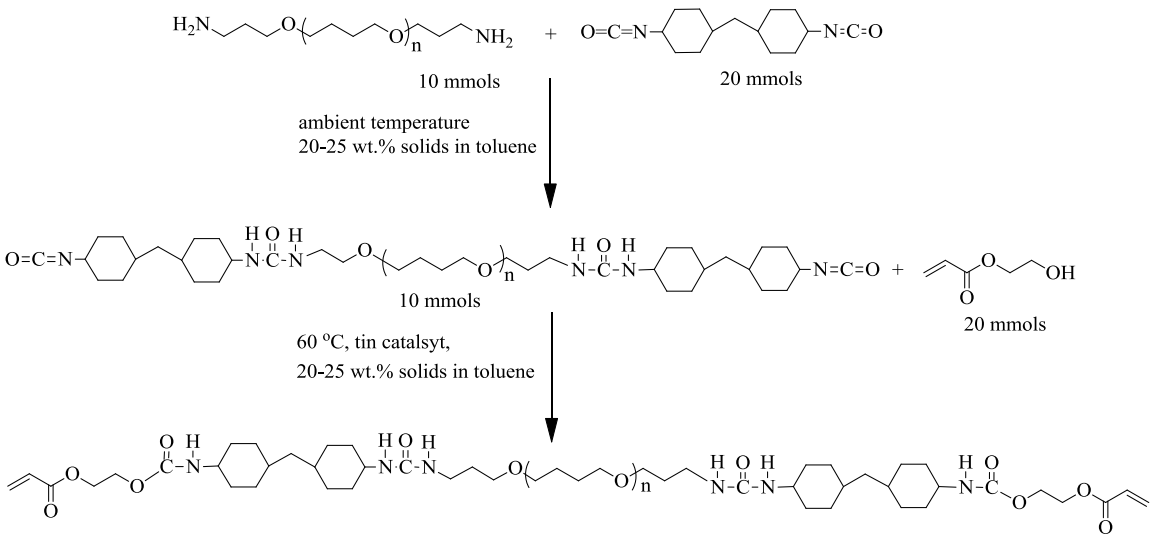

Scheme 2.2. Two-step synthesis of PTMO-based urea diacrylates (UrDA)

In situ IR spectroscopy tracked the progress of the reaction and determined the reaction conditions. Figure 2.1 A) and Figure 2.1 B) shows the –NCO group absorbance in the first and second steps of the synthesis respectively. Gradual decrease in the absorption of –NCO absorption indicates end-capping of –OH functionalities with –HMDI in the first step and functionalization of -NCO end-groups with HEA in the second step.

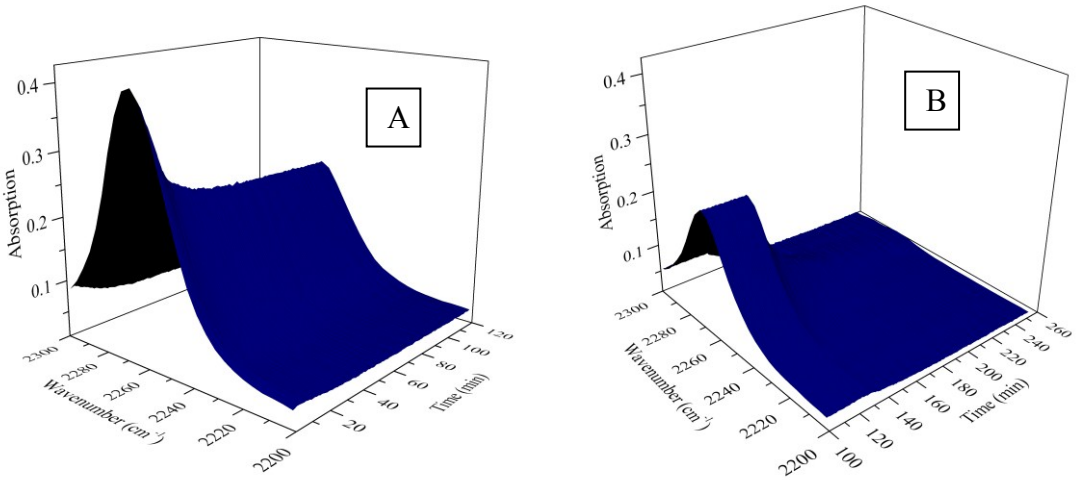

Figure 2.1. Waterfall plots of –NCO absorption during urethane diacrylate synthesis

PTMO-based ester diacrylates of 1000 g/mol and 2000 g/mol PTMO (EtDA 1000-2000) were synthesized as controls to H-bonding containing urethane and urea networks. (**Scheme 2.3)**

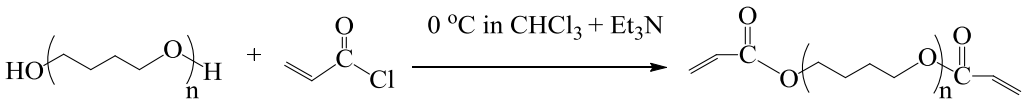

Scheme 2.3. Synthesis of PTMO-based ester diacrylates (EtDA)

End group analysis of the diacrylates by ^{1}H NMR was used to determine the M_n of the Michael acceptors (**Table 2.1**)**.** End group analysis of the hydroxyl and aminopropyl end groups on the PTMO precursors (measured by NMR) plus the molecular weight of two HMDI and two HEA molecules to account for the end groups were utilized to obtain the calculated values in Table 1. Comparison of the calculated molecular weights to those derived experimentally from NMR on the isolated polymers agreed well in all cases.

Table 2.1. Comparisons of compositions and M_n of the oligomeric Michael acceptors

Precursor	**Wt %PTMO**	**Calculated M_n (g/mol)**	**^{1}H NMR M_n (g/mol)**
UtDA 1000	24	1050	1110
UtDA 2000	53.5	1900	1850
UtDA 3000	70.6	2700	2760
UtDA 3600	77.7	3550	3670
EtDA 1000	100	1210	1150
EtDA 2000	100	1910	1950
UrDA 1000	100	900	930
UrDA 2000	100	1900	1940

Acetoacetylation of 1,4-butanediol or a 250 g/mol PTMO according to a method adapted from Long *et al.* [53](**Scheme 2.4**) yielded the Michael donors, 1,4-BD BisAcAc and PTMO 250

BisAcAc respectively. The reactions were conducted holding the system at toluene reflux under mild vacuum (100 mm Hg) to remove the t-butyl alcohol by-product to drive the reaction to completion. Finally high vacuum (0.1 mmHg) at 110 °C were applied for 3 hours to remove volatile starting reagents, solvent and reaction by products.

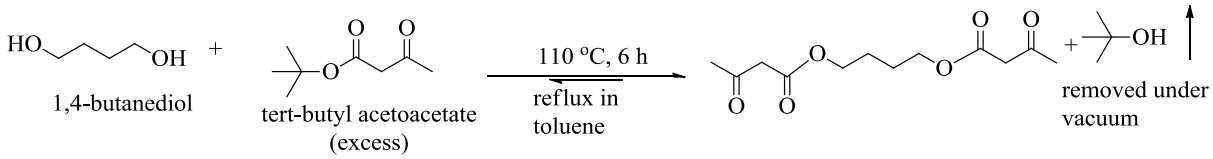

Scheme 2.4. Acetoacetylation of 1,4-butanediol

Isothermal DSC was performed on the diacrylate precursors to establish the thermal stability of the acrylate end groups under conditions to be utilized for rheological measurements. The absence of exothermic peaks in Figure 2 indicated that the diacrylates were thermally stable at 90 ºC for an hour.

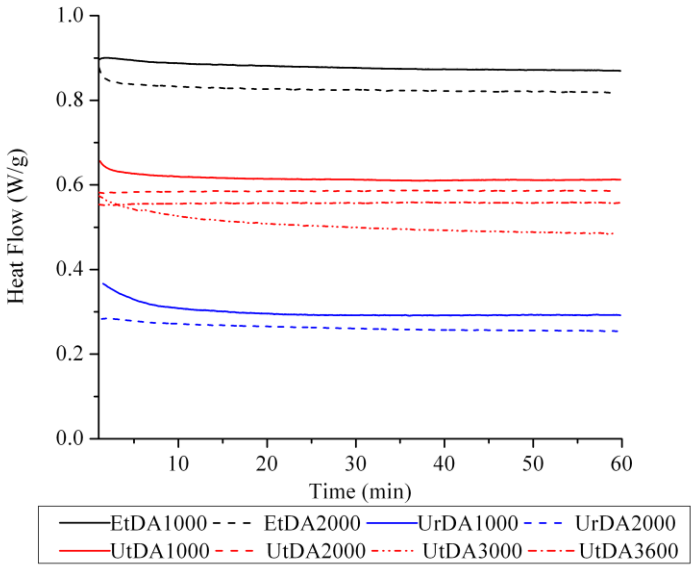

Figure 2.2. Isothermal DSC thermograms of diacrylates at 90 °C for 1h.(Exo DOWN)

Rheological measurements showed the effect of molecular weight on viscous flow properties of the diacrylates under shear. As expected, **Figure 2.3** shows that the viscosities of the diacrylates decreased with decreasing molecular weight and increasing temperature. Moreover, **Figure 2.4** indicates that the oligomers containing urea groups had substantially higher viscosities than the urethane oligomers, and the ester diacrylates without hydrogen bonding have the lowest viscosities. It is reasoned that the hydrogen bonds introduce physical crosslinks that increase viscosity.

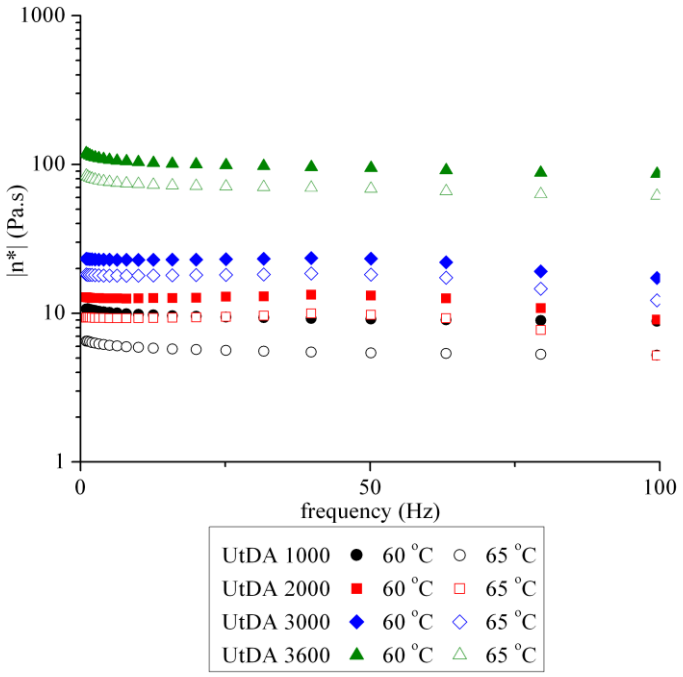

Figure 2.3. Viscosity profiles of urethane diacrylates at 60 and 65 °C from 1 to 100 Hz

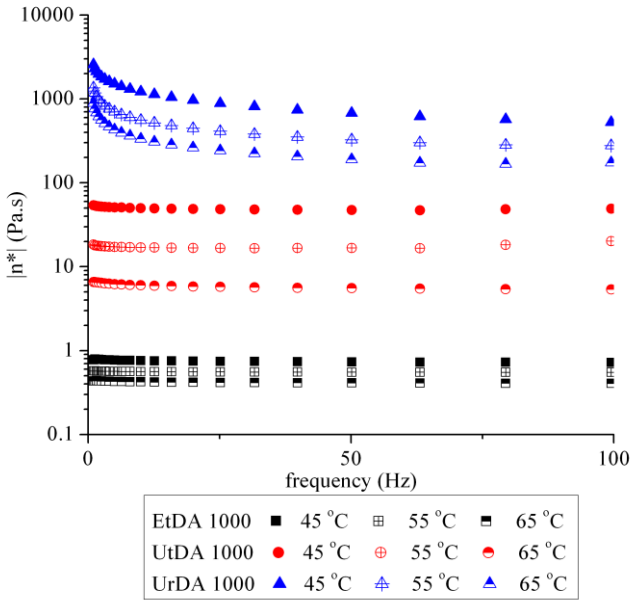

Figure 2.4. Viscosity profiles of ester, urethane, urea diacrylates at 45, 55, and 65 °C from 1 to 100 Hz

Viscosities of each urethane diacrylate were also measured with a temperature ramp at constant frequency (1 Hz). Their activation energies for flow were calculated from Arrhenius plots (R^2 values > 0.99, **Figure 2.5**). **Equation 2.1** shows the relationship between viscosity (η) and activation energy (E_a) where A is a constant, R is the gas constant, and T is temperature in K. The plot of ln η vs. 1/T yields a slope of (E_a/R). **Table 2.2** summarizes the activation energies for flow of the urethane diacrylates. As the molecular weight of the PTMO segment in the diacrylate increases, the relative content of the hydrogen bonded terminal groups decrease and this increases E_a. Moreover, **Figure 2.6** (R^2 values > 0.99) shows a direct comparison between viscosity profiles of ester, urethane and urea diacrylates as a function of temperature. Viscosities were measured with a temperature ramp at constant 1 Hz frequency. The nature of hydrogen-bonding (urea>urethane>ester) has a thickening effect on viscosity and increases E_a (**Table 2.3**).

Equation 2.1

$$\eta = A\ e^{\left(\frac{E_a}{RT}\right)}$$

$$\ln \eta = \ln A + \left(\frac{E_a}{R}\right)\frac{1}{T}$$

Equation 2.1. Arrhenius relationship between viscosity (Ƞ) and activation energy (E_a)

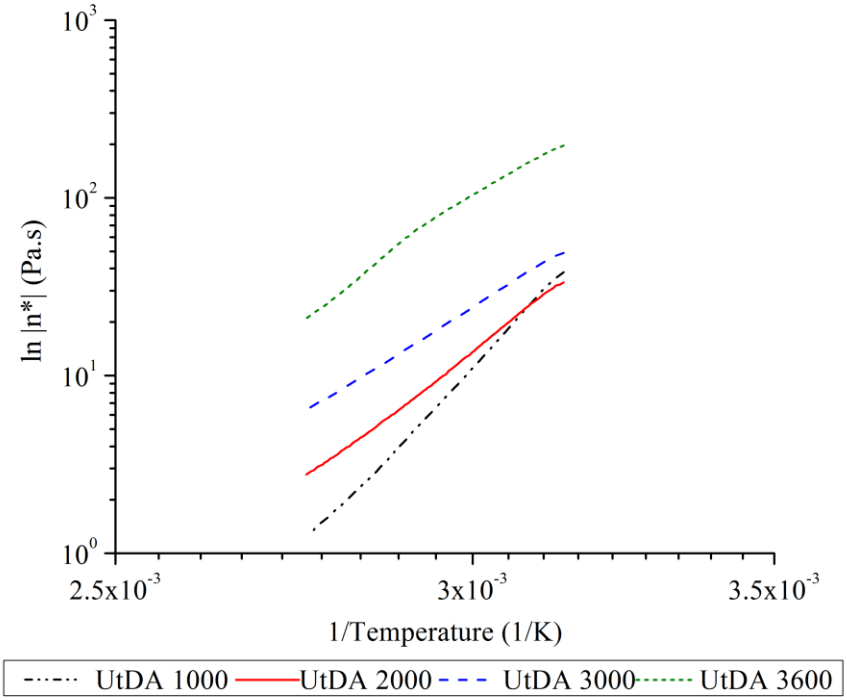

Figure 2.5. Viscosity profiles of urethane diacrylates from 45 to 90 °C at 1 Hz

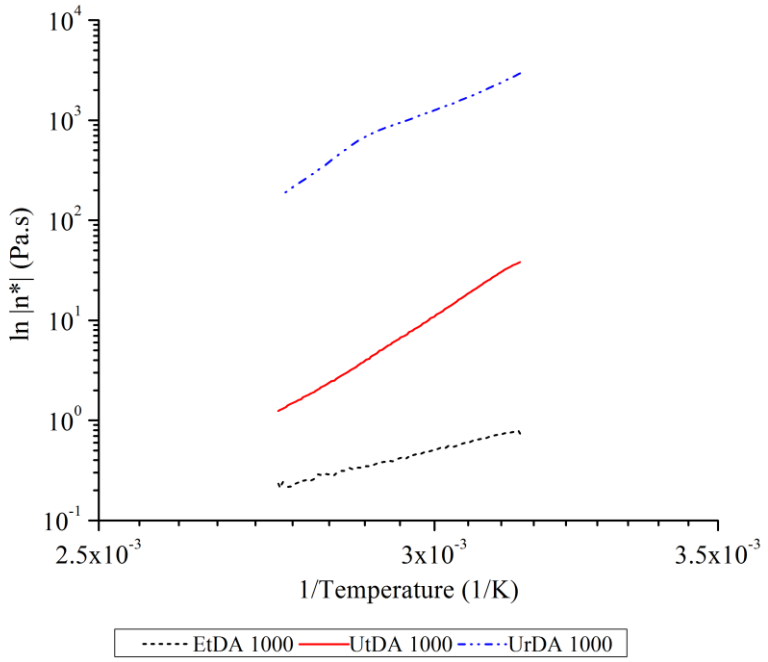

Figure 2.6. Viscosity profiles of ~1000 g/mol ester, urethane and urea diacrylates from 45 to 90 °C at 1 Hz.

Table 2.2. Activation energies of flow (E_a) for UtDA

Precursor	HMDI -HEA Segment wt.%	Slope (E_a/R) (K)	E_a (kJ x mol^{-1})
UtDA 1000	76	3956	32.89
UtDA 2000	46.5	2885	23.99
UtDA 3000	29.4	2346	19.50
UtDA 3600	22.3	2065	17.68

Table 2.3. Activation energies of flow (E_a) for diacrylates

Precursor	HMDI -HEA Segment wt.%	Slope (E_a/R) (K)	E_a (kJ x mol^{-1})
EtDA 1000	0	1467	12.20
UtDA 1000	76	3953	32.87
UrDA 1000	77.4	4576	38.04

The E_a values in **Table 2.3** demonstrate that with the increasing percentage of hydrogen-bonding segments per diacrylate molecule, the E_a increases. The E_a for non-hydrogen-bonding EtDA was less than one-third of the similar molecular weight UrDA. The percentages of H-bonding segments (HMDI-HEA) in UrDA were significantly higher than for EtDA and UtDA.

FT-IR spectroscopy showed the presence of hydrogen-bonding in urethane and urea diacrylates. Thin films of each precursor were cast on polished KBr discs and FT-IR spectra were collected in transmittance mode (**Figure 2.7**).

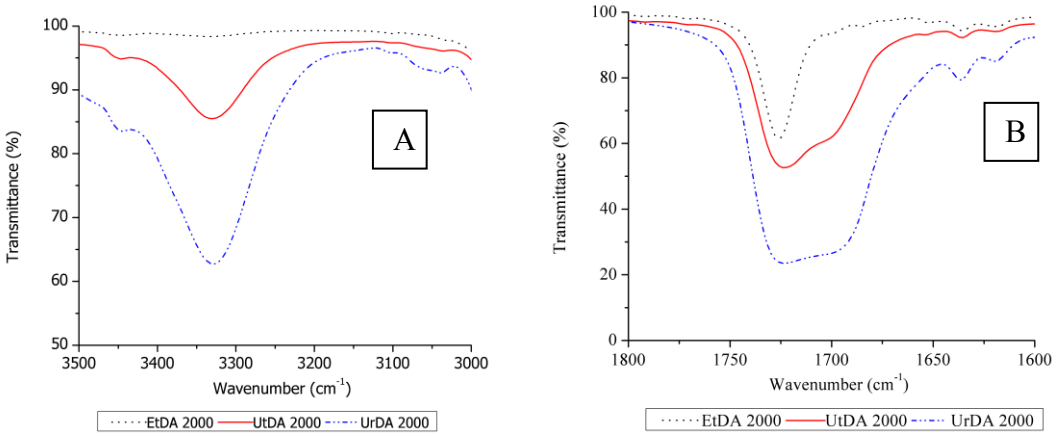

Figure 2.7. (A) FT-IR spectrum of NH region. (B) FT-IR spectrum of C=O region.

FT-IR spectra in **Figure 2.7 A)** show the presence of N-H bond absorption for urethane, and urea diacrylate, and the absence of the same absorption for the ester diacrylate. The absorption of non-hydrogen bonded carbonyls in ester diacrylate is sharper and at 1725 cm^{-1} compared to hydrogen-bonded urethane and urea diacrylates (**Figure 2.7 B**). Consistent with the literature,[14] the presence of H-bonding in the diacrylates caused broadening and a shift of the peak to lower wavenumbers (1700 to 1690 cm^{-1}).

The Michael acceptors reacted with 1,4-BD BisAcAc in the presence of DBU as a base catalyst. The networks were comprised of 1.40 equivalents of acrylate per 1.00 equivalents of

acetoacetate and the base concentration was 3 weight % based on the bis acetoacetates. **Scheme 2.5** depicts the reaction for this process. Literature precedent on Michael carbon addition networks from our group indicated that 1.4:1.0 stoichiometry of diacrylates to bis acetoacetates yielded higher gel fractions, greater tensile strengths and Young's moduli than crosslinked networks of those with other stoichiometric ratios.[56]

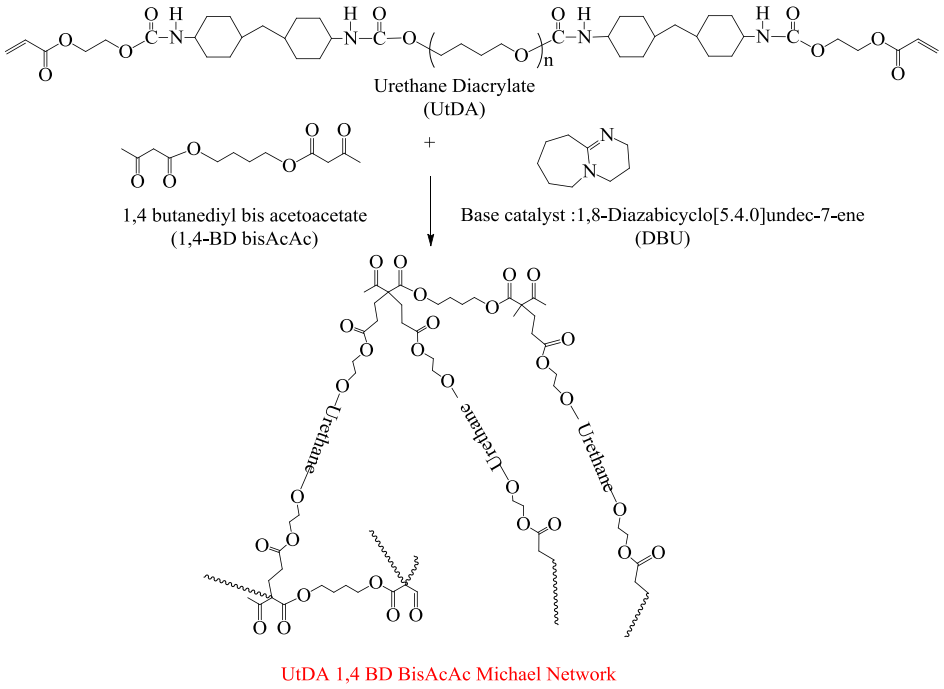

Scheme 2.5. Carbon Michael addition of Michael donor UtDA to Michael acceptor 1,4-BD BisAcAc

FT-IR spectroscopy showed the consumption of acrylate functional groups. The films of 1.40 mol equivalents of 1000 g/mol urethane diacrylate per 1.00 mol equivalent of 1,4-BD BisAcAc were cast on polished KBr discs and FT-IR spectra were recorded. A second spectrum was collected 24 hours after the addition of base catalyst (Graphs were offset on Y axis **Figure 2.8**). Disappearance of the acrylate carbon-carbon double bond absorption at 815 cm^{-1} indicates addition of the urethane diacrylate to the BisAcAc. FTIR spectrum showed the Michael carbon addition reaction reached to completion.

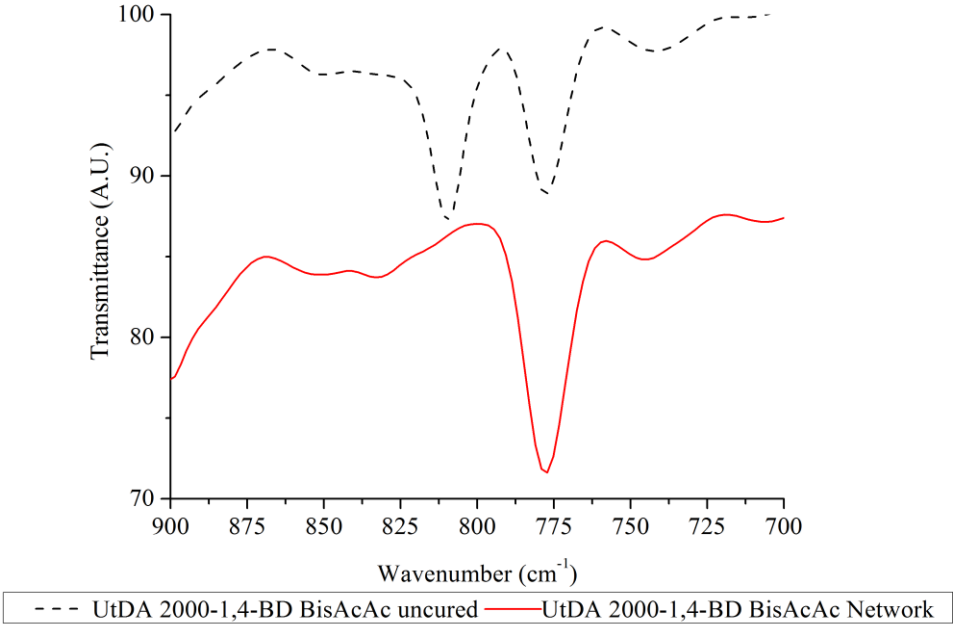

Figure 2.8. FTIR spectra of UtDA 2000-1,4-BD BisAcAc uncured mixture (dashed line) and cured sample (solid line).

Gel fraction analyses of the Michael networks showed the efficiency of the crosslinking reaction. The gel fractions were about 90% or higher which indicated that the networks were well crosslinked (**Table 2.4).**

Table 2.4. Gel fraction analysis for diacrylate -1,4BD BisAcAc networks

Network	Gel Fraction %
EtDA 1000 – 1,4-BD BisAcAc	89 ± 2
EtDA 2000 – 1,4-BD BisAcAc	92 ± 2
UtDA 1000 – 1,4-BD BisAcAc	92 ± 3
UtDA 2000 – 1,4-BD BisAcAc	96 ± 2
UtDA 3000 – 1,4-BD BisAcAc	96 ± 2
UtDA 3600 – 1,4-BD BisAcAc	94 ± 2
UrDA 1000 – 1,4-BD BisAcAc	93 ± 2
UrDA 2000 – 1,4-BD BisAcAc	90 ± 2

Isothermal TGA demonstrated that presence of urethane and urea groups improved thermal stability of diacrylates. This was determined at 125 and 175 ºC for 5 hours (**Table 2.5**). **Figure 2.9** show representative TGA curves of different types of diacrylates at 175 °C. Since eters and polyethers are inherently unstable to oxidative conditions, the urea and urethane networks which contain lower compositions of ethers are substantially more stable than the control ester diacrylates. The weight losses of urethane and urea films were only 1-2 % at 125 °C. After 5 hours at 175 °C, only 5 to 6% of the crosslinked urethane films and 3 to 4 % of the urea films were degraded. By contrast EtDA lost almost 30% of its weight under these conditions.

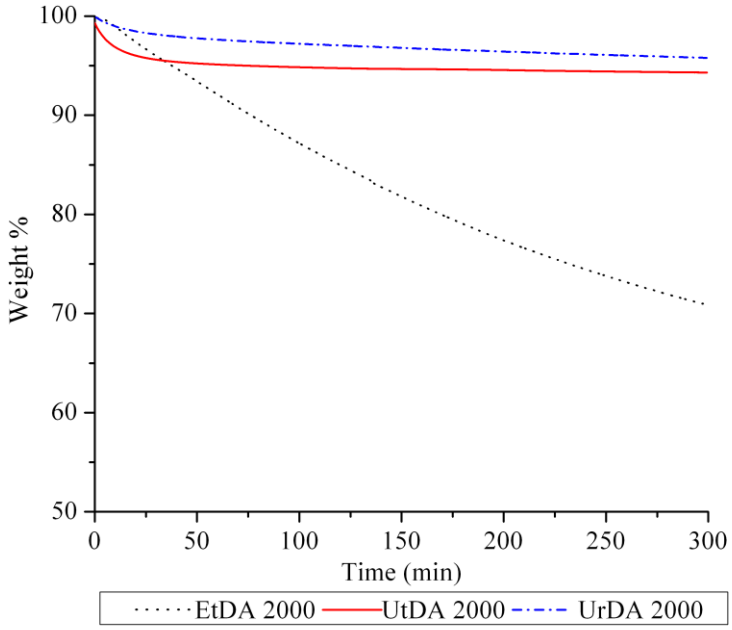

Figure 2.9. Isothermal TGA of the EtDA 2000, UtDA 2000, UrDA 2000-1,4-BD BisAcAc networks.

The general trend of oxidative stability was attributed the lower percentage of ether segments in urethane and urea diacrylates. The networks of the same type (ester, urethane, or urea) with different molecular weights had a similar extent of oxidative degradation.

Table 2.5. Comparison of degradation of different diacrylates at 125 and 175 °C in air.

Network	Weight % Remaining at 125 °C	Weight % Remaining at 175 °C
EtDA 2000 – 1,4-BD BisAcAc	98	72
UtDA 2000 – 1,4-BD BisAcAc	99	95
UrDA 2000 – 1,4-BD BisAcAc	94	97

2.5.2 Impact of Hydrogen-Bonding on Thermo-Mechanical Properties of Networks

DSC was utilized to analyze thermal transitions of Michael networks. The DSC thermograms showed a wide distribution of T_g's ranging from -61 to 52°C. DSC indicated that the UtDA–1,4-BD BisAcAc networks have T_g's of 52, 23, -55, and -61 ºC (UtDA 1000-3600). The network T_g decreased with increasing molecular weight of the PTMO segment, and this behavior was attributed to a lower crosslink density. Moreover, UtDA 3000 and 3600 showed crystallization and melting transitions, attributed to the presence of longer and more mobile PTMO segments in these networks. (**Figure 2.10**)

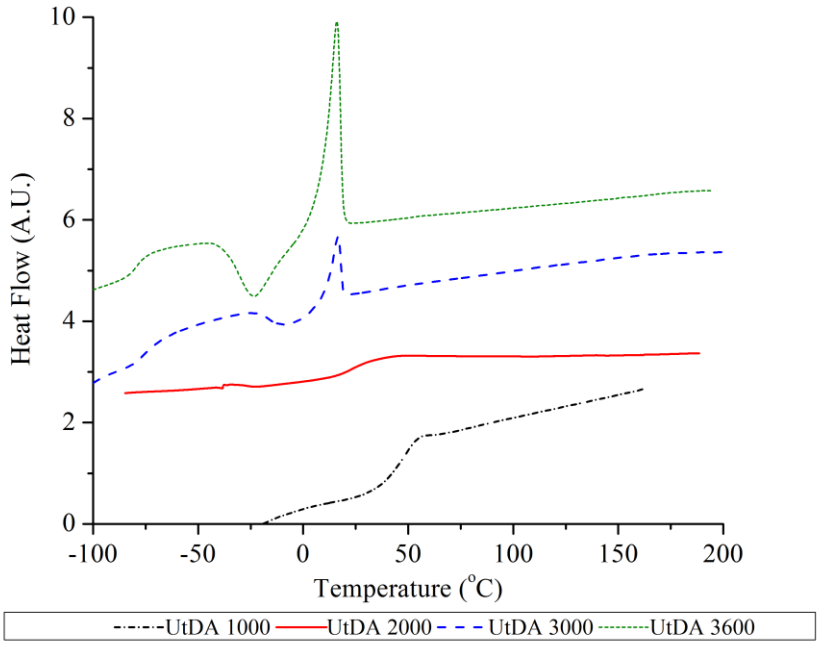

Figure 2.10. Overlay of DSC curves of different molecular weight UtDA (Exo Down)

DSC indicated the 1000 g/mol UtDA – 1,4-BD BisAcAc network has a T_g 52 °C, 2000 g/mol The effect of bis acetoacetate molecular weight (1,4-BD BisAcAc 258.27 g/mol, PTMO 250 BisAcAc 420.15 g/mol) on the network properties was compared utilizing DSC. **Figure 2.11**

shows the UtDA 1000-PTMO 250 BisAcAc network has a slightly lower T_g compared to the UtDA 1000-1,4-BD BisAcAc network. This result agrees with the DSC analysis of urethane diacrylate network series showing further proof on increasing crosslinking density on limits the mobility of segments between crosslink points.

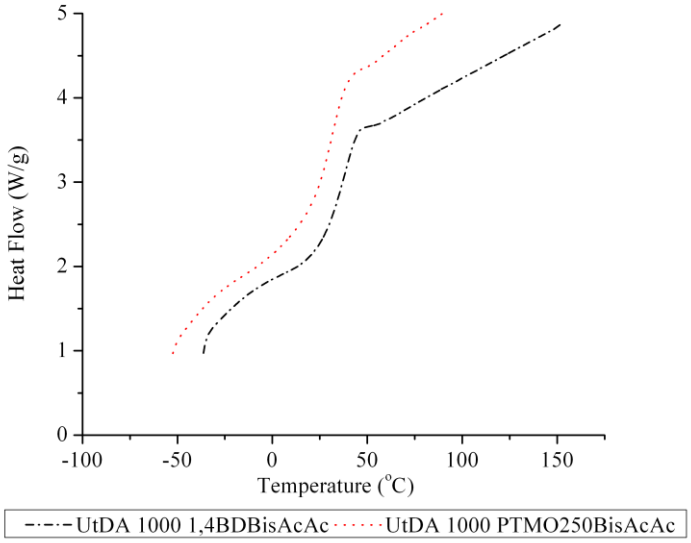

Figure 2.11. Comparison of DSC thermograms of networks crosslinked with different M_n BisAcAc.(Exo Down)

The influence of presence hydrogen bonding on the thermal transitions of Michael networks were also investigated using DSC (**Figure 2.12**). The DSC thermograms indicate that increasing the hydrogen-bonded segment have a profound effect. The network T_g change from -63 to 63 °C with increasing hydrogen-bonding (ester <urethane< urea). This result was attributed to hydrogen-bond introducing physical crosslinks into networks which further restricts the molecular motion and increases the network T_g.

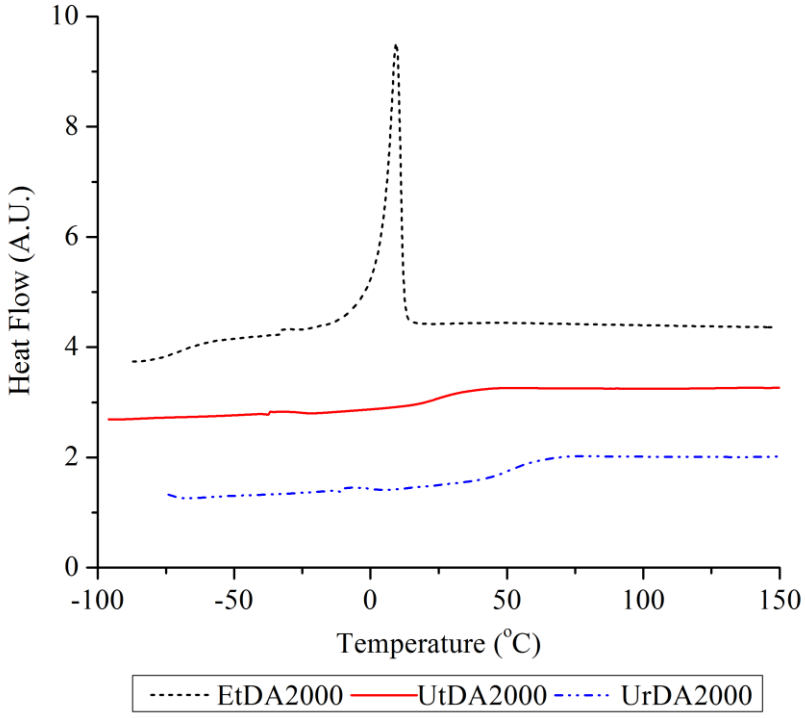

Figure 2.12. Overlay of DSC thermograms of EtDA 2000, UtDA 2000, and UrDA 2000– 1,4-BDBisAcAc networks.(Exo Down)

The mechanical properties of the Michael addition networks were investigated by DMA. **Figure 2.13** includes the tan δ and storage modulus versus temperature plots of urethane diacrylate networks. The tan δ curves show that the T_g's are 52, 23, -45 and -61 ºC for 1000, 2000, 3000 and 3600 g/mol UtDA–1,4-BDBisAcAc networks. The T_g's from tan δ data agrees with the thermal results regarding the influence of precursor molecular weight on the network T_g. **Figure 2.14** presents DMA thermogram of UtDA 2000-based network crosslinked with 1,4-BD BisAcAc show a T_g of 25°C which is ~5°C higher compared to its counterpart crosslinked with PTMO 250 BisAcAc.

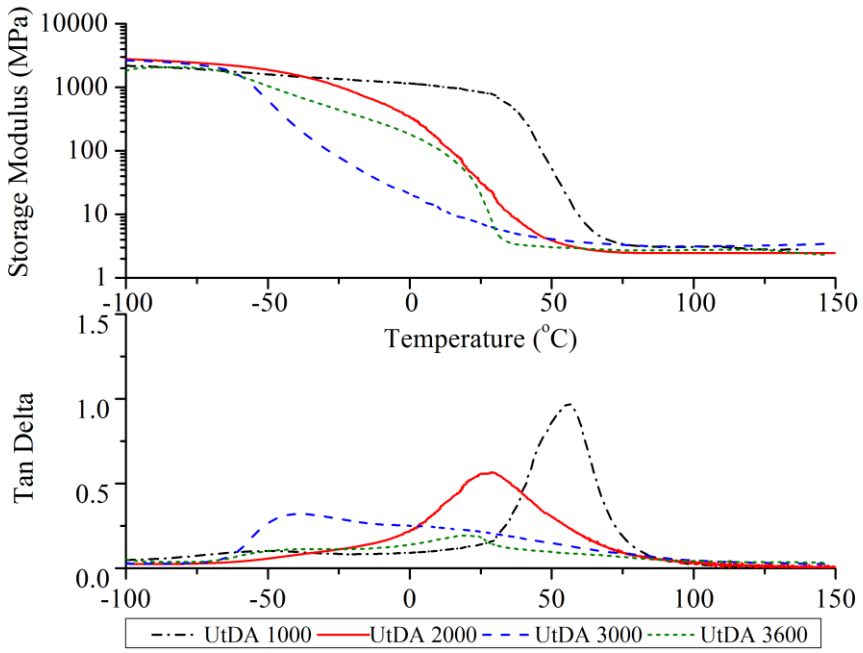

Figure 2.13. Tan δ and storage modulus vs. temperature plots of UtDAs.

The DMA curves show a breadth of the T_g's. DMA tan δ curves showed the T_g's of the Michael addition networks vary from 52 ºC for the 1000 g/mol UtDA – 1,4-BDBisAcAc network, 23 ºC for the 2000 g/mol UtDA – 1,4-BDBisAcAc network, -45 ºC for the 3000 g/mol UtDA –1,4-BDBisAcAc network, and -61 ºC for the 3600 g/mol UtDA – 1,4-BDBisAcAc. The T_g's decreased with increasing molecular weight of the PTMO segment, and this observation was attributed to less restriction on segmental motion due to increased molecular weight between crosslink points. As the molecular weight between crosslink points decreased, the segmental motion close to the crosslink junctions is more limited. This results in the broadening of the glassy region, and the relaxation occured at a higher temperature. DMA curves of UtDA 100-1,4-BD BisAcAc and UtDA 100- PTMO 250 BisAcAc networks showed slight variation in network T_g. **Figure 2.14** shows the network crosslinked with 1,4-BD BisAcAc showed ~5°C

higher network T_g compared to its counterpart crosslinked with PTMO 250 BisAcAc (T_g = 20 °C).

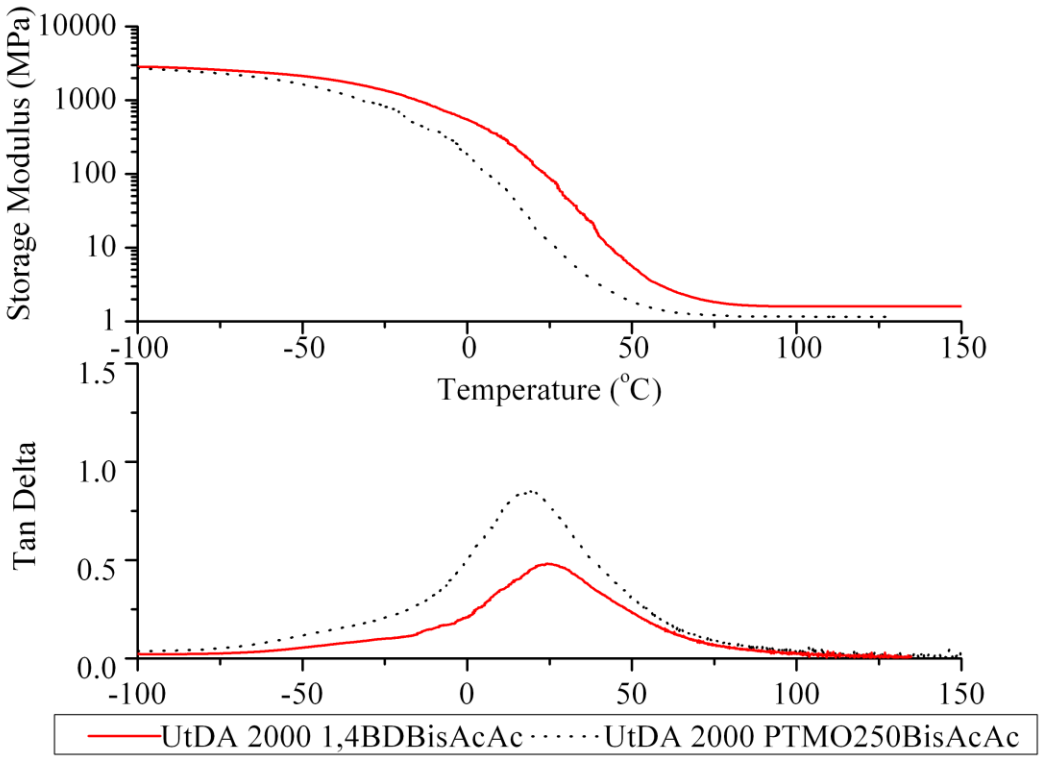

Figure 2.14. Tan δ and storage modulus vs. temperature plots of UtDA 2000 networks crosslinked with 1,4-BD BisAcAc and PTMO 250 BisAcAc

DMA demonstrated that T_g increased with decreasing molecular weight of the diacrylate and bis acetoacetate segments. Increased rubbery plateau moduli were observed with a decrease in precursors' molecular weight. The plateau moduli for the two lowest urethane diacrylate molecular weights were nearly identical. These observations were attributed to increasing restriction on segmental motion due to increased crosslink density yielding shorter segments between crosslink points. DMA results also supported the presence of a crystalline phase for the networks with higher molecular weight PTMO (Figure 13). Networks having longer PTMO

segments of 2000 and 2900 g/mol demonstrated lower glass transition temperatures and presence of melting transitions in tan δ curves that were attributed to the presence of crystallinity. The storage modulus, plateau modulus, and glass transition of the networks were dependent on the molecular weight of the PTMO segment because of the difference in crosslink density and the degree of crystallinity.

The mechanical properties of ester, urethane, and urea diacrylates were also compared using DMA. **Figure 2.15** shows the overlay of storage modulus and tan δ vs. temperature curves of EtDA, UtDA, and UrDA 2000–1,4-BDBisAcAc networks. The network T_g's were -54, 24 and 63 °C for these networks. Increasing HMDI-HEA content in networks introduced a higher degree of inter- and intra-molecular H-bonding interactions which results in formation of a physical network. These interactions improve storage moduli and rubbery plateau moduli of the networks. Secondary interactions such as hydrogen-bonding also restrict segmental motion of the polymer chains between the crosslink points, ultimately resulting enhanced mechanical properties.

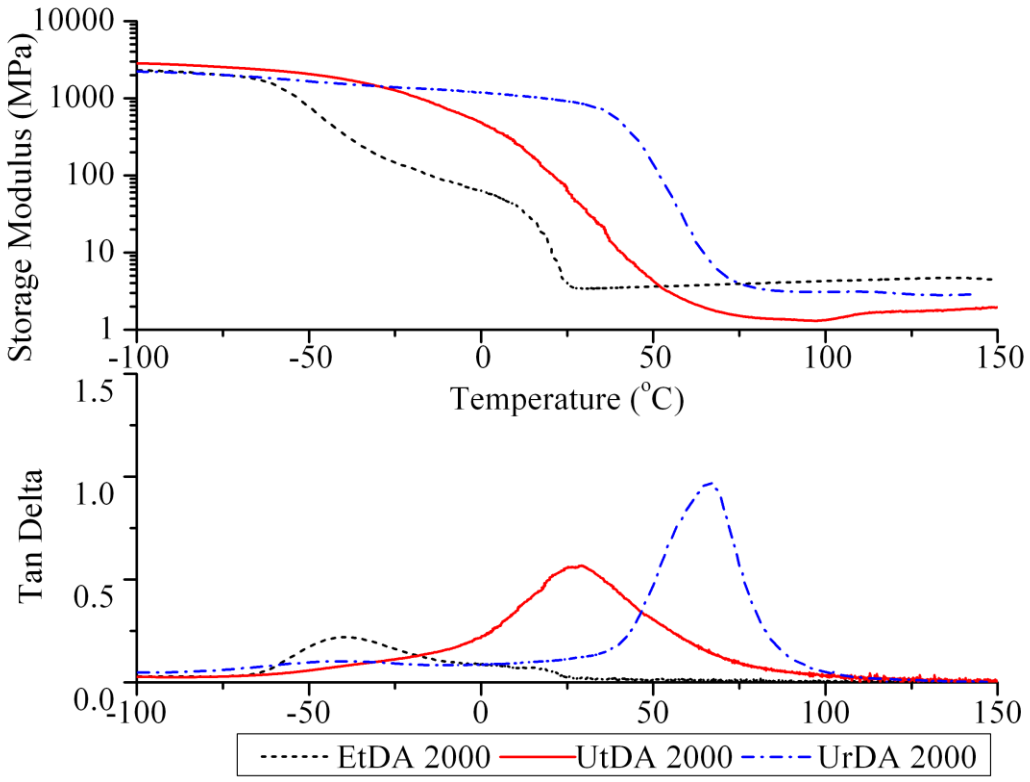

Figure 2.15. Tan δ and storage modulus vs. temperature plots of 2000 g/mol EtDA, UtDA and UrDA networks

Figure 2.16 shows the stress–strain curves corresponding to the networks obtained from reaction of urethane diacrylates with molecular weights of 1000, 2000, 3000 and 3600 g/ mol with 1,4-butanediyl bis acetoacetate precursors. Tensile testing confirmed the dependence of mechanical properties on the molecular weight of the network precursors. The Young's moduli decreased from 25.3 to 2.0 and the elongation at break increased from 255 to 775% with increasing urethane diacrylate molecular weight. (**Table 2.6**). Tensile testing was also performed on the urethane diacrylate networks crosslinked with either 1,4-BD bisAcAc or PTMO 250 bisAcAc (**Figure 2.17**). Tensile data of these networks also indicate a significant drop in

Young's modulus, stress at break and an increase in elongation at break of the networks (**Table 2.7**). These trends were attributed to the different compositions of diacrylates and drop in the crosslinking density of the networks. The increased elongation at break is due to increase in the flexible PTMO content present in urethane diacrylates which caused a drop in the crosslinking density of the networks. The reduced crosslinking density of networks results in a significant drop in Young's modulus. Moreover, increasing content of hydrogen-bonded segment in these networks yields tougher films (**Table 2.6**)

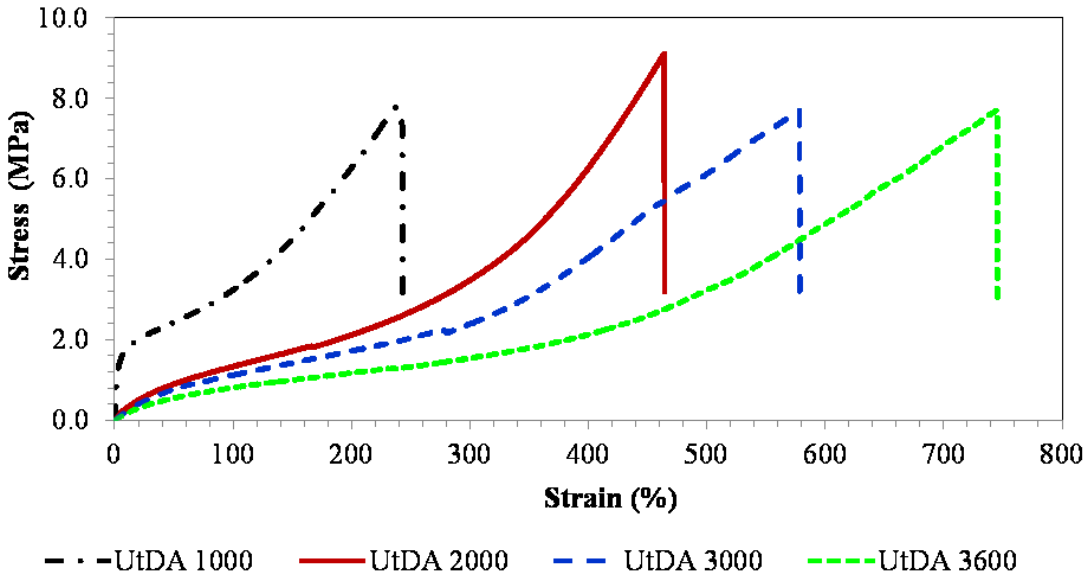

Figure 2.16. Tensile testing comparison stress vs. strain of UtDA networks

Table 2.6. Comparison of tensile properties of UtDA – 1,4-BD BisAcAc networks

Network	Young's Modulus (MPa)	Stress at Break (MPa)	Elongation at Break (%)
UtDA 1000 – 1,4-BD BisAcAc	25.3 ± 5.7	7.2 ± 1.3	255 ± 25
UtDA 2000 – 1,4-BD BisAcAc	3.5 ± 0.6	9.1 ± 0.9	468 ± 13
UtDA 3000 – 1,4-BD BisAcAc	2.8 ± 0.2	5.8 ± 0.7	578 ± 15
UtDA 3600 – 1,4-BD BisAcAc	2.0 ± 0.4	8.8 ± 1.5	775 ± 42

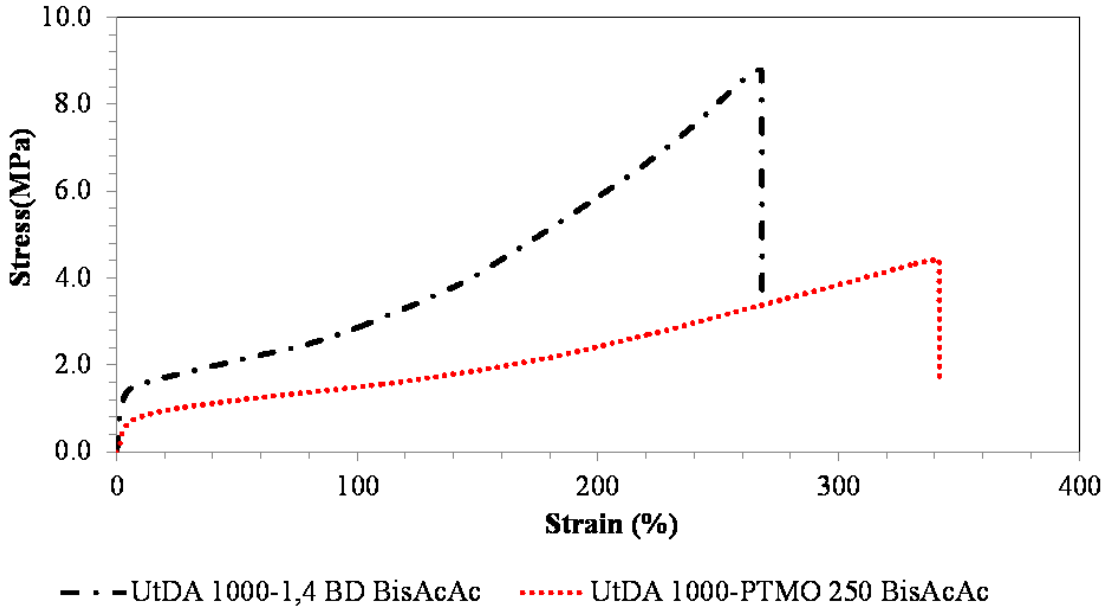

Figure 2.17. Tensile testing comparison stress vs. strain of UtDA 1000 networks crosslinked with different BisAcAc

Table 2.7. Tensile data for UtDA 2000-1,4-BD BisAcAc and PTMO 250 BisAcAc networks

Network	Young's Modulus (MPa)	Stress at Break (MPa)	Elongation at Break (%)
UtDA 1000 – 1,4-BD BisAcAc	25.3 ± 5.7	7.2 ± 1.3	255 ± 25
UtDA 1000 – PTMO 250 BisAcAc	4.5 ± 0.6	4.3 ± 1.6	358 ± 13

Tensile testing was also performed on EtDA and UrDA. The urea diacrylate networks have T_g's above 40 °C , which is ~ 20 °C higher than the ambient testing temperature thus the Young's moduli and stress at break of UrDA networks are superior compared to UtDA and EtDA networks whose T_g's are at or below the ambient temperature. The Young's modulus and stress at break values for UrDA networks are significantly higher than both EtDA and UtDA networks (Table 8). Presence of both physical and covalent crosslinks changes have a substantial influence of tensile properties. This change impacts rigidity, and toughness of the networks and overall tensile properties of the networks. These results indicate that manipulating the precursor molecular weight and/or changing different type of secondary interactions one can fine-tune the stress-strain properties of these networks to achieve the desired properties.

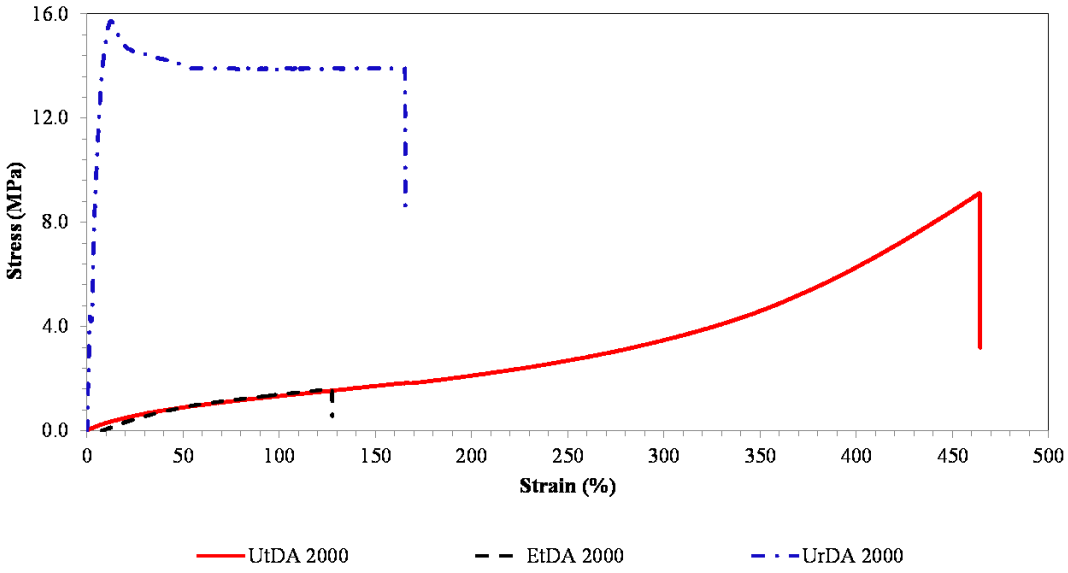

Figure 2.18. Tensile testing comparison stress vs. strain of 2000 g/mol EtDA, UtDA, and UrDA

The Young's modulus and stress at break of UrDA networks are significantly higher than both EtDAs and UtDAs. The T_g's of UrDA networks are above 40 °C , which is ~ 20°C higher than the ambient testing temperature thus the tensile properties of UrDAs are higher than UrDAs and

EtDAs whose T_g's are at or below the room temperature. **Table 2.8** shows the summary of tensile testing results.

Table 2.8. Tensile data for UrDA and EtDA -1,4-BD BisAcAc networks

Network	Young's Modulus (MPa)	Stress at Break (MPa)	Elongation at Break (%)
UrDA 1000 – 1,4-BD BisAcAc	368.1± 17.1	17.5±3.2	8.5± 4.3
UrDA 2000 – 1,4-BD BisAcAc	311.3 ± 25.2	13.7 ±1.4	150 ± 21
EtDA 1000 – 1,4-BD BisAcAc	4.69 ± 0.35	1.66± 0.15	41 ± 8
EtDA 2000 – 1,4-BD BisAcAc	3.27 ± 0.15	1.18 ±0.12	115± 24

2.6 Conclusions

Three different series of diacrylate precursors were synthesized from α,ω-aminopropyl-terminated PTMO polyol, α,ω-hydroxy-terminated PTMO polyol, Bis(4-isocyanatocyclohexyl)methane and 2-hydroxyethyl acrylate. Two bis acetoacetates were prepared from acetoacetylation of 1,4-butanediol, PTMO 250 g/mol hydroxy-terminated polyol with t-butyl bis acetoacetate. ^{1}H NMR spectroscopy confirmed the structures and molecular weight. *In situ* FTIR spectroscopy was utilized to determine the reaction conditions. The flow properties of synthesized diacrylates were studied and activation energy of flow for ester, urethane and urea diacrylates were obtained. FT-IR spectroscopy revealed the presence of H-bonding in diacrylate precursors. Michael carbon addition of diacrylates to bis acetoacetates yielded covalent networks. FT-IR spectroscopy showed disappearance of acrylate which ascribed the completion of crosslinking reaction. Networks had gel fractions above 90 %. DSC and DMA experiments revealed that diacrylate networks showed a broad distribution of glass transition temperatures depending on the molecular weight and/or degree of H-bonding present in their

backbone structures. UtDA network had a variation in the T_g's between -49 °C and 54 °C. The network T_g's of urethane and urea-based networks of the comparable molecular weight precursors varied between -49 ºC and 63 ºC ascribed to increasing degree of H-bonding present in the networks. The UtDA and UrDA networks showed an improved thermal stability compared to EtDA networks. Tensile testing also revealed a dependence on the molecular weight of the diacrylates. In correlation with increasing molecular weight of urethane diacrylate precursor the storage moduli of networks dropped from 25.3 to 2.0 MPa and elongation at break improved from 255 to 755 %. The Young's moduli increased from 3.27 for EtDA 2000 to 311.1 for UrDA 2000 networks to due to presence of urethane and urea hydrogen bonds in the networks.

2.7 Acknowledgements

We acknowledge Ninad Dixit for FR-IR measurements from Dr. Robert Moore's group at Virginia Tech. Research was sponsored by the Army Research Laboratory and was accomplished under Cooperative Agreement Number W911NF-06-2-0014. The views and conclusions contained in this document are those of the authors and should not be interpreted as representing official policies, either expressed or implied, of the Army Research Laboratory or the U.S. Government. The U.S. Government is authorized to reproduce and distribute reprints for Government purposes not withstanding any copyright notation here on.

2.8 References

(1) Klinedinst, D. B.; Yilgor, E.; Yilgor, I.; Beyer, F. L.; Sheth, J. P.; Wilkes, G. L. *Rubber Chemistry and Technology* **2005**, *78*, 737.
(2) Das, S.; Cox, D. F.; Wilkes, G. L.; Klinedinst, D. B.; Yilgor, I.; Yilgor, E.; Beyer, F. L. *Journal of Macromolecular Science, Part B: Physics* **2007**, *46*, 853.
(3) Chang, C.-C.; Chen, K.-S.; Yu, T. L.; Chen, Y.-S.; Tsai, C.-L.; Tseng, Y.-H. *Polymer Journal (Tokyo)* **1999**, *31*, 1205.
(4) Silver, J. H.; Karayianni, E.; Cooper, S. L. *Journal of Colloid and Interface Science* **1996**, *178*, 219.
(5) Lim, H.-O.; Bark, G.-M.; Jo, N.-J. *Proceedings of SPIE* **2007**, *6423*, 64234F/1.
(6) Ghosh, S.; Krishnamurti, N. *Polymer-Plastics Technology and Engineering* **2001**, *40*, 539.
(7) Sheth, J. P.; Klinedinst, D. B.; Wilkes, G. L.; Yilgor, I.; Yilgor, E. *Polymer* **2005**, *46*, 7317.
(8) Hernandez, R.; Weksler, J.; Padsalgikar, A.; Choi, T.; Angelo, E.; Lin, J. S.; Xu, L.-C.; Siedlecki, C. A.; Runt, J. *Macromolecules (Washington, DC, United States)* **2008**, *41*, 9767.
(9) Lomax, G. R. *Journal of Materials Chemistry* **2007**, *17*, 2775.
(10) Chattopadhyay, D. K.; Raju, K. V. S. N. *Progress in Polymer Science* **2007**, *32*, 352.
(11) Kumari, S.; Mishra, A. K.; Chattopadhyay, D. K.; Raju, K. V. S. N. *Journal of Polymer Science, Part A: Polymer Chemistry* **2007**, *45*, 2673.
(12) Kojio, K.; Mitsui, Y.; Furukawa, M. *Polymer* **2009**, *50*, 3693.
(13) Eceiza, A.; Martin, M. D.; de la Caba, K.; Kortaberria, G.; Gabilondo, N.; Corcuera, M. A.; Mondragon, I. *Polymer Engineering and Science* **2008**, *48*, 297.
(14) Caracciolo, P. C.; Buffa, F.; Abraham, G. A. *Journal of Materials Science: Materials in Medicine* **2009**, *20*, 145.
(15) Williams, S. R.; Wang, W.; Winey, K. I.; Long, T. E. *Macromolecules (Washington, DC, United States)* **2008**, *41*, 9072.
(16) Mather, B. D.; Miller, K. M.; Long, T. E. *Macromolecular Chemistry and Physics* **2006**, *207*, 1324.
(17) Mather, B. D.; Williams, S. R.; Long, T. E. *Macromolecular Chemistry and Physics* **2007**, *208*, 1949.
(18) Williams, S. R.; Mather, B. D.; Miller, K. M.; Long, T. E. *Polymer Preprints (American Chemical Society, Division of Polymer Chemistry)* **2007**, *48*, 833.
(19) Williams, S. R.; Miller, K. M.; Long, T. E. *Progress in Reaction Kinetics and Mechanism* **2007**, *32*, 165.
(20) Williams, S. R.; Mather, B. D.; Miller, K. M.; Long, T. E. *Journal of Polymer Science, Part A: Polymer Chemistry* **2007**, *45*, 4118.
(21) Clemens, R. J.; Del Rector, F. *Journal of Coatings Technology* **1989**, *61*, 83.
(22) Kilambi, H.; Stansbury, J. W.; Bowman, C. N. *Journal of Polymer Science, Part A: Polymer Chemistry* **2008**, *46*, 3452.
(23) Yamauchi, K.; Lizotte, J. R.; Long, T. E. *Macromolecules* **2002**, *35*, 8745.
(24) Coca, S.; Jasieczek, C. B.; Beers, K. L.; Matyjaszewski, K. *Journal of Polymer Science, Part A: Polymer Chemistry* **1998**, *36*, 1417.
(25) Ozturk, G.; Long, T. E. *Journal of Polymer Science, Part A: Polymer Chemistry* **2009**, *47*, 5437.

(26) Yilgor, I.; Yilgor, E.; Guclu Guler, I.; Ward, T. C.; Wilkes, G. L. *Polymer* **2006**, *47*, 4105.

Chapter 3. Urethane Diacrylate-Functionalized Multiwalled Carbon Nanotube Composites

3.1 Abstract

A two-step reaction of bis (4-isocyanatocyclohexyl) methane with α,ω-hydroxy-terminated poly(tetramethylene oxide) (PTMO, M_n 250, 1000, 2000 and 2900 g/mol), and 2-hydroxyethyl acrylate yielded urethane diacrylates (UtDA). Acetoacetylation reaction of 1,4-butanediol with *tert*-butyl acetoacetate produced 1,4-butanediyl-bis acetoacetate (1,4-BD BisAcAc). ^{1}H NMR spectroscopy confirmed the structures and end group analysis revealed the M_n of the precursors. Acid functionalization of C70 P Baytubes multiwalled carbon nanotubes (MWCNT) generated MWCNT-COOH. 0.01 wt. % MWCNT-COOH suspensions were prepared in organic solvents (chloroform, toluene, THF, DMF and 2-propanol). DLS of 0.01 wt. % of MWCNT-COOH suspensions indicated that average diameter for MWCNT-COOH particles in DMF and in 2-propanol were 139 nm and 162 nm respectively. FESEM of suspensions revealed that MWCNT-COOH dispersed free off aggregates in DMF and in 2-propanol. Incorporation of MWCNT-COOH yielded composite Michael networks. FESEM images of fracture surfaces of composites showed MWCNT-COOH dispersed homogeneously in the composites. DMA showed an increase in the rubbery plateau modulus, which correlated with the MWCNT-COOH content in the networks. Tensile testing also revealed a relationship between MWCNT-COOH content and Young's moduli and strain at break of networks. Storage moduli of networks increased from 25 MPa to 211 MPa with increasing MWCNT-COOH content whereas elongation at break decreased from 255 % to 146 %.

Keywords: crosslinking, multi-walled carbon nanotubes, composite, mechanical properties, Michael addition

3.2 Introduction

Iijima [75,76] observed multi-wall carbon nanotubes (MWCNT) for the first time in 1991 and single-wall carbon nanotubes (SWCNT) in 1993 and they attracted significant interest. Nanotubes have tubular structures that are typically of nanometer diameter and many micrometers in length. Due to their size and unique shape, these nanotubes exhibit interesting properties. Their lightweight, high tensile strength (50-100 GPa) and high modulus (1-2 TPa) enable them to be well-suited as reinforcing fillers for lightweight composite applications.[77] Researchers focused on various methods to disperse CNT in composite matrix such as ultrasonication,[78-80] high shear mixing of CNT composites,[81-85] melt mixing,[86-90] using polymeric compatiblizers,[91] and chemical functionalization.[77,92-109] The intrinsic van der Waals interactions prevent nanotubes to disperse resulting in large aggregates of bundles and ropes.[77] Acid functionalization of CNT exists as an alternative functionalization method. Acid functionalization of CNT surface provides many advantages over other functionalization reactions. Carboxylic acid groups on CNT (CNT-COOH) (i) increase solubility and dispersion in polar solvents such as water and ethanol; (ii) improve dispersion of CNT in polymers matrices; (iii) introduce possible chemical functionalization sites.[93,101,106,107,110,111]

Lee and others[127] described the preparation of 4-methoxybenzoic acid (4-MeO-BA) and 4-ethoxybenzoic acid (4-EtO-BA) functionalization of MWCNTs. Homogeneous dispersion of acid-functionalized and pristine MWCNTs was demonstrated in ethylene glycol. The results showed that MWCNT/poly(ethylene terephthalate) (PET) nanocomposites were achieved through polymerization of nanoparticle-containing ethylene glycol with terephthalic acid. Lee and colleagues characterized the composites utilizing SEM.

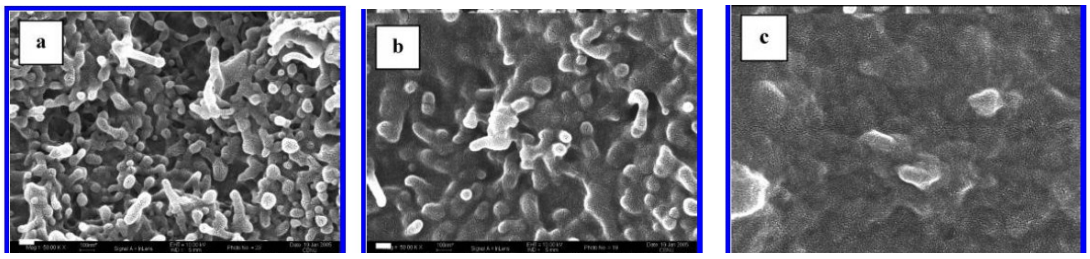

Figure 3.1 SEM images (X 50 K) of (a) MWCNT/PET (b) MeO-MWCNT/PET (c) EtO-MWCNT/PET. Scale bar is 100 nm. [127]

SEM images of the fracture surfaces of each film were captured. SEM showed that the dispersion of MWCNT in PET matrix improves through acid functionalization of MWCNTs. Large scale aggregates existed in MWCNT/PET nanocomposites (**Figure 3.1.a**).

Chen et al.[128] studied the functionalized MWCNT poly(L-lactic acid) composites of several poly(L-lactic acid) M_n. They reported further functionalization of the MWCNT-COOH into acyl-chloride-MWCNT and reacting them with poly(L-lactic acid) to graft polymer on to the MWCNT surface. The authors also reported preparation of solution dispersed MWCNT-poly (L-lactic acid) as controls. They characterized the nanocomposite morphology utilizing SEM and TEM. The SEM images showed grafted composites differ in dispersability from the solution-blended composites. Solution dispersed MWCNT-COOH demonstrated a reasonable dispersion within the polymer matrix; the amount of MWCNT-COOH and the degree of dispersion of grafted samples were superior to solution dispersed samples. These efforts show functionalization of MWCNT greatly improves the dispersion of MWCNT within the polymer matrix.

3.3 Experimental

3.3.1 Materials

tert-Butyl acetoacetate (t-BuAcAc, reagent grade, 98%), 1,4-butanediol (1,4-BD, reagent plus, >99%), 1,8-diazobicyclo[5.4.0]undec-7-ene (DBU, 98%), dibutyl tin dilaurate (DBTDL, 95%), 2,6-di-*tert*-butyl-4-methylphenol (BHT, >99%), magnesium sulfate (reagent plus, anhydrous, 99 %) were purchased from Sigma Aldrich and were used as received. 2-hydroxyethyl acrylate (HEA, 96%) was purchased from Aldrich and purified as previously described.[126] PTMO polyols (Mn 250, 1000, 2000 and 2900 g/mol) were purchased from Sigma Aldrich were purchased and degassed at 60 °C for ~12h. Bis (4-isocyanatocyclohexyl) methane (HMDI, >99.5%) and C70 P BayTubes multiwall carbon nanotubes (MWCNT) were graciously donated by Bayer Material Science. Toluene (Fischer, HPLC grade) was distilled from magnesium sulfate and was stored over activated 4Å molecular sieves immediately prior to use. Methanol (Fischer, HPLC grade) was used without purification. 2-propanol (>99.5%, anhydrous) was purchased from Sigma Aldrich and used without further treatment. Dibutyl tin dilaurate (DBTDL, 95%) was dissolved in THF as a 1 wt. % solution. Ultrahigh-purity nitrogen gas was used as inert reaction atmosphere.

3.3.2 Synthesis of PTMO-Based Urethane Resins

Freshly distilled toluene (35 mL), HMDI (10.49 g, 40.0 mmol), and DBTDL solution (0.01 mL) were introduced into a two-neck, round-bottomed flask equipped with a stir bar, addition funnel and nitrogen inlet. The PTMO polyol (1100 g/mol by ^{1}H NMR, 22.0 g, 20.0 mmol) was dissolved in toluene (68 mL) and was charged into the addition funnel. Dropwise addition of PTMO into the HMDI solution was completed over ~30 min. The reaction was

allowed to proceed for 2 h and the temperature was maintained at 80 °C for 2 h. The reaction temperature was reduced to 60 °C. HEA (4.70 g, 40.5 mmol) was dissolved in toluene (16 mL), charged into the addition funnel and added dropwise over ~30 min. The reaction proceeded for 3 h at 60 °C after completion of the addition of HEA. BHT (50 mg) was added to prevent polymerization of the product. The solvent was removed in a rotary evaporator. The resulting viscous liquid was dried at reduced pressure (0.1 mm Hg) at room temperature for 24 h to a constant weight.

3.3.3 Synthesis of 1, 4-Butanediol-Based Michael Donor

Acetoacetylation of 1,4-butanediol with t-BuAcAc adapted from a procedure described previously in the literature yielded 1,4-BD BisAcAc.[53-55,58] Briefly, PTMO polyol and t-BuAcAc (1:4 mol eq.) were dissolved in toluene (30 wt. % solution) and the solution was charged into a flask equipped with a short-path distillation head, receiving flask, and magnetic stirrer. The mixture was maintained at 110 °C for 3 h under gentle vacuum (100 mmHg) was applied to remove the tert-butanol by-product and excess t-BuAcAc. An additional 2 mol eq. of t-BuAcAc was added and heating continued for another 3 h at 110 °C. Finally high vacuum (0.1 mmHg) at 110 °C was applied to remove volatile starting reagents, solvent and reaction by products. The BisAcAc oligomer structure was confirmed by ^{1}H NMR spectroscopy. ^{1}H NMR (400 MHz, 50 mg/mL, $CDCl_3$) of the 1,4-BD BisAcAc, δ= 1.49 ppm(t, 4H), δ= 2.26 ppm (s, 6H), δ= 3.4 ppm (s, 4H), δ=4.14 ppm (m,4H), δ=4.90 ppm (s, -enol C=CH-C=O).

3.3.4 Acid Functionalization of MWCNT

MWCNT were surface functionalized with a similar procedure previously described in the literature. [77,106] C 70 P type Baytubes MWCNTs (10 g.) and 50 mL of 8M Nitric acid was charged in a 2-neck round bottom flask equipped with a nitrogen inlet and a condenser. MWCNTs were refluxed for 24h, filtered and washed subsequently DI water. Collected sample was charged in a 2-neck round bottom flask 50 mL of 1 M HCl was added. This mixture was refluxed for 24h. After cooling down to room temperature MWCNT suspension was filtered and washed with 200 mL of DI water (5 X) and subsequently 100 mL of methanol (5X). Acid-functionalized MWCNT (MWCNT-COOH) was filtered off and dried under reduced pressure (0.1 mm Hg) at 100 °C for 24 h.

3.3.5 Preparation of MWCNT-COOH Suspension in Organic Solvent

2-propanol was filtered through a 0.45-μm filter. Dried 1.00 g of MWCNT-COOH, 99.00 g of 2-propanol, and a magnetic stir bar was charged into a 150 mL 1-neck round bottom flask. This suspension was sonicated in a sonicator bath for 1 h and subsequently sonicated with a sonicator probe and simultaneously stirred with a magnetic stirrer for 1 h. 1.00 wt. % of MWCNT-COOH in 2-propanol suspension was obtained.

3.3.6 Preparation of MWCNT-COOH-containing UtDA Michael Networks

7.25 g of 1.00 wt. % MWCNT-COOH suspension in 2-propanol, 1,4-BD BisAcAc (2.26 g, 0.875 mmol eq.), UtDA 1000 (1.365 g, 1.23 mmol, 1.4 mol eq.) were mixed thoroughly to form a homogeneous mixture. This mixture was sonicated for 30 min in a sonicator bath. DBU catalyst was quickly added and mixed thoroughly. 500μ-layer of this mixture was coated on

Mylar® substrate with an adjustable film applicator. Coatings were allowed to crosslink for 24 h at room temperature. The films were dried at reduced pressure (0.1 mmHg) at 60 °C for 24 h.

3.4 Characterization

^{1}H NMR spectroscopy confirmed PTMO diacrylate and bisAcAc oligomer composition, end group analyses yielded number average molecular weight of diacrylates. A 400 MHz Varian Inova NMR spectrometer was used to characterize the oligomers in $CDCl_3$ at 23 °C. FESEM was conducted on a Zeiss EVO40 XVP FESEM, at EHT=10kV and WD= 5.5 mm. DLS was conducted on a Malvern Instruments Nano ZS (633 nm He-Ne red laser), with a detector angle of 173°. DSC was conducted on a TA Instruments Q100, under nitrogen at 10 ºC/min heating rate. DMA was performed on a TA Instruments Q800 Dynamic Mechanical Analyzer in tension mode at a frequency of 1 Hz, an oscillatory amplitude of 15 μm, and a static force of 0.01 N. The temperature ramp was 3 °C/min. T_g's were determined at the peak of the tan δ curve. Sample films were solution-cast from 2-propanol on a Mylar® substrate, and films were annealed at 60 °C under reduced for 24 h. Tensile tests were performed on an Instron 4411 universal testing instrument with a cross-head speed of 20 mm/min using manual grips at ambient temperature. Stress–strain experiments were conducted with rectangular film specimens. The reported data represents an average of at least five specimens. The networks were characterized for gel fraction using Soxhlet extractions in THF reflux for 6 h. Extracted samples were subsequently dried in an oven at reduced pressure (0.1 mmHg) at 60 °C for 24 h, until constant weight was observed. The gel fraction was determined gravimetrically, via dividing the initial mass (mi) by the final mass (mf). 90 % or higher gel fractions were observed.

3.5 Results and Discussion

A 2-step "prepolymer" method was utilized to synthesize urethane diacrylates from reaction of HMDI with α,ω-hydroxyl-terminated PTMO polyol, and HEA. ^{1}H NMR spectroscopy confirmed the composition and the absence of by-products in the precursors. **Scheme 3.1** depicts the synthesis of urethane diacrylates (UtDA).

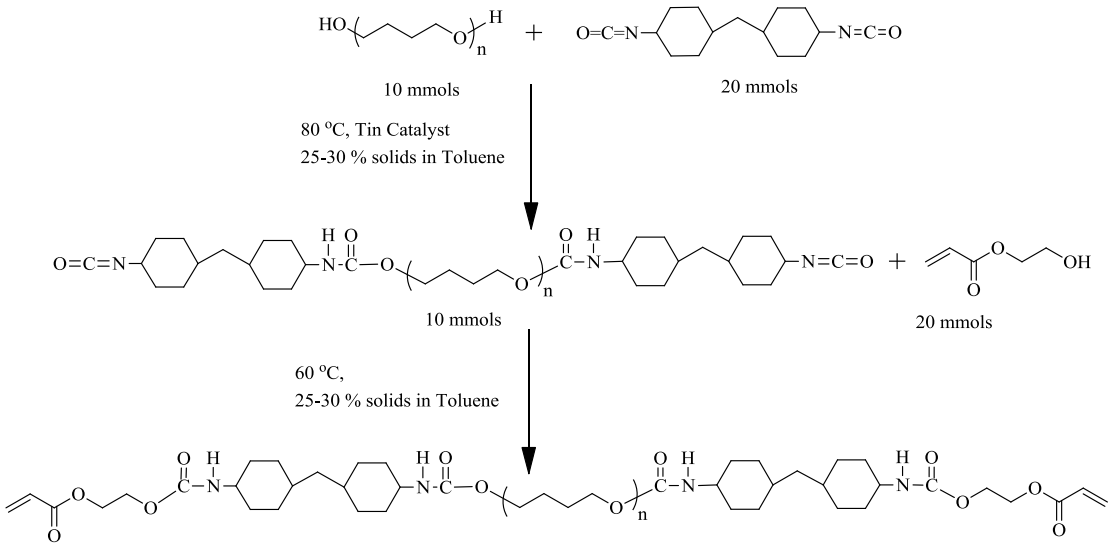

Scheme 3.1. Two-step synthesis of PTMO-based urethane diacrylates (UtDA)

The Michael donor 1,4-BD BisAcAc was synthesized using acetoacetylation of 1,4-butanediol according to a method adapted from Long *et al.* [53](**Scheme 3.2**). The reactions were conducted holding the system at toluene reflux under mild vacuum (100 mm Hg) to remove the t-butyl alcohol by-product to drive the reaction to completion. Finally high vacuum (0.1 mmHg) at 110 °C were applied for 3 hours to remove volatile starting reagents, solvent and reaction by products.

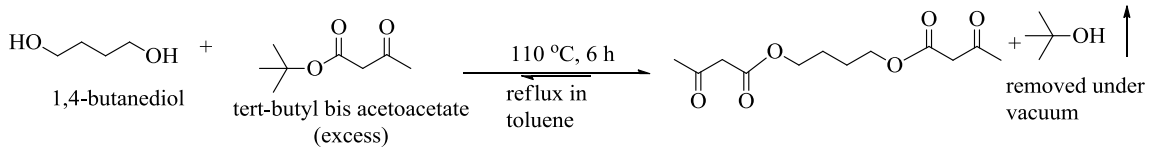

Scheme 3.2. Acetoacetylation of 1,4-butanediol

The Michael acceptors consist of 1000, 2000, 3000, 3600 g/mol M_n UtDA. DLS was performed with 0.01 wt. % suspension of MWCNT-COOH in (DMF, 2-propanol, THF, toluene, chloroform) HPLC grade solvents. Solvents were passed through a 0.45-µ filter. Previously prepared 1.00 weight % MWCNT-COOH suspension was diluted with required amount of different solvents to achieve 0.01 weight % suspensions. These suspensions were sonicated in a sonicator bath for 1 hour prior to DLS experiments. The suspensions showed different degrees of dispersion/aggregation.

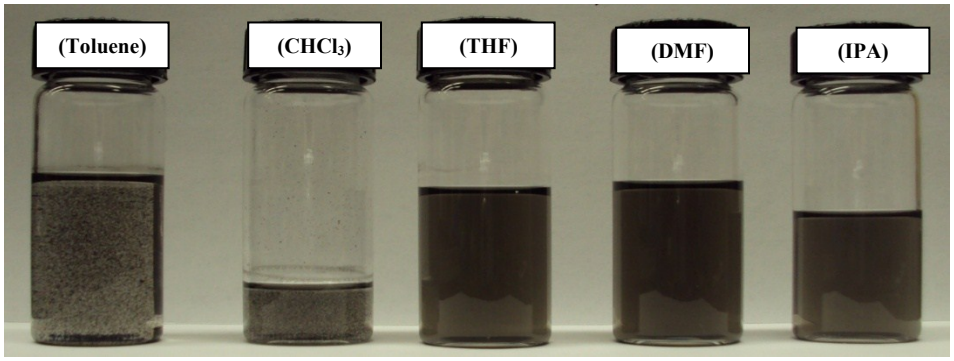

Figure 3.2 0.01 weight % suspensions of MWCNT-COOH after 30 min.

Figure 3.2 shows the images of 0.01 weight % MWCNT-COOH suspensions 30 minutes after sonication. MWCNT-COOH in toluene and chloroform formed visible aggregates. **Figure 3.3** shows the DLS curves of these MWCNT-COOH suspensions.

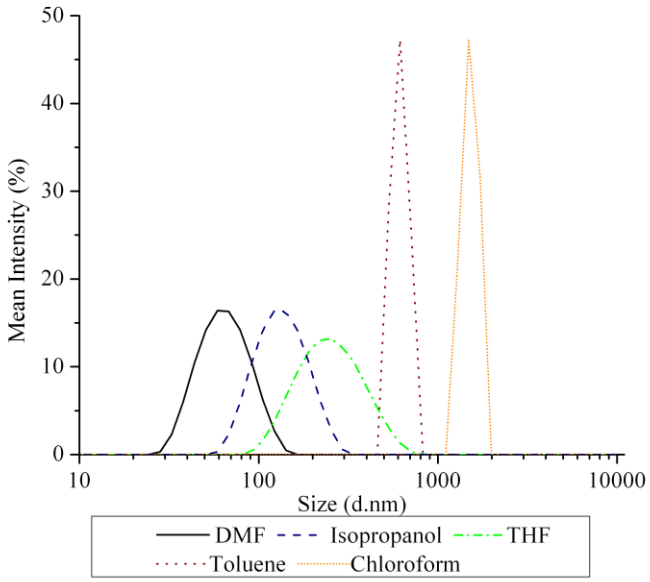

Figure 3.3. DLS traces of 0.01 weight % suspensions of MWCNT-COOH

DLS of 0.01 wt. % of MWCNT-COOH suspensions indicated that average diameter for MWCNT-COOH particles 139 nm for DMF, 162 nm for 2-propanol, 229 nm for THF, 615 nm for toluene, and 1561 nm for chloroform. Toluene and chloroform suspensions showed significant amount of aggregation. MWCNT-COOH dispersed homogeneously in DMF and 2-propanol. 2-propanol was selected as the casting solvent for MWCNT-COOH-UtDA composites since DMF was a poor casting solvent for UtDAs.

FESEM was conducted on a Zeiss EVO40 XVP FESEM. 0.01 weight % suspensions of MWCNT-COOH in chloroform, 2-propanol, DMF, THF, and toluene, was prepared as described above. These suspensions were cast on silicone substrates. Electron high tension was set to 10 kV, working distance was set to 5.5 mm.

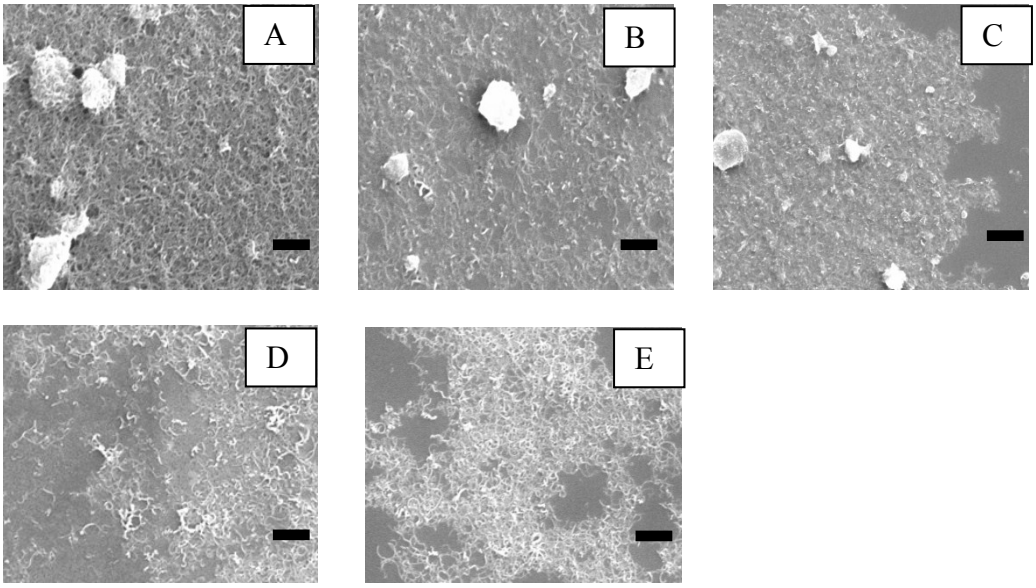

Figure 3.4. FESEM images of (X 20k) of MWCNT-COOH suspensions in (A)Toluene (B)Chloroform (C)THF (D) DMF (E) 2-propanol. (1μ Scale bars)

FESEM revealed the presence of large MWCNT-COOH aggregates in chloroform, THF, and toluene suspensions (**Figure 3.4**). MWCNT-COOH coils were homogeneously dispersed in 2-propanol and DMF. FESEM images agreed with the particle size distribution measurements with DLS. FESEM confirmed 2-propanol and DMF are good dispersion solvents for MCWNT-COOH suspensions.

Composite networks of MWCNT-COOH in urethane diacrylates were prepared to investigate the influence of MWCNT-COOH in urethane network matrix. 1.00 weight % 2-propanol-MWCNT-COOH suspension, 1,4-BD BisAcAc, and PTMO UtDA (1.365 g, 1.23 mmol, 1.4 mol eq.) were mixed thoroughly to form a homogeneous mixture. This mixture was sonicated for 30 min in a sonicator bath. DBU catalyst was quickly added and mixed thoroughly. 500μ-layer of the mixture was coated on Mylar® substrate with an adjustable film applicator (**Scheme 3.3**).

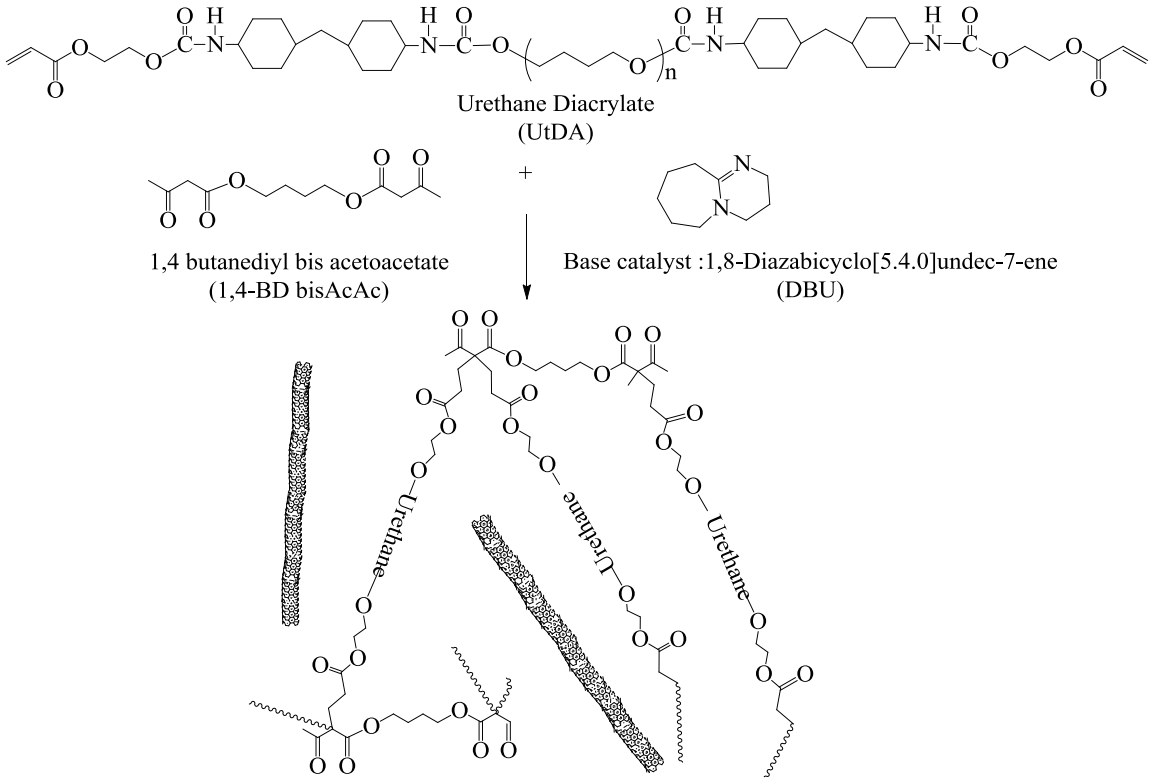

UtDA-1,4 BD BisAcAc MWCNT-COOH composite network

Scheme 3.3. Michael addition of MWCNT-COOH containing UtDA to 1,4-BD BisAcAc

FESEM was conducted on fracture surfaces of UtDA 1,4-BD BisAcAc-MWCNT-COOH composites. These polymer films were sputter coated with gold for 45 s. Electron high tension (EHT) was set to 10 kV, working distance (WD) was set to 5.5 mm. **Figure 3.5** shows fracture surfaces of 3 different composite matrices.

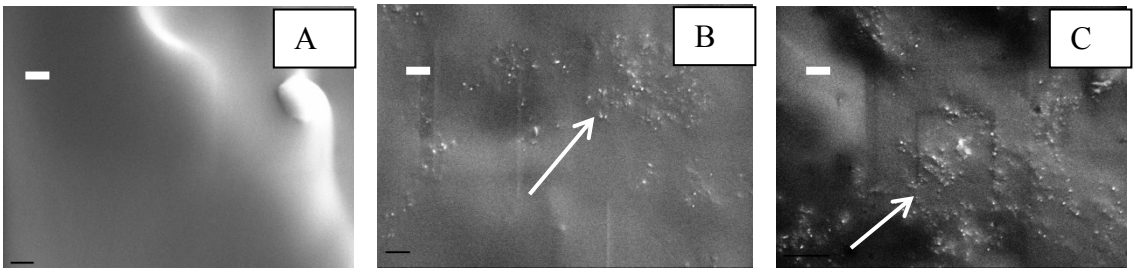

Figure 3.5 FESEM images (X20 K) of UtDA 1000-1,4BD BisAcAc-MWCNT-COOH. A) Pristine network. B) 1.0 wt. % C) 2.0 wt. % MWCNT-COOH containing networks. 1µ Scale bars.

The fracture surface of 2.0 wt. % MWCNT-COOH composites contains a higher density of MWCNT-COOH surfaces which provides a visual confirmation for presence of a higher concentration of MWCNT-COOH in the UtDA network. FESEM images also show a random distribution of MWCNT-COOH on the polymer fracture surface. This result indicates relatively even dispersion of MWCNT-COOH within the polymer matrix.

The thermal transitions of MWCNT-COOH-containing networks were investigated using DSC. **Figure 3.6** shows an overlay of DSC thermograms UtDA 1000 containing different amounts of MWCNT-COOH particles.

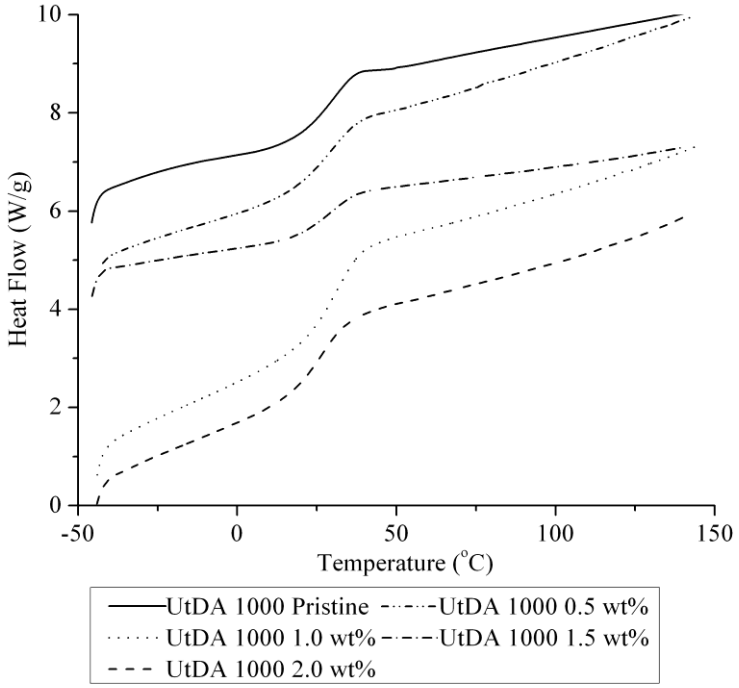

Figure 3.6 DSC comparison of UtDA 1000-1,4 BD BisAcAc- MWCNT-COOH networks

DSC thermogram indicates the 1000 g/mol UtDA – 1,4-BD BisAcAc network has a T_g of 23 °C, and with increasing MWCNT-COOH content network T_g remains constant. This result was

attributed to inability of small scale MWCNT-COOH in composites restrict the long range segmental motion of polymer chains between crosslink points.

The storage modulus and rubbery plateau modulus of composites improved with presence of MWCNT-COOH. The DMA curves showed a constant T_g (25 °C for UtDA 1000- 1,4 BD BisAcAc composite networks) for 3 different concentrations (1.0, 2.0, and 5.0 wt.%) of MWCNT-COOH-UtDA composite networks (**Figure 3.7**)**.** Increasing MWCNT-COOH content enhanced the storage moduli of the composites. The tan δ curves also indicate rubbery plateau moduli improve with increasing MWCNT-COOH content. This observation was attributed to higher restriction of segmental motion due to mixing of MWCNT-COOH with UtDA on a molecular level.

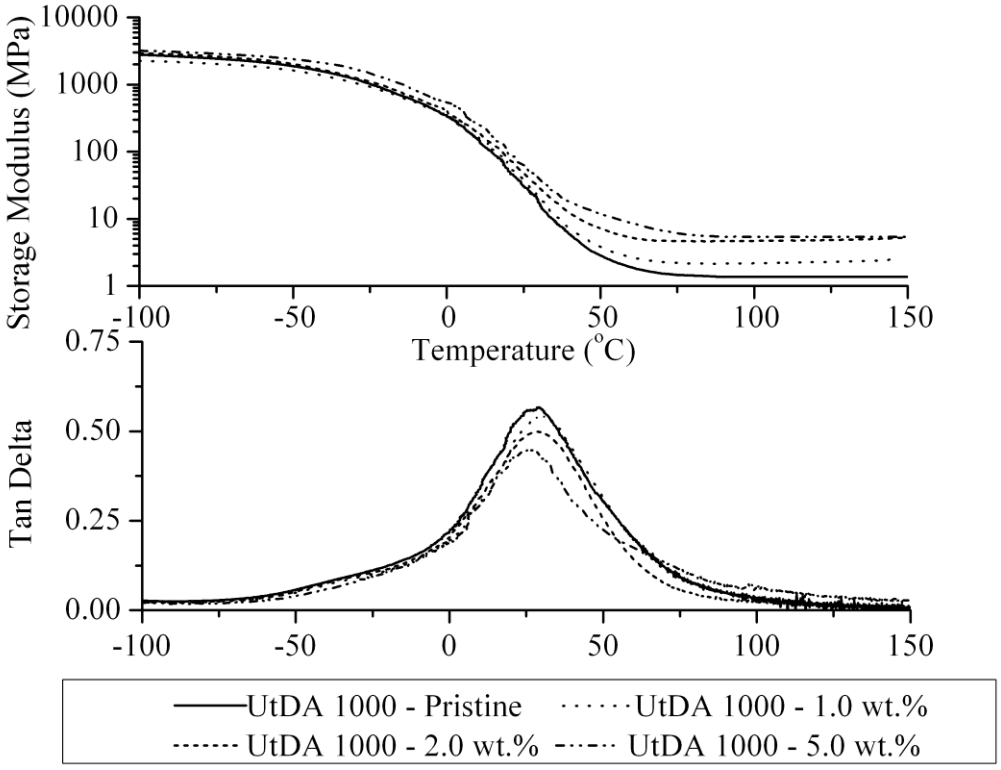

Figure 3.7 DMA comparison of UtDA 1000-1,4 BD BisAcAc- MWCNT-COOH networks

Tensile properties of the networks were analyzed using an Instron 4411 testing machine with a minimum of five samples for each network. **Figure 3.8** shows a representative plot of tensile tests for each MWCNT-COOH content in UtDA 1000 1,4 BD BisAcAc networks.

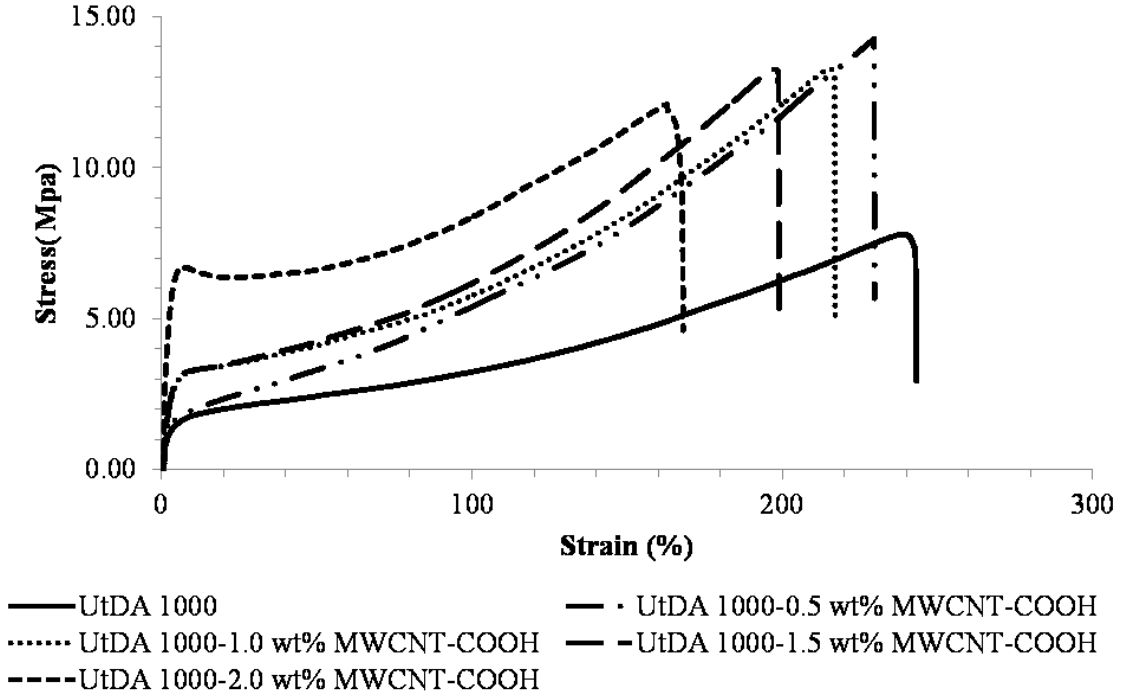

Figure 3.8 Tensile comparison of urethane diacrylate-1,4BD BisAcAc networks with 0 to 2 weight % MWCNT-COOH content.

Tensile test results indicate Young's moduli increases with and increasing MWCNT-COOH content. The toughness of networks improved significantly even with the 0.5 weight % MWCNT-COOH content. The Young's modulus of networks shows a sharp increase as the MWCNT-COOH content reaches 1.5 wt. % of the network. This outcome ascribed to reaching the percolation threshold of MWCNT-COOH in networks resulting in enhanced mechanical properties. Elongation of composite networks decreases with increasing MWCNT-COOH content. These results indicate the stiffness of the composite networks increases with higher

nanoparticle content which we attributed to interaction of high modulus of MWCNT with composite networks in a molecular level (**Table 3.1)**.

Table 3.1 Tensile data comparison for urethane diacrylate-1,4-BD BisAcAc networks with 0 to 2 weight % MWCNT-COOH contents

Network	Young's Modulus (MPa)	Stress at Break (MPa)	Elongation at Break (%)
UtDA 1000 – 0 wt.%	25.3 ± 5.7	7.2 ± 1.3	255 ± 25
UtDA 1000 – 0.5 wt.%	23.5 ± 2.8	12.2 ± 0.8	220 ± 14
UtDA 1000 – 1.0 wt.%	54.91 ± 5.2	11.6 ± 1.3	207 ± 9
UtDA 1000 – 1.5 wt.%	156.7 ± 33.1	12.9 ± 0.8	202 ± 31
UtDA 1000 – 2.0 wt.%	211.4 ± 24.4	10.6 ± 0.6	146 ± 21

The surface resistivity measurements indicated increasing MWCNT-COOH content reduces the surface resistivity. The unmodified polymer coating had surface resistivity above 10^{12} ohm/cm^2 and composites became less resistive with increasing MWCNT-COOH content. 2 weight percent of MWCNT-COOH improved surface resistivity of these films by three orders of magnitude. Similar trend in surface resistivity was observed throughout all samples with the same weight percent of MWCNT-COOH.

Table 3.2 Surface resistivity for urethane diacrylate-1,4BD BisAcAc networks

Network	Surface Resistivity (Ω/cm^2)
UtDA 1000 – 0 wt.%	10^{12}
UtDA 1000 – 0.5 wt.%	10^{12}
UtDA 1000 – 1.0 wt.%	10^{11}
UtDA 1000 – 1.5 wt.%	10^{10}
UtDA 1000 – 2.0 wt.%	10^{9}

3.6 Conclusions

PTMO-based urethane diacrylate precursors were synthesized from, α,ω-hydroxy-terminated PTMO polyol, bis (4-isocyanatocyclohexyl) methane and 2-hdroxyethyl acrylate. 1,4-butanediyl-bis acetoacetate was prepared from acetoacetylation of 1,4-butanediol, with tert-butyl bis acetoacetate. ^{1}H NMR spectroscopy confirmed the structures and M_n of the precursors. Acid functionalization of C70 P Baytubes multiwalled carbon nanotubes (MWCNT) generated MWCNT-COOH. Magnetic stirring and sonication of Baytubes MWCNT in 2-propanol and MWCNT-COOH in chloroform, toluene, THF, DMF and 2-propanol yielded MWCNT-COOH suspensions (0.01 wt. % of nanoparticle concentration). FESEM images showed MWCNT-COOH dispersed free of aggregates compared to MWCNT suspension in 2-propanol. DLS of 0.01 wt. % MWCNT-COOH suspensions revealed presence of large particles of MWCNT-COOH in toluene, THF and chloroform. Average particle size of MWCNT-COOH dispersed in THF, toluene, and chloroform were 229, 615, and 1561 nm respectively. Average particle size of MWCNT-COOH dispersed in DMF and 2-propanol were 139 and 162 nm respectively. FESEM images of 0.01 weight % MWCNT-COOH suspensions showed μ-scale aggregates of MWCNT-COOH in toluene, chloroform and some aggregation in THF. FESEM images of 0.01 wt. % MWCNT-COOH suspensions revealed aggregate free dispersion of MWCNT-COOH in DMF and 2-propanol. Michael reaction of MWCNT-COOH-UtDA precursor mixtures to 1,4-BD BisAcAc yielded composite networks. FESEM images of fracture surfaces of UtDA showed a random distribution of MWCNT-COOH on the fracture surface which indicated well dispersion of MWCNT-COOH in network matrix. DSC and DMA experiments revealed that T_g of diacrylate networks was not effected with MWCNT-COOH content in the composites. DMA showed an increase in the rubbery plateau modulus which correlated with the MWCNT-COOH

content in the networks. Tensile testing also revealed a relationship between MWCNT-COOH content and Young's moduli and strain at break of networks. Storage moduli of networks increased from 25 MPa for pristine to 211 MPa 2.0 wt. % MWCNT-COOH containing networks whereas elongation at break decreased from 255 to 146 % for the same networks. Surface resistivity measurement showed, increasing MWCNT-COOH content increases the amount of MWCNT-COOH on the surface which improves the surface resistivity.

3.7 Acknowledgements

Research was sponsored by the Army Research Laboratory and was accomplished under Cooperative Agreement Number W911NF-06-2-0014. The views and conclusions contained in this document are those of the authors and should not be interpreted as representing official policies, either expressed or implied, of the Army Research Laboratory or the U.S. Government. The U.S. Government is authorized to reproduce and distribute reprints for Government purposes not withstanding any copyright notation here on.

3.8 References

(1) Iijima, S. *Nature (London, United Kingdom)* **1991**, *354*, 56.
(2) Iijima, S.; Ichihashi, T. *Nature (London, United Kingdom)* **1993**, *363*, 603.
(3) Zhu, J.; Kim, J.; Peng, H.; Margrave, J. L.; Khabashesku, V. N.; Barrera, E. V. *Nano Letters* **2003**, *3*, 1107.
(4) Biercuk, M. J.; Llaguno, M. C.; Radosavljevic, M.; Hyun, J. K.; Johnson, A. T.; Fischer, J. E. *Applied Physics Letters* **2002**, *80*, 2767.
(5) Coleman, J. N.; Dalton, A. B.; Curran, S.; Rubio, A.; Davey, A. P.; Drury, A.; McCarthy, B.; Lahr, B.; Ajayan, P. M.; Roth, S.; Barklie, R. C.; Blau, W. J. *Advanced Materials (Weinheim, Germany)* **2000**, *12*, 213.
(6) Ajayan, P. M.; Schadler, L. S.; Giannaris, C.; Rubio, A. *Advanced Materials (Weinheim, Germany)* **2000**, *12*, 750.
(7) Cao, S.-z.; Sun, X.-g.; Zeng, X.-s. *Jixie Gongcheng Cailiao* **2008**, *32*, 50.
(8) Andrews, R.; Jacques, D.; Minot, M.; Rantell, T. *Macromolecular Materials and Engineering* **2002**, *287*, 395.
(9) Chen, G.-X.; Shimizu, H. *PMSE Preprints* **2007**, *96*, 685.
(10) Obrzut, J.; Douglas, J. F.; Kharchenko, S. B.; Migler, K. B. *Physical Review B: Condensed Matter and Materials Physics* **2007**, *76*, 195420/1.
(11) Chen, G.-X.; Li, Y.; Shimizu, H. *Carbon* **2007**, *45*, 2334.
(12) Masuda, J. i.; Torkelson, J. M. *Macromolecules (Washington, DC, United States)* **2008**, *41*, 5974.
(13) Broza, G.; Schulte, K. *Polymer Engineering and Science* **2008**, *48*, 2033.
(14) Poetschke, P.; Bhattacharyya, A. R.; Abdel-Goad, M.; Janke, A.; Goering, H. *ACS Symposium Series* **2005**, *898*, 164.
(15) Pujari, S.; Ramanathan, T.; Kasimatis, K.; Masuda, J. i.; Andrews, R.; Torkelson, J. M.; Brinson, L. C.; Burghardt, W. R. *Journal of Polymer Science, Part B: Polymer Physics* **2009**, *47*, 1426.
(16) Manchado, M. A. L.; Valentini, L.; Biagiotti, J.; Kenny, J. M. *Carbon* **2005**, *43*, 1499.
(17) Zhang, J. X.; Zheng, Y. P.; Yu, P. Y.; Mo, S.; Wang, R. M. *Carbon* **2009**, *47*, 2776.
(18) Gotovac, S.; Yang, C.-M.; Hattori, Y.; Takahashi, K.; Kanoh, H.; Kaneko, K. *Journal of Colloid and Interface Science* **2007**, *314*, 18.
(19) Balasubramanian, K.; Burghard, M. *Small* **2005**, *1*, 180.
(20) Titus, E.; Ali, N.; Cabral, G.; Gracio, J.; Babu, P. R.; Jackson, M. J. *Journal of Materials Engineering and Performance* **2006**, *15*, 182.
(21) Liang, F.; Sadana, A. K.; Peera, A.; Chattopadhyay, J.; Gu, Z.; Hauge, R. H.; Billups, W. E. *Nano Letters* **2004**, *4*, 1257.
(22) Dyke, C. A.; Tour, J. M. *Journal of Physical Chemistry A* **2004**, *108*, 11151.
(23) Agrawal, S.; Raghuveer, M. S.; Kroger, R.; Ramanath, G. *Journal of Applied Physics* **2006**, *100*, 094314/1.
(24) Bekyarova, E.; Itkis, M. E.; Cabrera, N.; Zhao, B.; Yu, A.; Gao, J.; Haddon, R. C. *Journal of the American Chemical Society* **2005**, *127*, 5990.
(25) Wang, C.; Cao, Q.; Ozel, T.; Gaur, A.; Rogers, J. A.; Shim, M. *Journal of the American Chemical Society* **2005**, *127*, 11460.
(26) Tobias, G.; Shao, L. D.; Ballesteros, B.; Green, M. L. H. In *2nd ChemOnTubes International Conference* Zaragoza, SPAIN, 2008; Vol. 9, p 6072.

(27) Lin, S.-T.; Wei, K.-L.; Lee, T.-M.; Chiou, K.-C.; Lin, J.-J. *Nanotechnology* **2006**, *17*, 3197.
(28) Xia, W.; Jin, C.; Kundu, S.; Muhler, M. *Carbon* **2009**, *47*, 919.
(29) Yu, H.; Jin, Y.; Peng, F.; Wang, H.; Yang, J. *Journal of Physical Chemistry C* **2008**, *112*, 6758.
(30) de Heer, W. A. *MRS Bulletin* **2004**, *29*, 281.
(31) Escobar, M.; Goyanes, S.; Corcuera, M. A.; Eceiza, A.; Mondragon, I.; Rubiolo, G. H.; Candal, R. J. In *2nd ChemOnTubes International Conference* Zaragoza, SPAIN, 2008; Vol. 9, p 6228.
(32) Peng, H.; Alemany, L. B.; Margrave, J. L.; Khabashesku, V. N. *Journal of the American Chemical Society* **2003**, *125*, 15174.
(33) Zeng, L.; Zhang, L.; Barron, A. R. *Nano Letters* **2005**, *5*, 2001.
(34) Long, B.; Wu, T. M.; Stellacci, F. *Chemical Communications (Cambridge, United Kingdom)* **2008**, 2788.
(35) Geng, H.; Rosen, R.; Zheng, B.; Shimoda, H.; Fleming, L.; Liu, J.; Zhou, O. *Advanced Materials (Weinheim, Germany)* **2002**, *14*, 1387.
(36) Zhang, L.; Kiny, V. U.; Peng, H.; Zhu, J.; Lobo, R. F. M.; Margrave, J. L.; Khabashesku, V. N. *Chemistry of Materials* **2004**, *16*, 2055.
(37) Jian Chen, M. A. H., Hui Hu, Yongsheng Chen,; Apparao M. Rao, P. C. E., Robert C. Haddon **1998**, *282*, 95.
(38) Lee, H.-J.; Oh, S.-J.; Choi, J.-Y.; Kim, J. W.; Han, J.; Tan, L.-S.; Baek, J.-B. *Chemistry of Materials* **2005**, *17*, 5057.
(39) Chen, G.-X.; Kim, H.-S.; Park, B. H.; Yoon, J.-S. *Journal of Physical Chemistry B* **2005**, *109*, 22237.
(40) Coca, S.; Jasieczek, C. B.; Beers, K. L.; Matyjaszewski, K. *Journal of Polymer Science, Part A: Polymer Chemistry* **1998**, *36*, 1417.
(41) Ozturk, G.; Long, T. E. *Journal of Polymer Science, Part A: Polymer Chemistry* **2009**, *47*, 5437.
(42) Williams, S. R.; Miller, K. M.; Long, T. E. *Progress in Reaction Kinetics and Mechanism* **2007**, *32*, 165.
(43) Williams, S. R.; Mather, B. D.; Miller, K. M.; Long, T. E. *Polymer Preprints (American Chemical Society, Division of Polymer Chemistry)* **2007**, *48*, 833.
(44) Williams, S. R.; Mather, B. D.; Miller, K. M.; Long, T. E. *Journal of Polymer Science, Part A: Polymer Chemistry* **2007**, *45*, 4118.

Chapter 4. Preparation of UV Cured Poly(tetramethylene oxide)-Based Urethane Networks

4.1 Abstract

A two-step reaction between bis(4-isocyanatocyclohexyl)methane, α,ω-hydroxy-terminated Poly(tetramethylene oxide) (PTMO M_n 250, 1000, 2000 and 2900 g/mol**)** polyols, and 2-hydroxyethyl acrylate produced urethane diacrylate precursors (UtDA). ^{1}H NMR spectroscopy utilized to determine the structures and molecular weights of UtDAs. The mixtures of pentaeriythritol tetra acrylate (PETA) and UtDA were prepared in 1:2 mol ratios. 2,2-dimethoxy-2-phenylacetophenone (DMPA) (1 wt. % of the mixture) containing mixtures were cast on glass slides. These slides were passed through a Fusion UV system at 6 ft.min^{-1} belt speeds and 1.42 ± 0.05 W.cm^2 for each pass to achieve photo-crosslinking. UV exposure of thin films yielded covalent network with 90% or above gel fractions. FT-IR spectroscopy showed disappearance of acrylate which ascribed the completion of crosslinking reaction. UV/Vis spectroscopy investigation showed the decrease in the UV absorption of the films upon UV irradiation. DMA demonstrated the presence of broad glass transition regions with a range of T_g's. The T_g's varied from -60 °C to -30 °C. Tensile testing also revealed the relationship between Young's moduli, strain at break and the molecular weight of the diacrylates. The increasing M_n of urethane diacrylates resulted in a significant drop in the storage moduli of the networks from 15.8 to 1.4 MPa and an increase in elongation at break from 76 to 132 %.

4.2 Introduction

Polyurethanes (PU) are a unique class of polymers that have a wide range of applications because their properties can be readily tailored by the variations of their components. Crosslinked polyurethanes have a wide range of applications in membranes, coatings[39], adhesives[40,41], medicine[42], biomedical and bioengineering applications[43-45], and in electronic devices[46]. The major advantages of crosslinking introduce to polyurethanes are additional mechanical resistance and high temperatures of deformation and/or degradation. The presence of crosslinks provides enhanced tensile strength, abrasion resistance as well as acid and solvent resistance. UV curing of linear SPU precursors with acrylic-functionality (hydroxyl ethyl acrylate, HEA, or 2-hydroxyl ethyl methacrylate HEMA) remains as another alternative to prepare crosslinked networks.[35,59-66] UV curing saves energy and reduces or eliminates solvent compared with solvent-based systems because most formulations consist of only reactive oligomers and diluents. [59,60,63-66] UV-curable urethane acrylates also minimizes possible side reactions upon application and has excellent optical properties.[45] A UV-curable system is typically composed of reactive urethane oligomers, reactive diluents, and photoinitiators.[64] Reactive urethane precursor is the most important component that determines the ultimate physical properties of UV-cured networks. Traditionally, it is a segmented PU oligomer end-capped with acrylic functionality, such as 2-hydroxyethylacrylate (HEA) and 2-hydroxyethyl methacrylate (HEMA).[60] In some cases reactive acrylic monomers such as acrylamide and acrylic acid are present to modify the properties and to reduce the viscosity of the precursor mixtures.[64] Compared to 2-component (solvent-based) urethane resins, PU-based UV resins have advantages concerning environment, health and safety. One of the main disadvantages of 2-component systems is the long curing times. UV curing provides with high hardness, high

solvent and stain resistance due to the high crosslink density. However, most UV cures systems inevitably lack flexibility due the high crosslinking density.[65]

Kim and others [64] studied synthesis of UV-curable PU acrylates were prepared from various PEGs (400, 600, 1000,2000, 4000 g/mol M_n) , aliphatic, cycloaliphatic, and aromatic diisocyanates, acrylamide, and acrylic acid diluents. Authors investigated the influence of PEG M_n, the type of diisocyanate, and the diluent content in terms of mechanical properties. Tensile testing of the UV-cured PU acrylates that are based on PEGs with different molecular showed Young's modulus and the stress at break decrease and elongation at the break) increased with increasing M_n of PEG. Presence of crystallinity in networks prepared from PEG 4000 g/mol increased the Young's modulus stress at break. Authors showed the presence of crystalline domains both with DSC and x-ray diffraction experiments. Authors also compared the tensile properties of the UV-cured PU acrylates that are based on PEG 2000 with different types of diisocyanate. Young's moduli, stress at break and strain at break improved in the order of IPDI, HDI, TDI, HMDI. They attribute these results to the decreasing degree of flexibility and the increasing symmetry of the urethane segments in the given order. Ahn and others [65] synthesized tri-armed PU prepolymers of various molecular weights, utilizing PTMO, a hexane diisocyanate (HDI) trimer, and using HEA, pentaerythritol triacrylate, aminopropyl triethoxy silane as end-capping agents. They investigated the effect of prepolymer molecular weight M_n and type of capping agent in terms of mechanical properties of the cured and UV-cured PU networks. Dynamic mechanical properties of the UV cured films showed where the storage modulus increased with the decrease in M_n due to increase in the crosslinking density of the networks. Tensile testing of the networks demonstrated that Young's moduli increased and elongation at break decreased for the networks with decreasing M_n . Tensile testing also showed the capping

agents, pentaerythritol triacrylate had the greatest and aminopropyl triethoxy silane had the lowest strength for the same precursor M_n.

4.3 Experimental

4.3.1 Materials

PTMO polyols (M_n 250, 1000, 2000 and 2900 g/mol) were purchased from Sigma Aldrich and degassed at 60 °C for ~12h. 2-hydroxyethyl acrylate (HEA, 96%) was purchased from Aldrich and purified as previously described.[126] Bis (4-isocyanatocyclohexyl) methane (HMDI, >99.5%) was graciously donated by Bayer Material Science. Pentaerythritol tetraacrylate (PETA), dibutyl tin dilaurate (DBTDL, 95%), 2,2-dimethoxy-2-phenylacetophenone (DMPA, purum, > 98%), 2,6-di-tert-butyl-4-methylphenol (BHT, >99%), magnesium sulfate (reagent plus, anhydrous, 99 %), anhydrous 2-propanol (>99.5 %) were purchased from Sigma Aldrich and used as received. Toluene (Fischer, HPLC grade,) was distilled from magnesium sulfate and was stored over activated 4Å molecular sieves immediately prior to use. Dibutyl tin dilaurate (DBTDL, 95%) was dissolved in THF as a 1 wt. % solution. Ultrahigh-purity nitrogen gas was used as inert reaction atmosphere.

4.3.2 Synthesis of UV-Active PTMO-Urethane Resins

Freshly distilled toluene (35 mL), HMDI (10.49 g, 40.5 mmol), and DBTDL solution (0.01 mL) were introduced into a two-neck, round-bottomed flask equipped with a stir bar, addition funnel and nitrogen inlet. The PTMO polyol (1000 g/mol, 20.0 g, 20.0 mmol) was dissolved in toluene (68 mL) and charged into the addition funnel. The reaction was allowed to proceed for 2 h at 80 °C. Dropwise addition of PTMO into the HMDI solution was completed in

~30 min. HEA (4.70 g, 40.5 mmol) was dissolved in toluene (16 mL), charged into the addition funnel and added dropwise over ~30 min. The reaction proceeded for 3 h at 60 °C after completion of the addition of HEA. BHT (50 mg) was added to prevent polymerization of the product. The resulting viscous liquid was dried in vacuum (0.1 mm Hg) at room temperature for 24 h.

4.3.3 Procedure for UV-Curing of PTMO-Urethane Resins

UtDA 1000 (2.20 g, 2 mmol) PETA (0.352 g 1 mmol) and 2-propanol (1 g) were mixed thoroughly to form a homogeneous mixture. 2-propanol was used to utilize a homogeneous mixture. DMPA UV initiator (1 wt. % of total weight ~ 25 mg) was added into mixture and mixed thoroughly. Mixture was cast on this glass slides and passed through a LC-6B Fusion UV system at 6 $ft.min^{-1}$ belt speed and 1.42 ± 0.05 $W.cm^2$ for each pass to achieve photo-crosslinking.

4.4 Characterization

^1H NMR spectroscopy was utilized to determine composition and M_n of PTMO diacrylates. A 400 MHz Varian Inova NMR spectrometer was used to characterize the oligomers in $CDCl_3$ at 23 °C. FTIR analysis was performed on thin films cast on polished KBr discs on a Varian 6700 FTIR spectrometer at ambient temperature in transmittance mode. Qualitative UV/Vis spectroscopy was performed on an Analytical Instrument Systems, Inc. spectrometer that was equipped with fiber-optic light guides, a DT1000CE light source, and an Ocean Optics USB2000 on thin films cast on glass slides, absorption of glass slides was subtracted. DMA was conducted on a TA Instruments Q800 Dynamic Mechanical Analyzer in tension mode at a frequency of 1 Hz, an oscillatory amplitude of 15 μm, and a static force of 0.01 N. The

temperature ramp was 3 °C/min. T_g's were determined at the peak of the tan δ curve. TGA was carried on a TA Instruments Q100 with a temperature ramp from 25 to 600 ºC under a N_2 atmosphere to determine the oxidative stabilities of networks. The remaining weight percent was measured. Tensile tests were performed on an Instron 4411 universal testing instrument with a cross-head speed of 20 mm/min using manual grips at ambient temperature Stress–strain experiments were conducted with rectangular film specimens. The reported data represents an average of at least five specimens. Soxhlet extraction studies in THF reflux for 6 hour determined the gel fractions. Extracted films were subsequently dried in an oven at reduced pressure (0.1 mmHg) at 60 °C for 24 h, until constant weight was observed. The gel fraction was determined gravimetrically, dividing the initial mass (mi) by the final mass (mf). 90 % or better gel fractions were observed.

4.5 Results and Discussion

4.5.1 Synthesis and Characterization of UV-Active PTMO-Based Resins

A 2-step "prepolymer" method was employed to synthesize urethane diacrylates from α,ω-hydroxyl-terminated PTMO polyol, HMDI, and HEA. ^{1}H NMR spectroscopy confirmed the composition of the diacrylates. **Scheme 4.1** depicts the synthesis of urethane diacrylates (UtDA).

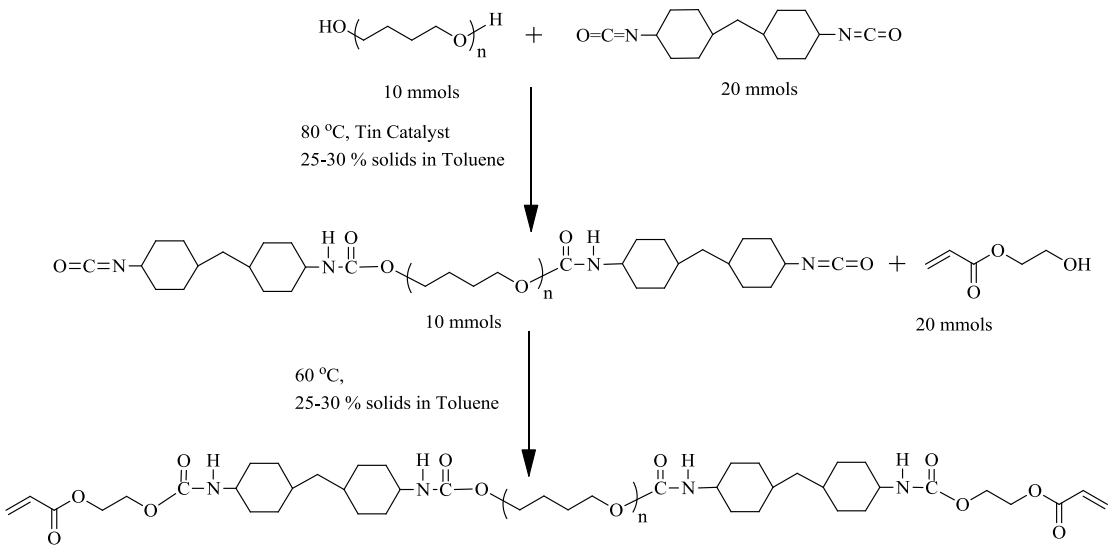

Scheme 4.1. Two-step synthesis of PTMO-based urethane diacrylates (UtDA)

FT-IR spectroscopy was also employed to track the UV crosslinking reaction UtDA with PETA. The thin films of each precursor were cast on a polished KBr disc and FT-IR spectra were collected in transmittance mode. **Figure 4.1** shows the gradual decrease in FTIR absorption at 815 cm^{-1}. The absorption of acrylate end-groups reach to baseline after 6 cycles of UV-exposure.

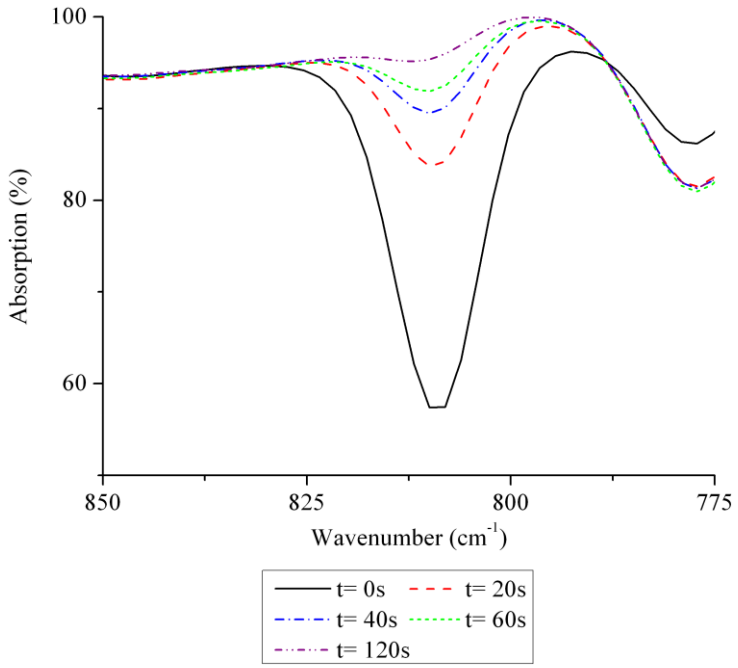

Figure 4.1. FT-IR of acrylate absorption. (UV irradiation conditions: at 6 ft. min $^{-1}$ belt speeds, 1.42 ± 0.05 W cm^2 and 20 s. for each pass.)

The thin films of UtDA and PETA mixtures were applied on a glass slides and UV/Vis spectrum were collected. **Figure 4.2** shows significant change in the pre- and post- UV exposure UV/Vis absorption of thin films. The absorption of acrylate end-groups reach to baseline after 6 cycles of UV-exposure. **Scheme 4.2** shows the UV curing of UtDA with PETA. 1:2 mol equivalence of PETA to UtDA was employed.

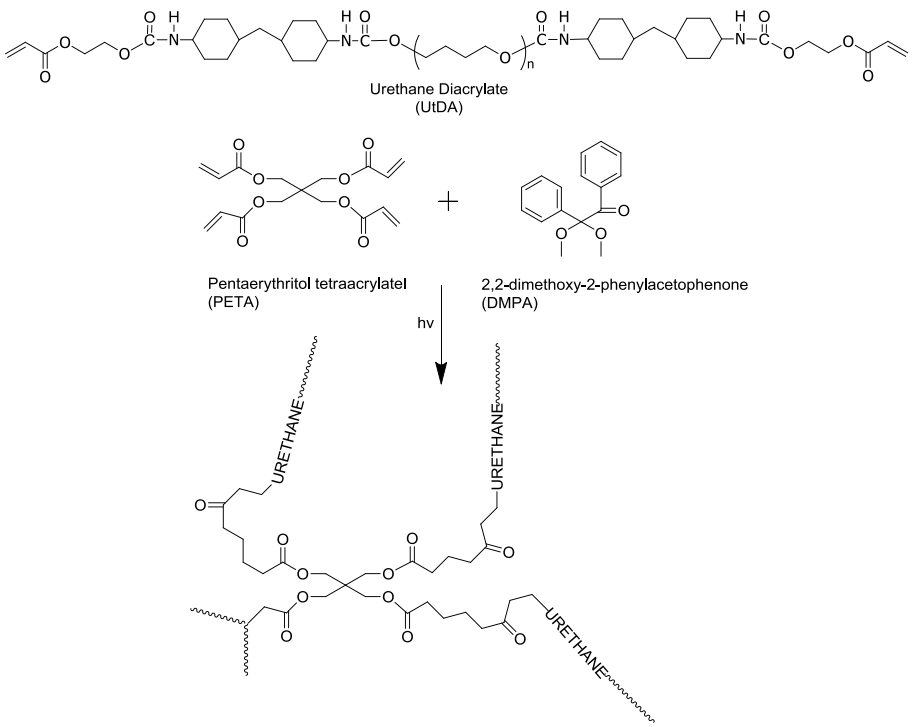

Scheme 4.2. UV crosslinking of UtDA with PETA.

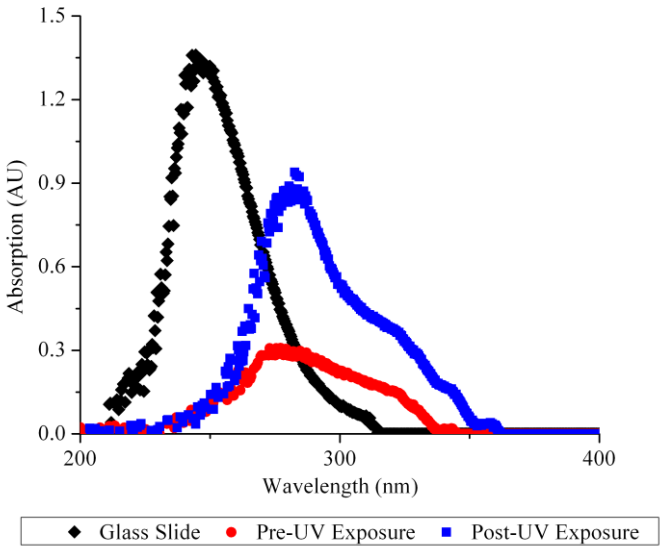

Figure 4.2. UV/Vis UtDA2000–PETA mixture before and after UV-exposure.

4.5.2 Effect of Urethane Diacrylate Molecular Weight on Thermal and Mechanical Properties of Networks

TGA thermogram revealed UtDA-PETA networks show a two-step thermal degradation starting around 320 °C. This result was attributed to consecutive degradation of PETA and UtDA segments. Remaining weight percent calculations revealed that weight loss in the first and second steps corresponded to weight percent of PETA and UtDA in each sample. **Figure 4.3** includes overlay plots of TGA thermograms of UtDA-PETA networks.

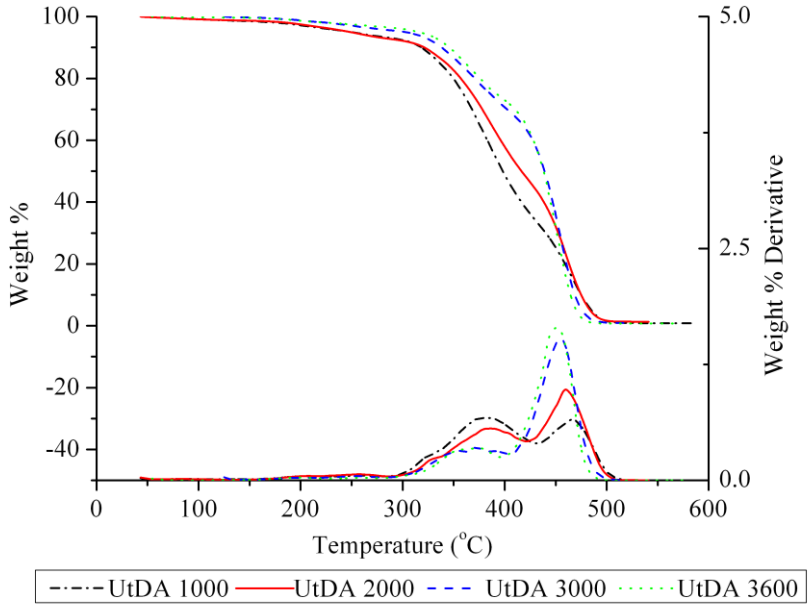

Figure 4.3. TGA thermogram of UtDA-PETA networks.

DMA was conducted to study the influence of UtDA M_n on thermo-mechanical properties of networks. The DMA curves showed a very broad T_g transition for UtDA-PETA networks. This result was attributed non-selective crosslinking reaction between PETA and UtDA. Random reaction between PETA and UtDA yielded a variety of structures which resulted broadening of T_g transition. **Figure 4.4** shows a DMA overlay plot of four UtDA-PETA

networks. UtDA 3000 and UtDA 3600 show a 2 step transition due to crystallization of long PTMO segments present between the crosslink points.

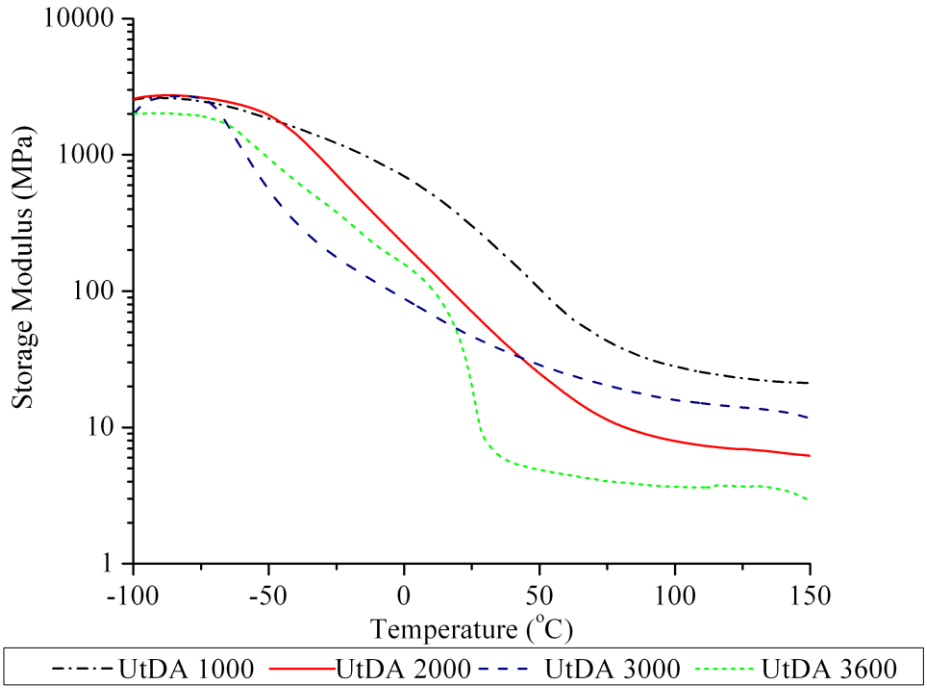

Figure 4.4. DMA curves of UtDA-PETA networks

Tensile properties of the networks were analyzed using an Instron 4411 testing machine with a minimum of five samples for each network. **Figure 4.5** shows a representative plot of tensile tests for each UtDA. The films exhibited moderate Young's moduli, stress at break values, and elongations. The Young's modulus decreased from 15.8 to 1.4 for UtDA-PETA networks as the UtDA precursor molecular weight increased. The elongation at break of the same urethane networks showed an opposite trend decreasing from 76 to 132%. These trends were attributed to the decrease in crosslink density of the networks. **Table 4.1** summarizes the tensile testing results.

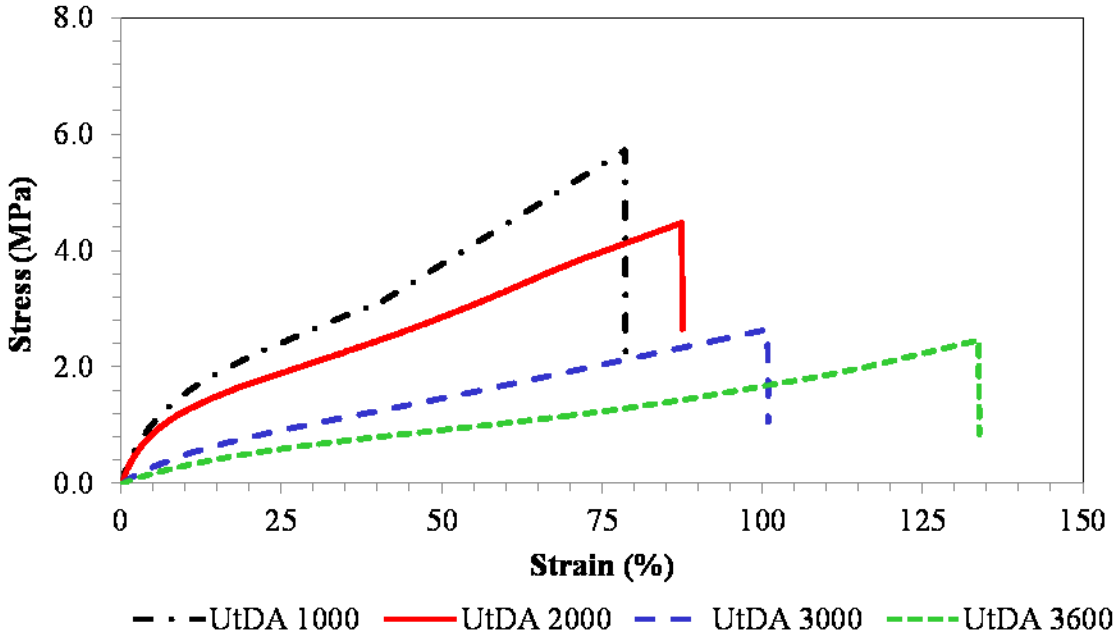

Figure 4.5. Stress-strain curves of UtDA-PETA networks

Table 4.1. Tensile data for urethane diacrylate-PETA networks

Network	Young's Modulus (MPa)	Stress at Break (MPa)	Elongation at Break (%)
UtDA 1000 – PETA	15.8 ± 1.7	6.2 ± 1.4	76 ± 17
UtDA 2000 – PETA	9.6 ± 1.8	3.9 ± 0.4	85 ± 20
UtDA 3000 – PETA	3.3 ± 1.2	2.2 ± 0.6	103 ± 12
UtDA 3600 – PETA	1.4 ± 0.4	1.9 ± 0.5	132 ± 9

4.6 Conclusions

PTMO-based diacrylate precursors were synthesized from α,ω-hydroxy-terminated PTMO polyol, bis (4-isocyanatocyclohexyl) methane and 2-hydroxyethyl acrylate. ^{1}H NMR spectroscopy confirmed the compositions and M_n of the diacrylates. UV exposure of mixtures of UtDA-PETA thin films on glass substrates yielded covalent networks. 1 wt. % DMPA of total weight was employed as UV initiator. FT-IR spectroscopy showed disappearance of acrylate which ascribed the completion of crosslinking reaction. UV/Vis spectroscopy investigation

revealed the decrease in the UV absorption of the films upon UV irradiation. Gel fraction analysis of networks showed gel fractions above 90 %. DMA experiments demonstrated that diacrylate networks showed a very broad distribution of glass transition region. UtDA network had a variation in the T_g's between -60 °C and -30°C. Tensile testing also revealed the relationship between Young's moduli, strain at break and the molecular weight of the diacrylates. In correlation with increasing molecular weight of urethane diacrylate precursor the storage moduli of networks dropped from 15.8 to 1.4 MPa and elongation at break improved from 255 to 755 %.

4.7 Acknowledgements

Research was sponsored by the Army Research Laboratory and was accomplished under Cooperative Agreement Number W911NF-06-2-0014. The views and conclusions contained in this document are those of the authors and should not be interpreted as representing official policies, either expressed or implied, of the Army Research Laboratory or the U.S. Government. The U.S. Government is authorized to reproduce and distribute reprints for Government purposes not withstanding any copyright notation here on.

4.8 References

(1) Kim, B. K.; Lee, K. H.; Kim, H. D. *Journal of Applied Polymer Science* **1996**, *60*, 799.
(2) Ghosh, S.; Krishnamurti, N. *Polymer-Plastics Technology and Engineering* **2001**, *40*, 539.
(3) Crawford, D. M.; Escarsega, J. A. *Thermochimica Acta* **2000**, *357-358*, 161.
(4) Lawson, G.; Bartram, S.; Fitchner, S.; Woodland, E. D. *Analyst (Cambridge, United Kingdom)* **2000**, *125*, 115.
(5) Cho, Y. B.; Jeong, H. M.; Kim, B. K. *Macromolecular Research* **2009**, *17*, 879.
(6) Abraham, G. A.; de Queiroz, A. A. A.; Roman, J. S. *Biomaterials* **2001**, *22*, 1971.
(7) Karabanova, L. V.; Lloyd, A. W.; Mikhalovsky, S. V.; Helias, M.; Phillips, G. J.; Rose, S. F.; Mikhalovska, L.; Boiteux, G.; Sergeeva, L. M.; Lutsyk, E. D.; Svyatyna, A. *Journal of materials science. Materials in medicine* **2006**, *17*, 1283.
(8) Jaffrennou, B.; Droger, N.; Mechin, F.; Halary, J.-L.; Pascault, J.-P. *e-Polymers* **2005**, No pp given.
(9) Bruin, P.; Meeuwsen, E. A.; van Andel, M. V.; Worst, J. G.; Pennings, A. J. *Biomaterials* **1993**, *14*, 1089.
(10) Figovsky, O. L.; Sklyarsky, L. S.; Sklyarsky, O. N. *Journal of Adhesion Science and Technology* **2000**, *14*, 915.
(11) Srivastava, A.; Agarwal, D.; Mistry, S.; Singh, J. *Pigment & Resin Technology* **2008**, *37*, 217.
(12) Kumari, S.; Mishra, A. K.; Chattopadhyay, D. K.; Raju, K. V. S. N. *Journal of Polymer Science, Part A: Polymer Chemistry* **2007**, *45*, 2673.
(13) Lin, Y.-H.; Chou, N.-K.; Chen, K.-F.; Ho, G.-H.; Chang, C.-H.; Wang, S.-S.; Chu, S.-H.; Hsieh, K.-H. *Polymer International* **2007**, *56*, 1415.
(14) Wang, F.; Hu, J. Q.; Tu, W. P. *Progress in Organic Coatings* **2008**, *62*, 245.
(15) Kim, B. K.; Paik, S. H. *Journal of Polymer Science, Part A: Polymer Chemistry* **1999**, *37*, 2703.
(16) Ahn, B. U.; Lee, S. K.; Lee, S. K.; Park, J. H.; Kim, B. K. *Progress in Organic Coatings* **2008**, *62*, 258.
(17) Lin, Y. H.; Liao, K. H.; Chou, N. K.; Wang, S. S.; Chu, S. H.; Hsieh, K. H. *European Polymer Journal* **2008**, *44*, 2927.
(18) Coca, S.; Jasieczek, C. B.; Beers, K. L.; Matyjaszewski, K. *Journal of Polymer Science, Part A: Polymer Chemistry* **1998**, *36*, 1417.

Chapter 5. Future Directions

5.1 Synthesis and Characterization of Sulfonated Urethane Michael Networks

In Chapter 2 the influence of presence and degree of H-bonding both on networks precursors and networks was demonstrated. Incorporation of sulfonate groups into urethane diacrylates may even further enhance the thermal and mechanical properties of the networks. Sulfonate groups can be introduced into soft segment of the urethane diacrylates via transesterification reaction between Dimethyl 5-sulfoisophthalate sodium salt and PTMO. This reaction will yield sulfonate group bearing PTMO diol structure as shown in **Scheme 5.1**. The synthesis of ester and urethane diacrylates can be achieved as previously described in Chapter 2. Michael networks can be synthesized through crosslinking of diacrylates with bis acetoacetates. The thermal and mechanical properties of the network should be investigated. Moreover sulfonate group containing short chain bis acetoacetates can be synthesized utilizing the reaction of Dimethyl 5-sulfoisophthalate sodium salt and 1,4-butanediol. Further reaction of the product as described in Chapter 2 should yield sulfonate group-containing bis acetoacetates. The influence of sulfonate groups on the polymer properties should be investigated via comparing pristine urethane diacrylate networks, sulfonated soft segment-containing networks and sulfonated bis acetoacetate containing networks.

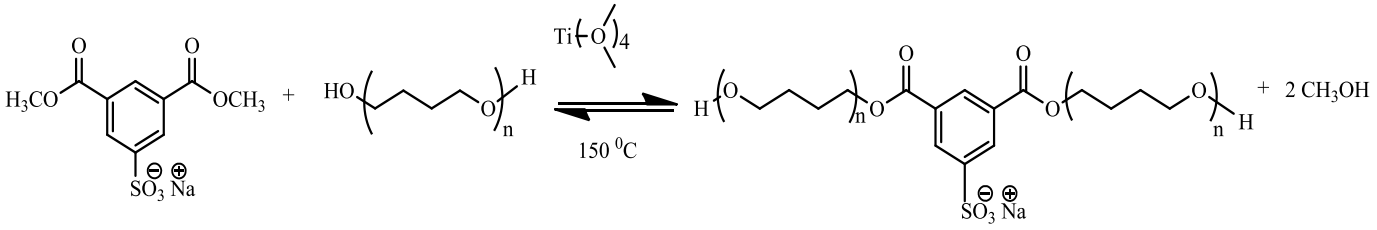

Scheme 5.1 Proposed transesterification reaction between Dimethyl 5-sulfoisophthalate sodium salt and PTMO.

5.2 Electrospinning of Thin Fiber Mats of PTMO-Based Diacrylates

PTMO-based diacrylates are soluble in most organic solvents. In addition to melt rheology behavior of PTMO-based diacrylates as demonstrated in Chapter 2, solution rheology of both H-bonding and non-H bonding diacrylates should also be investigated. The influence of H-bonding on the solution rheology of various diacrylates can be determined. The influence of precursor molecular weight and type of base catalyst on viscosity upon curing should be assessed. The mixture of urethane diacrylates and bis acetoacetates can be electrospun from various organic solvents upon initiation of Michael addition via catalyst addition. The influence of soft segment and bis acetoacetate molecular weight on fiber length, diameter and shape should be investigated.

5.3 Electrospinning of Thin Fiber Mats of PTMO-Based Network-Acid Functionalized MWCNT Composites

Surface-functionalization of carbon nanotubes improves their dispersability in organic solvents, as well as their dispersability within polymer matrices as shown in Chapter 3. The dispersion of acid-functional MWCNT and network precursors in solution should be studied. The influence of surface carboxylic acid groups on the dispersion and alignment of MWCT during electrospinning should be investigated.

5.4 Incorporation of MWCNT with Various Functionalities into Michael Networks

Acid functionalization of CNT introduces the ability to functionalize CNT further with thionyl chloride and long-chain amines as discussed in Chapter 1. Previously reaction of surface carboxylic acid groups of CNT with amine and isocyanate functional groups were demonstrated. As previously discussed in our group, Figure 5.2 shows a series of surface functionalization of carboxylic acid groups with short and long chain amines. The further functionalization of

carboxylic acids with short and long chain amines and their influence of dispersability in organic solvents, as well as their dispersability within polymer matrices should be investigated. The interaction between the amine-functionalized MWCNT and network precursors should be studied. The influence of long and short amine on the dispersion and alignment of MWCT within the polymer matrix should be studied.

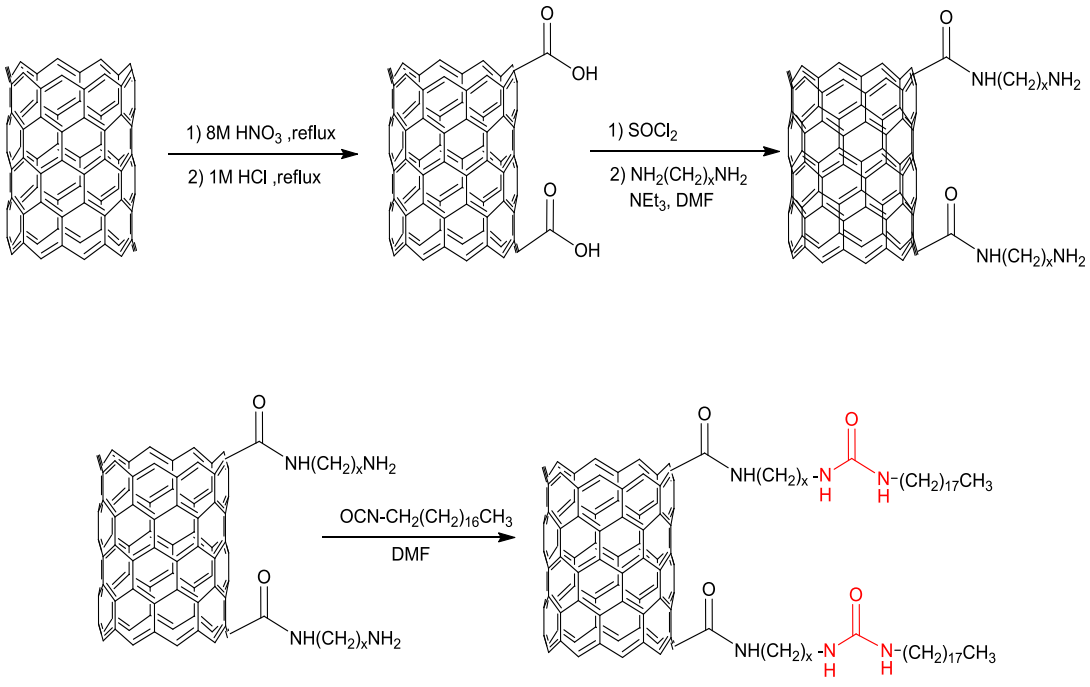

Scheme 5.2 Functionalization of MWCNT-surface.

5.5 Electrospinning of Thin Fiber Mats of PTMO-Based Network-Amine Functionalized MWCNT Composites

Surface-functionalization of carbon nanotubes significantly improves their dispersability both in organic solvents, and within the polymer matrices as demonstrated earlier in Chapter 3. The dispersion of amine-functional MWCNT and network precursors in solution should be studied. The influence of surface amine groups on the dispersion and alignment of MWCT during electrospinning should be investigated.